960

WEAR IN SCREW EXTRUDERS

by

David Roger Carlile

February 1978

A thesis submitted for the Degree of Doctor of Philosophy of the University of London.

Department of Mechanical Engineering,
Imperial College of Science and Technology,
Exhibition Road,
London. SW7 2BX

ABSTRACT

Wear in Screw Extruders

by

D.R. Carlile

Wear resulting from metal-to-metal contact between the screw flight and the barrel of a single screw polymer extruder is considered in this work.

An experimental investigation of the lubricating action of molten polymers is described. A critical shear stress in the clearance between the screw flight and the barrel is found, below which good lubrication is encouraged with no metallic contact between the screw and barrel, and above which there will always be inferior lubrication and some contact.

An analytical investigation of the forces acting on the screw and the resulting deflections is described.

The results of both sets of work are combined to define screw design criteria to minimise screw and barrel wear.

CONTENTS

ACKNOWLEDGEMENTS

I should like to thank Shell International for their financial support during this project. I should also like to thank my present colleagues at I.C.I. Plastics Division for their encouragement during the period spent writing this thesis, in particular T.A. Stanley.

I should like to thank the staff of the Mechanical Engineering Department of Imperial College for their assistance during the course of this work, in particular S. Kasinathan, J.E. Miller and G.R. Williamson.

Lastly I wish to thank my supervisor, Dr. R.T. Fenner for his help and encouragement throughout this project.

CHAPTER 1

Introduction

Most polymers pass through an extruder at some time. Polymer manufacturers use extruders to compound, or mix, polymer with additives such as pigments, stabilisers,glass etc. Extruders are also used to densify polymer powder into regular shaped granules. In the case of polyethylene, where the material is polymerised in a molten form, an extruder can be used to homogenise the polymer and form it into granules. The extruder, with a suitable die, is used to form articles with a constant cross-section such as pipes. It is also the first component in a film line.

The heart of an extruder is its screw. The screw rotates inside a closely fitting barrel. The initial radial clearance between the screw and the barrel is very small, typically of the order of one thousandth of its diameter. It is not surprising that eventually the screw and barrel wear. The wear rates are reduced by either hard facing the flight tips and sometimes the screw root, or by manufacturing the screw out of hardened steel. The barrel liner is also protected in a similar way. Normally the barrel liner is harder than the screw flight tip. Thus the screw, which is easier to replace than the barrel liner, wears out at a faster rate. This wear has an adverse effect on the extrusion process, and eventually the screw and sometimes the barrel liner have to be replaced.

Maddock (Ref. 1) considered the effect of wear on reducing the throughput rate of extruder screws. He carried out a cost analysis on a 2½" extruder and came to the conclusion that the increased leakage flow over the flights, and hence reduced throughput rate made it uneconomic to

extrude polyethylene when the radial clearance was 15% of the metering section channel depth. This analysis, using simple flow equations, was based on screw and polymer costs in 1959. However, even today, this screw wear limit is still a good guide to screw replacement. Barr and Chung (Ref. 2) suggested that an increase in radial clearance decreases the ability of the screw to scrape polymer off the surface of the barrel wall. This will probably lead to degradation of the polymer on the barrel wall and could produce harmful black speck contamination of the product. More recently Klein (Ref. 3) carried out a theoretical study on the effect of wear using a computer program to predict the action of a plasticating screw with a progressively increasing clearance. He also concluded that wear reduces the throughput rate of a screw at a given screw speed. More seriously, he concluded that as a screw wears a longer screw length is required to melt the polymer, i.e. the screw will wear until it reaches a stage when it is not long enough to fully melt the polymer.

Replacement screws are expensive, but this may not be the only significant cost of a worn screw. "Down-time" can be expensive, particularly if a replacement screw is not readily available. Worn screws can therefore adversely affect the melting rate and hence stability of the extrusion process and eventually be costly when replacement is essential.

There are two basic types of wear, abrasive and corrosive. Corrosive wear is a result of adverse chemical reactions inside the extruder and is outside the scope of this work. Abrasive wear can be caused by metal-to-metal contact between the screw and the barrel. The wear rate will be accelerated by abrasive additives, such as glass, being ground between the screw flight and the barrel. Abrasive additives will presumably produce higher wear rates as the degree of metal-to-metal contact between the screw and the barrel increases. This work therefore investigates the

basic wear mechanism of metal-to-metal contact between the screw and barrel. Metal-to-metal contact can be produced by a bent screw or barrel, or a misaligned screw. However this can be avoided by attending to manufacturing tolerances and by careful alignment of the screw in the barrel. These secondary causes of metal-to-metal contact are therefore ignored in this investigation and the primary cause, deflections caused by self-generated forces acting on the screw is considered. The investigation also only considers the generally used one-start single screw extruder. Two-start and twin-screw extruders are not considered.

The work is split into two parts. Polymer lubrication of the screw is investigated in Chapter 2. An experimental rig is used to find what form of lubrication if any, prevails under different extruder operating conditions with different screw geometries and feedstock. In Chapter 3, the potential deflections of a screw and the self-generated forces producing the deflections are estimated using a computer program.

CHAPTER 2

EXPERIMENTAL INVESTIGATION INTO THE LUBRICATING EFFECT OF POLYMERS

2.1 Introduction

In this Chapter the polymer's ability to prevent the screw touching the barrel is considered. An analogy may be drawn between a journal bearing and a single screw extruder. The screw acts as a journal, the barrel as the bearing housing, and the polymer as the lubricant.

This analogy assumes that the polymer acts as a lubricant. Practical experience seems to show this assumption to be true. Very large screws with diameters of up to 500 mm are offered by screw manufacturers. The radial clearance between the barrel and the screw is usually .001 times the diameter. A number of loads act on the screw to potentially produce contact between, and hence wear of the barrel and the screw flight. These include the weight of the screw, self-generated polymer forces, due to the rotating screw and the polymer being forced through the extruder, a bent screw etc. Presumably screw and barrel wear would be more of a problem than it is if the polymer had no lubricating effect. However, it must be shown whether or not there is polymer lubrication, and if so what type of lubrication and how the extruder operating conditions and screw geometry affect it.

2.1.1 Bearing Capacity Measurement

Ideally measurements should be made on an extruder. Unfortunately there are a number of problems:

(i) The exact load acting on any section of the screw is not known.

(ii) A large number of screws would be required to vary the geometry sufficiently.

(iii) The screw must be concentric with the barrel bore so the lubricating effect can be precisely known. A bent or misaligned screw could obscure the true size of it.

(iv) It is difficult to know when the screw touches the barrel.

Therefore a rig must be devised where the above objections are overcome and at the same time the action of the extruder is simulated as closely as possible.

2.2 Mechanical Principles of the Rig

2.2.1 General Principles

A general view of the rig is shown in Fig. 2.1. A 38.1 mm diameter Bone Bros. extruder is used to supply polymer to the working section barrel which is bolted onto its end (Fig. 2.2). A short screw section rotates inside the barrel and conveys the supplied polymer through an annulus between the shaft and the barrel flange. The screw section is grub screwed to a closely fitting shaft and a known lateral load applied to the shaft, and hence the screw section, via a pulley (Fig. 2.3). The shaft rotates in a bearing housing which sits on 3 jacking screws used to align the screw section concentrically with the barrel bore (Fig. 2.4). An electric motor drives the shaft. The torque is transmitted to the shaft through a toothed rubber belt requiring minimal tension. A simple circuit is used to measure the electrical resistance between the screw section and the barrel. If there is polymer present the resistance will be very high. If there is metal-to-metal contact the resistance will be very low. This circuit, the Furey circuit, is widely used in

oil lubrication experiments and will be explained in more detail in Section 2.4. Each part of the rig will now be considered in greater detail.

2.2.2 The Working Section (Figs. 2.2 and 2.5)

This is where the action of a single screw extruder is simulated. The working section barrel may be seen as an extension of the extruder barrel, and the screw section as a separated extension of the extruder screw. This separation allows the screw geometry to be varied by simply changing the screw section on the end of the shaft. It also allows accurate alignment with the barrel and a simple circuit can be used to find when contact occurs between the screw section and the barrel. The screw sections have a pitch equal to their diameter. All screw sections are 2 pitches long, i.e. 2D in length. The short barrel is spigoted onto the extruder breaker plate. Fig. 2.5 shows the screw being pushed into the working section barrel before alignment. Fig. 2.2 shows the split barrel flange bolted round the shaft. The nominal bore of the barrel and O.D. of the screw section are the same as that of the extruder barrel (38.1 mm). The pumping rate of the short screw section should be the same as the extruder screw. Nine screw sections are used to vary the screw geometry. The 3 nominal flight width to diameter ratios (e/D) are .05, .1 and .15. The 3 nominal radial clearance to diameter ratios (δ/D) are .002, .005 and .008. The normal clearance ratio is .001. A range of clearances is used to consider the effect of a progressively worn screw and an atypical geometry. It was not necessary to have a ratio of .001 as the .002 ratio produced a final lubrication condition as will be shown later.

The channel depth, i.e. the distance between the barrel wall and the screw root, of all screw sections is the same as the extruder screw

metering section channel depth, 2.03 mm. This continuity in channel depth does not ensure equal pumping rates because there is a variation in screw section flight width and hence channel width. The extruder screw channel width obviously remains constant. The required balance is produced by running the screw section at a different speed to the extruder screw to compensate for this difference in channel width.

The whole point of the rig is to see under what running conditions and with which screw geometry the screw section touches the barrel. Therefore there must be sufficient clearance between the shaft and the flange to allow the screw to deflect to the barrel. This clearance will cause polymer sealing problems. However a die hole is also required to allow the polymer to be pumped out of the barrel. Therefore the annular clearance was enlarged to become this die hole. This enlargement also ensured that there would not be any unwanted polymer bearing effect between the shaft and the flange. Obviously the annular clearance could not be above a certain size otherwise the low viscosity, low speed runs would not generate any pressure inside the barrel. The consequent reduced lateral load to breakdown the polymer film is discussed later. Also the annular clearance could not be below a certain size otherwise the high viscosity, high speed runs would generate a pressure above that tolerated by the thrust bearings. Unfortunately, no one clearance satisfies these two conditions. Therefore a hole was tapped through the flange into the barrel bore to relieve the high pressure problem. At low speeds with low viscosity polymers this hole is blanked off. This remedy creates another possible problem if a significant lateral load is produced on the shaft when the hole is open. This was tested and the results will be given in the Running Conditions section (2.6).

The eventually required contact between the screw and the barrel is a potentially destructive test. Either the screw, the barrel, or both

will wear depending on their relative hardness. The barrel is used in all the tests whereas the screw sections are used for one set of running conditions, i.e. for a shorter time. Consequently the barrel was made very hard and the screw sections relatively soft. This ensured the barrel did not wear at all. The wear of the screw sections was noted and will be described later. A nitrided liner was shrunk inside the mild steel barrel and the screw sections were made of mild steel and ground to the required O.D. Some care was taken to damp out vibrations acting on the working section. The extruder is bolted to the concrete floor and an A-frame, also bolted to the floor, is used to hold the barrel steady (Fig. 2.3). The barrel is braced against the A-frame by steel plate. These two steps reduced the vibrations to negligible proportions. A scraper is bolted to the top of the barrel flange (Fig. 2.2), and this effectively removes the polymer from the shaft after it has been extruded out of the barrel. The scraper is positioned so it neither touches the shaft nor is a significant layer of polymer allowed to build up on the shaft.

Two holes were drilled and tapped through the barrel, one for a pressure gauge and one through the barrel for a melt thermocouple. Another hole was drilled into the barrel for the relatively shallow set thermocouple controlling the working section barrel heater (Fig. 2.2).

The rest of the rig performs 5 mechanical functions:

(i) It drives the screw section.

(ii) It ensures the screw section deflects sensibly parallel to the barrel bore.

(iii) It does not produce any significant resistance to lateral screw movement.

(iv) It initially aligns the screw section concentric with the barrel bore.

(v) It allows a known lateral load to be applied to the screw section.

The way these functions are carried out will now be described.

2.2.3 The Drive

Obviously a torque must be applied to the screw section to enable it to shear the polymer. The required torque is applied to the shaft and hence the screw section by a toothed rubber belt which is driven by an English Electric 1½ H.P. 3-phase induction motor (Fig. 2.1). The rubber belt isolates the shaft from earth. The electrical circuit used to indicate contact or no contact between the screw and the barrel, described in section 2.4,requires the shaft to be isolated from earth.

2.2.4 Parallel Shaft Deflection

The shaft is held in the bearing housing (Fig. 2.4). A set of opposed angular contact bearings are used as the location bearing, and a roller bearing is used as the floating bearing. The screw section should be able to deflect as nearly parallel to the barrel bore as possible to produce a consistent clearance along the length of the screw section between it and the barrel. The longer the shaft the more parallel will be the deflection. This requirement implies having a very long shaft.

2.2.5 Resistance to Screw Movement

There are two resistances to screw section movement when a load is applied to the shaft:

(i) The shaft's stiffness.

(ii) The polymer's resistance.

The object of this work is to find the resistance of the polymer to the applied lateral load. Therefore the resistance of the shaft's stiffness has to be subtracted from the total resistance. However, to reduce errors, it is sensible to make the shaft's resistance small compared with that of the polymer. A compliant shaft implies reducing its diameter to a minimum.

2.2.6 Shaft Instability

The last two sections suggest using a very long shaft with a small diameter. The angular contact bearings are tightened against each other to give the inner races a good grip on the shaft. The screw section rotates in the polymer so the shaft may be seen as a cantilever with a damping pot to lateral movement at its far end. However this is an idealised picture and the true situation may be less stable. If the shaft diameter is too small there is a possibility of the shaft whirling, of elastic buckling, and eventually of plastic deformation when large loads are applied to it and it is rotated at high speeds. Also the larger the shaft the more difficult it becomes to machine it straight, which in turn makes it more difficult to align the screw section by adjusting the bearing housing position. A compromise is required.

2.2.7 The Shaft Dimensions

The shaft was made out of mild steel, centreless ground to a straightness over it's length within ±.025 mm. The shaft's final dimensions are given below.

DISTANCE BETWEEN THE END OF THE BEARINGS AND THE START OF THE SCREW SECTION (L)	= .84m
SHAFT DIAMETER	= 25mm

It is difficult to propose a method enabling easy calculation of the shaft length to ensure reasonably parallel deflection of the screw section. The ratio, $\frac{x_{r,i}}{x_{r,e}}$ will approach 1 the closer the deflections get to a truly parallel situation. Where $x_{r,i}$ is the deflection at the start of the screw section and $x_{r,e}$ is the deflection at the end of the section. This ratio may be calculated, ignoring the polymer constraint, by a simple cantilever model. However this would ignore the straightening of the shaft produced by the polymer in the working section barrel. A compromise calculation is to consider the shaft to be pivoted about the barrel end of the bearing housing. This ratio will then simply be $\frac{L}{L+s} = \frac{.84}{.916} = .92$, i.e. an 8% difference between the two deflections, where L is the length of the shaft and s the length of the screw section.

The load required to overcome the resistance of the shaft to a deflection equal to the maximum clearance used in the experiments is only .59 kg. The whirling speed of the shaft in free air is 1550 rpm which is well above the maximum speed dictated by the extruder's speed limitation (70 rpm).

A 152 mm gap is left between the start of the screw and the point of application of the load through the pulley (Fig. 2.3). The load should be applied as close as possible to the screw section, so that unnecessarily large loads do not have to be applied to the shaft to produce a given load on the screw section. However there should also be a gap sufficiently large to allow polymer to be easily removed from the shaft and also to allow easy access to strip the barrel between experimental runs (Fig. 2.2).

2.2.8 Alignment of the Shaft (Figs. 2.4 and 2.5)

This section describes the method used for initial concentric alignment of the screw section with the barrel bore circumference. Adjustments are made at the bearing housing end (Fig. 2.4) and the results noted at the barrel end.

The shaft may be moved axially through the bearings if retaining washers and nuts are removed. This enables easy removal of the screw section from the barrel and the re-alignment of the screw section when it is reinserted in the barrel. Fig. 2.5 shows the screw section being moved into the barrel before adjustment begins.

Initially measurements were taken using a dial gauge with an extended arm. The screw section was pushed inside the barrel, the dial gauge was fixed to the shaft next to the screw section and the extended arm touched the bore of the barrel. The shaft was slowly rotated by hand and adjustments made at the bearing housing end until there was an equal clearance all round the screw section. This was repeated with the gauge arm touching the end face of the barrel. In practice this is a difficult procedure because the gauge readings are meaningless until the screw section is not touching the barrel wall,which is the object of the alignment.

A simpler method was eventually used. This method relies on the small load required to deflect the screw section a distance equal to the maximum clearance encountered. This load, .59 kg, already described as the stiffness of the shaft is also the maximum force required to centralise the screw section if it is known to be not touching the barrel when extruding polymer with no load acting on the shaft. This procedure is simple. The screw section is held outside the barrel is the position shown in Fig. 2.5. The bearing housing position is then adjusted until the screw section is lined up with the barrel bore. The shaft is then

pushed through the bearings until the front face of the screw section is very close to the open face of the barrel. The shaft is then rotated and the bearing housing position again adjusted until the screw section will easily slide into the barrel. The shaft is moved until the back face of the screw section is level with the barrel face. The shaft is again slowly rotated and adjustments made until there appears to always be a gap between the flight tip and the barrel bore. This visual approach is checked by switching on the resistance circuit, to be fully described in section 2.4.2, and checking there is no metal-to-metal contact between the screw section and the barrel. A maximum centralising load of only .59 kg is then required. This load was found to be negligible compared with the lubrication breakdown loads found in practice.

The adjustments are carried out at the bearing housing end (Fig. 2.4). Three screws are used for vertical adjustment. They have three requirements to fulfill:

(i) Strength, to support the weight of the bearing housing.

(ii) Fineness of adjustment to give the small movements required.

(iii) Stiffness to prevent movement of the bearing housing and hence the screw section when lateral loads are applied to the shaft.

Differential screws have all these qualities. A hardened conical insert is shrunk into the head of each of the screws for steel balls to sit in. A nut connects the two screws and a feather key is cut into the bottom screw to prevent relative rotational movement between the screws. Hence there is the strength associated with large screws and the fineness of movement per turn given by the difference in pitch between the screws.

The bearing housing has three hardened steel inserts screwed into its bottom face. One insert is flat, another conical in shape and the

third one has a groove in it. These inserts fit over the balls sitting on the top of the three differential screws. Their shape ensures no strain and no degrees of freedom when the screws are moved.

The differential screws fit into holes drilled and tapped into a plate which slides over a table. The differential screws, located in the vertical members of a frame which covers the housing, move this plate laterally.The frame has nine other plain screws screwed through it. These screws are used to hold the bearing housing once adjustments have been carried out. One large screw, through the horizontal member of the frame, prevents the housing from tipping when a load is applied to the shaft. The other eight screws prevent any tendency of the housing to twist. Obviously the table, upon which the housing sits, has to be very rigid. It is bolted to the floor and this reduced the vibrations from the motor situated below it (Fig.2.1) to negligible proportions.

2.2.9 Application of Load to the Screw Section (Fig. 2.3)

The load is applied to the shaft through a pulley. The pulley supports a hanger, onto which weights are loaded. A null method of calibration was used to obtain the relationship between this shaft load and the resulting load acting at the centre of the screw section, (see Section 2.5).

2.3 Possible Lubrication Mechanisms

It is important to understand the possible forms of lubrication in the extruder before the load bearing capacity of the screw is considered. These are described in this section. The information was obtained from Refs. 4, 5 and 6.

The aim of lubrication is to reduce the wear that would otherwise

occur when two metal surfaces slide over each other. If these two surfaces are completely separated by a fluid then there will be no wear. It is necessary to generate a pressure in the film between the surfaces to separate them.

This pressure can be generated externally, or internally by viscous shear of the fluid through the relative motion of the surfaces. This advantageous lubrication is called hydrodynamic lubrication and depends on the gap between the surfaces reducing in size in the direction of sliding. The fluid is forced through the gap by the relative motion of the surfaces and the consequent increase in pressure supports the load. The wedge produced in a journal bearing, when the shaft has deflected from its central position, provides this change in clearance. Fig. 2.7 shows this wedge. The supporting load is found by integrating the vertical component of the pressure force in the film, round the shaft. This is the situation that may be produced in an extruder in the clearance between the flight and the barrel when the screw is deflected. Unfortunately this favourable form of lubrication may not always be posible, e.g. if in the journal bearing shown in Fig. 2.7, the load is increased above the maximum the bearing can support hydrodynamically then this film will break down. However there is a less effective form of lubrication between hydrodynamic lubrication and full contact of the surfaces. This is called boundary lubrication when the surfaces may be partially separated by a film only one or two molecules thick. The surfaces will be touching but not so completely as they would in the absence of this thin film. The viscosity of the lubricating fluid, unlike in hydrodynamic lubrication, is not important in boundary lubrication. The chemical composition of the lubricant and the metal surfaces become important.

There is another form of lubrication called elastic-hydrodynamic lubrication. If the film is reduced to a very small thickness then the

pressure generated between the metal surfaces may be large enough to produce significant elastic deformation of the surface. The lubrication then depends on the elastic deformation of the metal and the hydrodynamic behaviour of the fluid film. However this normally occurs in rolling bearings e.g. ball bearings, or gears where the full load is supported over a very small area. In the sliding situation encountered in journal bearings and also extruders this is not applicable. Therefore there are two possible lubrication mechanisms between the screw flight and the barrel:

(i) Boundary lubrication.

(ii) Hydrodynamic lubrication.

The next section describes the circuit used in the rig to show when each or neither form of lubrication exists.

2.4 Electrical Principles of the Rig

2.4.1 The Contact/No Contact Circuit

The contact sensing circuit is called the Furey circuit after the man who first used it. The circuit was first used to study the metallic contact and friction between a metal ball and a loaded lubricated cylinder (Ref. 7). The extent of metallic contact was measured by noting the electrical resistance between the ball and the cylinder, the resistance of the oil being about 10^6 to 10^{18} times greater than that of the metal junction. This gives a simple contact test. If the resistance is very high then there is no contact. If it is very low there is contact. The circuit is shown in Fig. 2.8. The resistance between the ball and the cylinder is represented by Γ_t

in the diagram. A 1½ volt battery was used. The voltage applied to the ball and the cylinder was reduced by a voltage divider $\Gamma_1\Gamma_2$. This is necessary to prevent any voltage discharge through the oil at a significant separation between the ball and the cylinder. Obviously discharge will occur but by adjusting the applied voltage to an appropriately low level the clearance at which this discharge will occur can be made to be insignificantly low compared with the surface finish of the test specimens, i.e. until the specimens are effectively touching. Furey tested the effect of applied voltage from .1 to 4500 mV and found no significant change in his readings up to 1.5 volts. He eventually used a voltage reduced to 15 mV by the divider.

The circuit theory is simple. Γ_2 is made large compared with the resistance of a metal junction, but low compared with the resistance of a significant lubricant film. If there is no contact between the metal specimens then the value of Γ_t will be high compared with Γ_2 and virtually all the current will pass through Γ_2. The voltage measured across Γ_t will be the voltage applied through the divided i.e. $\frac{\Gamma_2}{\Gamma_1+\Gamma_2}$ V. However if the specimens touch, the resistance of Γ_t will be very low, the current passes through Γ_t and the voltage measured across Γ_t is virtually zero. This instantaneous voltage was monitored by an oscilloscope connected across the ball and the cylinder. In the two extremes of hydrodynamic lubrication and full contact the voltage reading will be theoretically constant. However in the intermediate stage of boundary lubrication there will be intermittent contact over a very short time period. Fig. 2.9 shows the transition from hydrodynamic lubrication to full contact. Theoretically, square traces will be produced as the voltage changes instantaneously from 0 to $\frac{\Gamma_2}{\Gamma_1+\Gamma_2}$ V.

It is useful to know the time percentage contact because the larger this becomes the worse the boundary lubrication becomes. A time averaged value of the voltage is taken by the recorder in an integrating R-C circuit. Tallian et al. (Ref. 8) introduced a small improvement to this circuit (Fig. 2.10). They inserted a current limiter, Γ_3, in the circuit. This reduces the current flowing through the test pieces when they touch, thus preventing any damage to the specimens caused by the dissipation of power over a small contact area. It also ensures that the current is not maintained for a significant length of time due to a heavily ionized path of current in the lubricant after their specimens separated.

They also mentioned possible secondary effects of the circuit. There is a possibly finite capacitance between the specimens separated by an oil film. This capacitance, with the current limiting resister, may determine a significant circuit time constant. This has the effect shown in Fig. 2.11. The square waves are never produced, instead the peak values of the trace are reduced. This obviously has a disasterous effect on the time averaged voltage reading. The effect of applied voltage has already been mentioned in the description of Furey's circuit. The third possible effect may be caused by the current limiting resistor reducing the voltage below $\frac{\Gamma_2}{\Gamma_1+\Gamma_2} V$ when hydrodynamic lubrication exists. My circuit follows the same basic principles with a number of changes. The first difference is that no time averaged value of voltage and hence resistance is taken. The essential difference between the extruder and their lubrication system is that they have a steel ball loaded against a cylinder, in Furey's case, and a ball rotated against other steel balls in Tallian's experiments. When contact exists it will occur through one full revolution of the ball. An extruder screw with a

helical flight is very different. Obviously on the scale of size determined by the asperities of the screw and barrel the screw section will not deflect exactly parallel to the barrel bore and there will be one point, probably at the end of the screw section, where contact will occur. However, because the flight only covers a proportion of the outer circumference of the screw and the applied load is always vertically down and does not rotate with the screw, contact will only occur once per revolution when the flight passes through the position of minimum clearance. For this period there may be full contact or partial contact signifying boundary lubrication. It is therefore more difficult to use a time averaging device to find the time averaged contact. Also in Furey and Tallian's experiments the predominant lubrication mechanism was boundary lubrication. Fig. 11 in Furey's paper (Ref. 7) shows the load carried in hydrodynamic lubrication is less than a hundredth of that carried in boundary lubrication. Therefore it was very important for them to monitor this effect closely. As will be shown later, in an extruder the boundary lubrication effect is much lower than the hydrodynamic effect. Therefore this region is not so important. The second major difference is in the level of applied voltage. Neither Furey nor Tallian mention the noise problem associated with using such small applied voltages. Unfortunately the circuit in my rig passes through the bearing housing. This is a substantial piece of metal and consequently noise was a problem at low voltage levels, even though the cables in the circuit were screened.

2.4.2 The Rig's Circuit (Fig. 2.12)

2.4.2.1 Electrical Properties of Polymers Used in The Experiments

It is first necessary to establish the volume resistivity and

dielectric strength of the polymers used in these experiments in order to specify the values of circuit elements. The polymers used were ICI's low density polyethylene WNC71 and BP's crystal polystyrene XLP. Only the order of magnitude of the values of volumetric resistivity and dielectric strength are required to specify the circuit elements. Therefore general figures for low density polyethylene and polystyrene are used.

Measurement of volume resistivity is very difficult, particularly as a function of temperature. In POLYTHENE (Ref. 9) Renfrew and Morgan quote the results of Stanney and Schroff. They give the volume resistivity of low density polyethylene as 8×10^{15} ohm - cm at $84^{o}C$ and 10^{18} ohm - cm at $40^{o}C$. In the Modern Plastics Encyclopedia (Ref. 7) it is given as 10^{16} ohm - cm for both polyethylene and polystyrene at room temperature. A figure of 10^{12} ohm - cm at typical operating conditions is taken as the volume resistivity of the polymer.

The dielectric strength of a polyethylene is given as 10^{5} volts/mm at $150^{o}C$ in POLYTHENE. The strength of polyethylene of 3.18mm thickness over a short time is given in the range 1.77×10^{4} volts/mm to 3.94×10^{4} volts/mm in the Modern Plastics Encyclopedia (Ref. 10). The dielectric strength of polystyrene is given as 1.97×10^{4} volts/mm. The minimum dielectric strength of a thin film encountered in these tests is taken as 1.5×10^{4} volts/mm.

A voltage of 6 volts was divided by Γ_1 and Γ_2 (Fig. 2.12) into an increasing voltage applied between the shaft and the barrel. A final applied voltage of 5.55 volts was used to eradicate any trace of outside noise. This voltage produces a film breakdown at $\frac{5.55}{1.5 \times 10^{4}}$ mm i.e. 3.7×10^{-4} mm. The variation in surface finish in a well ground screw-section is of the order of 10^{-3} mm, so this breakdown film thickness

is relatively insignificant. The volume resistivity of 10^{12} ohm - cm of the polymer is within the range Furey estimated for his oils (Ref. 7). This produced an oil, and hence in this case polymer film resistance of 10^{6} to 10^{18} times as great as the metal junction resistance between the screw section and the barrel when they touch. A current limiting resistance (Γ_3) of magnitude 12KΩ was chosen.

The circuit capacitance effect mentioned in Tallian's paper did not exist in the rig circuit. Tests were carried out before the experimental runs were started and the boundary lubrication waves were always found to be square, not modified by the capacitance of the film as shown in Fig. 2.11. The other secondary effect of the current limiter resistance was not evident either. When no contact occurred the voltage reading was very close to 5.55 volts.

All the cables in the circuit are screened to earth as shown in Fig. 2.12. The current is taken from the end of the shaft to the oscilloscope by a slip ring (Fig. 2.6). The shaft and bearing housing are insulated from earth. The shaft is driven by a toothed rubber belt and the bearing housing is isolated by the use of mica strips (Fig. 2.4). The hardened inserts at the bottom of the housing have mica strips bolted between them and the housing. Strips glued to metal plates are used to transmit the pressure from the holding screws set in the frame to the bearing housing, again isolating the housing from the frame and thus earth.

2.4.2.2 Problems in Defining Full Contact Between The Screw and The Barrel

The oscilloscope was set on a time base of 10 mv/cm and the result of first contact and "full" contact noted in the tests before experimental runs. First contact readings were very easy to see and

very reproducible. The change between the full hydrodynamic lubrication trace and the single spike per screw revolution, signifying first contact between the screw and the barrel could be produced by adding a .2Kg weight and then a return to hydrodynamic conditions, shown by the full 5.55 voltage trace reading, was produced by removing this extra .2 Kg weight. Full contact did not occur, even with very large applied lateral load. The proportion of the trace covering zero voltage position increased with the applied load, (the boundary lubrication trace shown in Fig. 2.9), until the line appeared to jump once per revolution from a reading of 5.55 volts to zero volts. However, even with significant increases in the applied lateral load the full contact position shown in Fig. 2.9 was never reached because there were always a number of trailing spikes, i.e. there was always a very limited amount of boundary lubrication. However the view was taken that the hydrodynamic lubrication situation is of the greatest importance because when this condition is broken down wear will eventually occur. Also, as described later, the percentage increase in applied load from first contact to the final limited boundary lubrication condition was small. Therefore the very reproducible first contact load is used to present results.

2.5 Calibrations

In the experimental runs the load was applied to the screw section by hanging weights on the pulley which is fixed to the shaft (Fig. 2.3). This load must then be transformed into the actual load acting on the screw section. Two operations are required to do this:

(i) Subtract the load required to overcome the shaft's stiffness from the applied load.

(ii) Multiply the resulting load by a calibration factor which transforms it into the load acting on the screw section. Two calibrations are required to do this. In both calibrations the rig was as shown in Fig. 2.3 except the barrel was removed, exposing the screw section thus enabling easy access to it. Fig. 2.13 shows the layout used to find the shaft's stiffness. A dial gauge measures the deflection of the end of the screw section when the shaft is loaded. The resulting calibration graph is Fig. 2.15. If the clearance between the screw section and the barrel is known for a screw section then the load required to deflect the shaft this distance may be found from Fig. 2.15. A null method was used to derive the second calibration graph. The mid-point of the screw rests on a roller which sits on one pan of a balance (Fig. 2.14). A load is applied to the shaft and weights added to the free pan on the balance until equilibrium exists. The pointer on the balance was not very sensitive so after the balance had been adjusted in equilibrium to the weight of the roller a dial gauge rested against the screw root. This enabled a return to the original position by loading the pan appropriately. Fig. 2.16 shows the calibration graph. Hence

$$\text{SCREW LOAD} = .609 \times (\text{APPLIED LOAD} - \text{STIFFNESS LOAD}) \qquad 2.1$$

2.6 Running Conditions

Nine screw geometries were used in the tests. The exact dimensions of the screws were measured using a Universal Measuring apparatus. The barrel bore was measured using an extension arm attached to the Universal measuring apparatus. In both cases the accuracy of the measurement was to within ±.003 mm. The screw dimensions are given

in Table 2.1.

Two polymers were used:

(i) Low density polyethylene (ICI's WNC71).

(ii) Crystal polystyrene (BP's XLP).

The speed range of the runs was dictated by the upper limit of the extruder's speed and the lower limit of the motor driving the screw section. Unfortunately a feeding limitation of the extruder limited the range of polymers used in this investigation to two. The two polymers were extruded by each screw section at speeds from 30 RPM to 70 RPM.

The extruder and working section barrel heaters were set on a level temperature profile of either 155^{o}C or 220^{o}C when extruding polyethylene and 205^{o}C when extruding the polystyrene. The two very different temperatures used whilst extruding polyethylene were chosen to investigate the effect of temperature on the polymer lubrication. So for each screw section there were 3 runs, each over a screw section speed range of 30 RPM to 70 RPM.

2.6.1 Effect of Polymer Pressure Relief Hole on the Results

The reasons for having a pressure relief hole were mentioned in section 2.2.2.

The possible effect of a lateral load caused by this hole were investigated by extruding polyethylene using screw section 1 (Table 2.1). The tests were carried out with the barrel heaters set at either 155^{o}C or 220^{o}C and screw speeds of 50 RPM and 60 RPM respectively. In each case the only change in operating conditions was to remove the blanking bolt from the hole. This obviously produced a change in absolute pressure inside the barrel. However the pressure difference across the screw section not the absolute pressure should be important in the lubricating effect. An insignificant change in the load required

to overcome the polymer's resistance shows this procedure does not interfere with the lubricating load.

At 50 RPM and 155^{o}C the load for first contact changed from 63.6 Kg to 64.6 Kg when the bolt was inserted. At 60 RPM and 220^{o}C the load changed from 54.7 Kg to 57.3 Kg. These changes are within the experimental errors of this rig and the use of the relief hole is justified.

2.6.2 Balance of Pumping Rates

This problem has been discussed in the General Mechanical Principles section (2.2.1). However it is of some interest to see what effect an unbalanced pumping rate can have on the contact load. Polystyrene was extruded at a constant screw section speed of 50 RPM and a variable extruder screw speed. The graph of first contact and full contact loads versus the extruder screw speed are shown in Fig. 2.17.

At extruder speeds below 53 RPM the pumping rate of the screw section is greater than that of the extruder. Consequently the working section is not full of polymer and a limited amount of polymer is transported across the flights. This improves as the extruder speed increases until at 57.5 RPM the pumping rates are the same and the load is that required to overcome the resistance of the polymer under normal working conditions.

As the extruder pumping rate is increased the polymer is forced through the working section at a faster rate than it would be if it were just being pumped by a screw represented by the screw section. This probably forces the polymer more strongly over the flights. Although great care was taken to equalise the pumping rates the penalties of slight errors are clearly shown by this graph. This is obviously an unavoidable source of experimental error.

2.6.3 Dimensional Changes in the Screw Sections During the Experiments

It is important to know whether or not the dimensions of the screw section changed during the experimental runs. Although contact with the barrel occurred for a small time the harder barrel could have worn away some of the screw section, changing it s dimensions and altering the results of the experiments.

Screw number 1 (Table 2.1) was used in commissioning runs before the experimental programme was started. Consequently it had the heaviest duty of all the screw sections. This screw section was measured after all the experimental runs had been carried out. No changes in the dimensions were found, in fact the original grinding marks on the flight tip were still evident when viewed through a microscope.

2.7 Results

The results of the experimental runs are shown in Figs. 2.18 to 2.23.

In Figs. 2.18 to 2.20 the load required to break down the hydrodynamic lubrication of the polymer film, i.e. the first contact load, is plotted against the screw section speed.

In Figs. 2.21 to 2.23 the rather subjective minimum load at which the final limited boundary lubrication of the screw occurred, is divided by first contact load and this ratio is plotted against the screw section speed. The ratio gives an indication of the amount of boundary lubrication occurring between no contact and the final limited boundary lubrication. The screw section number is given on each line plotted on these graphs. The dimensions of these screw sections, referred to the screw section number is given in Table 2.1.

2.8 Discussion

2.8.1 Boundary Lubrication (Figs. 2.21, 2.22 and 2.23)

The prime importance of the hydrodynamic film breakdown or fist contact load has been emphasised earlier. After this has occurred some wear will take place over a period of time. However it is useful to know when the final boundary lubrication and hence the most damaging contact will occur. Unfortunately this is a rather subjective reading. The ratio of the load to produce this final boundary lubrication condition to the load to produce first contact is plotted against screw speed in Figs. 2.21 to 2.23 and the screw reference numbers given in Table 2.1 are noted in each case. The larger this value the more important is the boundary lubrication effect.

It can be seen from the graphs that the maximum extra load carried in significant boundary lubrication is 50% of that carried in hydrodynamic lubrication. Most of the ratios are below 1.20 i.e. a 20% boundary lubrication effect. The judgement errors in finding the final boundary lubrication load will tend to overestimate this load. This is because an increasing applied load does not produce a proportional increase in percentage contact. The point where an increase in load did not change the voltage trace was difficult to define because of the insensitive response. The first contact loads were relatively accurate and hence the ratio of the two will be on the high side if anything.

The problems in estimating the final boundary lubrication load are shown in Figs. 2.21 to 2.23. Unlike in the first contact load graphs no patterns emerged. Screw section geometry caused no definable effect.

It appears to be safe to say that the significant boundary lubrication effect is secondary to the hydrodynamic effect and its

probable maximum load bearing capacity is only about 30% of the hydrodynamic load bearing capacity until the final limited boundary lubrication occurs.

2.8.2 First Contact Between the Screw Section and the Barrel

2.8.2.1 General Observations (Figs. 2.18 to 2.20)

A similar pattern is shown in all three graphs. The maximum breakdown load at any speed is produced by the section with the largest clearance and flight width. The load bearing capacity reduces as the flight width and then the clearance decrease until for screw sections with a nominal radial clearance to diameter ratio of .002 no significant load bearing capacity is shown.

The effect of flight width is appreciable with screws of $\delta/D = .008$. However with screw sections of $\delta/D = .005$ the effect of flight width appears to be negligible.

2.8.2.2. Temperature Effects (Figs. 2.18 and 2.19)

The effect of temperature is shown in Figs. 2.18 and 2.19. The large clearance effects, i.e. for $\delta/D = .008$ are expected. At a given section speed for a given screw, and hence a constant shear rate, an increase in temperature produces a reduction in polymer viscosity, and hence a reduction in the load bearing capacity of the polymer.

However as δ/D is decreased to .005 the temperature effects became negligible. Screw sections 4, 5 and 6 give nearly identical responses at both barrel heater temperatures. This is probably because at this smaller clearance the increased shear heat generated between the flight tip and the barrel is large enough to make the heat

input from the barrel heaters less significant.

2.8.2.3 Flight Width Effect (Fig. 2.24)

In Fig. 2.24 the first contact load at an average screw section speed of 50 RPM is plotted against flight width for all three clearances and three polymer conditions.

If there were no flight edge effects and hydrodynamic lubrication then it is probably reasonable to assume that the first contact load would be proportional to the flight width as this may be viewed as the length of a small bearing. However the narrower the flight becomes obviously the more important are the edge effects. The two polyethylene curves for nominal $\delta/D = .008$ show this tendency. The polystyrene line is straight. It is unwise to make any fixed conclusions from these results as each line is drawn through only three points. However the trend for the first contact load to increase with flight width is there. This purely hydrodynamic lubrication trend is lost when δ/D is reduced to .005. There then appears to be no relationship between load and flight width.

2.8.2.4 Clearance Effect

Changes in clearance produce changes in the polymer shear rate and and consequently the viscosity of the essentially non-Newtonian polymers. It is therefore very difficult to separate the effect of clearance and viscosity.

2.8.2.5 Hydrodynamic Lubrication Theory

Ignoring the helical configuration of the flight an extruder screw may be seen as a series of narrow bearings with one disc per turn

representing the flight (Fig. 2.25). Each disc may be viewed as a separate bearing of length equal to the screw's flight width. If the polymer is assumed to have a Newtonian viscosity, edge effects are ignored, the flow to be isothermal and to have fully developed velocity and temperature profiles then theory for narrow oil lubricated bearings may be used. In Cameron (Ref. 4 pp. 290 to 293) an equation accurate for $L/D \leqslant 1/8$ and in the extruder screw's case $e/D \leqslant 1/8$, is used.

The heat generation in the small clearance, probably raising the local polymer temperature above that of the barrel, has already been mentioned. Another problem occurs in defining a reference shear rate. When the screw moves from its central position the clearance between the screw and the barrel in the circumferential direction may vary from the nominal clearance to a gap slightly larger than the asperity size on the flight. This produces a vast range of shear rates in a shear sensitive material and makes it difficult to calculate a representative viscosity using the unknown temperature and shear rate. This inaccuracy in viscosity doesn't justify complex analysis and this simple approach is used. The equation is

$$\frac{W_b}{LU\mu}\ \frac{\delta^2}{L^2} = \frac{\pi}{4}\ \frac{\varepsilon}{(1-\varepsilon^2)^2}\ (0.62\varepsilon^2 + 1)^{\frac{1}{2}} \qquad 2.2$$

ε is the eccentricity ratio, i.e. the radial movement of the screw divided by the nominal clearance, δ. When ε is o the shaft is central, when $\varepsilon = 1$ the shaft is running againgst the bearing. By knowing the surface finish of the shaft and the bearing the maximum tolerable value of ε before contact occurs may be calculated. The load bearing capacity of the bearing, W_b, can be calculated by knowing the bearing geometry and operating shaft peripheral velocity, U.

This equation is modified for an extruder to:

$$\frac{W_b \delta^2}{2\mu U e^3} = \frac{\pi}{4} \frac{\varepsilon}{(1-\varepsilon^2)^2} (0.62\ \varepsilon^2 + 1)^{\frac{1}{2}} \qquad 2.3$$

The factor of 2 is introduced on the LHS of the equation because W_b is supported by two representative discs, each of length e.

Unfortunately it may be shown that this equation does not model the results given in Figs. 2.18, 2.19 and 2.20. If the two groups represented by screw sections 1, 2, 3 and 4, 5, 6 are considered, each group has a constant clearance therefore assuming the same surface finish ε should be constant within a group, and $W_b\delta^2/U\mu e^3$ should also be constant.

The ratio of e's between 1 and 3 and 4 and 6 are 3:1. At a certain speed, δ is constant within a group, μ and U are constant therefore the ratio of W_b's should be 3^3:1 i.e. 27:1. The ratio is hardly 2:1 for 1 and 3 and about 1:1 for 4 and 6. Apparently pure hydroydnamic lubrication does not exist because even taking into account the large approximations in the equation this magnitude of error would not be expected.

The first obvious source of error is that the edge effects as the polymer is dragged over and leaves the flight are not considered. The other effect which will now be explained concerns the possible slip of the polymer above a critical shear stress.

2.8.3 Polymer Shear Stress Effects

So far no insight has been gained into why the response of the polymer changes drastically as a function of the radial screw clearance until at $\delta/D = .002$ there is no hydrodynamic lubricating effect at all. A nominal shear rate over the flights is taken as $\pi nD/\delta$

where δ is the nominal radial clearance. This shear rate, together with a polymer temperature equal to the barrel temperature can be used to find a nominal polymer shear stress over the flight. This stress is taken from a flow curve resulting from capillary rheometer work on the polymer. The first contact load is then plotted against this nominal shear stress in Figs. 2.26 to 2.28. In each graph a critical shear stress occurs, above which the polymer has no evident load bearing capacity and below which there is a load bearing capacity. This phenomenon has been noted before in a different context. This work will be reviewed in the next section.

2.8.3.1 Polymer Slip Above a Critical Shear Stress

For the purpose of analysis the velocity of the polymer is normally assumed to be zero at the wall when flowing through a die. It has been known for a number of years that this is not always true. If the wall shear stress is greater than a critical value then the polymer will slip and its velocity will be non-zero. Melt fracture of the polymer and slip are associated (Ref. 11) so it is important to ensure the shear stress is less than critical to ensure good product quality. This is done by taking care in specifying the die profile. Kennaway (Ref. 12) looked at the adhesion between polymers and metal surfaces. He measured the stress required to break the bond between the polymer and a metal surface. The typical bond and shear stresses were found to be 7×10^4 N/m^2 for polyethylene, 1.4×10^5N/m^2 for PMMA and only 3400 N/m^2 for unplasticised PVC.

This is the mechanism involved when slip occurs, i.e. the shear stresses generated in the polymer are large enough to overcome

the adhesion shear stress and the polymer slips over the wall surface. The precise mechanism is not known. The polymer could either completely slip over the metal surface or the high shear stresses encountered in the slip region could cause a layer to be torn off adjacent to the wall. A lot of research has been carried out using a piston and barrel arrangement to extrude the polymer through the barrel at a known temperature, pressure and shear stress. Some early work was carried out by Benbow and Lamb (Ref. 13) when they also found the material from which the die is contructed affects the onset of instability. From a wider range of work on melt fracture (Ref. 14) it appears that slip is associated with melt instability and the critical shear stress for most commercial polymers is around $10^5 N/m^2$. This is the result Kennaway obtained in his adhesion experiments except he used the exceptional unplasticised PVC which has a very low critical shear stress.

Relatively little work has been carried out to investigate the effect of slip in extruders. Shear stresses of $10^5 N/m^2$ are not normally found in the polymer in the screw channel but this order of shear stress may be found in the polymer in the clearance between the flight and barrel. Barr and Chung (Ref. 2) ran a 63.5 mm diameter extruder processing high density polyethylene with three different screws, identical except for a changing clearance between the flight and the barrel. The clearances used were .064 mm, .14 mm and .267 mm and the screw was run at 64, 72 and 134 RPM. The experiment was carried out mainly to find the effect of screw clearance on polymer throughout. However they also looked at the power requirements and found there was a sharp increase for the .064 mm clearance screw at all speeds. Their interpretation of this result was that either the screw or the barrel was eccentric causing contact between them at a small clearance. However, the nominal shear stresses over the flight at this clearance are in the

region of $10^5 N/m^2$ and it may be that this is where slip occurred. The high contribution of shear over the flight to the total power used is lost, but with no effective polymer lubricating film present the screw will run on the barrel thus producing a large increase in the power requirement. More recently Worth and Helmy (Ref. 15) looked at slip in an extruder and used a power consumption criterion to decide when slip occurs over the flight tip. They extruded silicone fluid through a 37.9 mm extruder, calculated the expected power requirements for leakage flow and compared them with those required by their extruder. They found an increasing discrepancy between calculated and experimental power requirements with increasing screw speed. Surprisingly, the calculated power requirements were above the experimental values. This would happen if, when the fluid slipped, little contact occurred between the screw and the barrel.

2.8.3.2 The Effect of Polymer Slip on the Results of this Investigation

Slip, predominantly viewed as a die phenomenon also appears to have an effect on the lubrication of the extruder screw. In Figs. 2.26 to 2.28 the first contact load is plotted against the nominal polymer shear stress over the screw flight. In all three graphs there is a very sharp discontinuity at a particular shear stress. At this point, and with increasing shear stress the polymer film cannot support a load. Below this shear stress, depending on the screw geometry and operating conditions, the screw section will support a load. The critical shear stress for polyethylene is 1.4×10^5 N/m^2 for a barrel setting of 155^oC and $.72 \times 10^5$ N/m^2 for a barrel setting of 220^oC. The critical shear stress for the crystal polystyrene is 1.18×10^5 N/m^2.

In deriving the viscosity curves for the materials used in these runs Cogswell (Ref. 16) noted melt instability at exit from the rheometer capillary at shear stresses of about 10^5 N/m^2.

All three critical shear stresses are around the 10^5 N/m^2 expected for slip to occur. It seems reasonable to suggest the polymer film breakdown and slip are connected. However in Benbow and Lamb's paper (Ref. 13) it is suggested that the critical shear stress is not a function of temperature, whereas it appears to be insensitively so for the different polyethylene temperatures used in this experiment. However in Kennaway's direct work on polymer adhesive stresses (Ref. 12) the bond stress for polyetheylene is seen to decrease with temperature as found in my results. Also errors may occur in estimating the values of shear stress which are only based on the nominal radial clearance between the screw section and the barrel and the barrel temperature.

2.8.4 Lubrication Mechanism

Another possible critical shear stress mechanism has not been mentioned yet. It is possible that the melt fractures at critical shear stresses over the flight, at which point the hydrodynamic film breaks and its load bearing capacity is removed. This would be similar to the cavitation effects seen in oil bearings. However the critical shear stresses derived in my experiments are very close to those derived in slip experiments and this indicates that polymer slip causes the film breakdown.

At sub-critical shear stresses the polymer is sheared by the flight against the barrel wall. This shearing depends on good adhesion to the barrel wall. The shearing action builds up pressure as the clearance between the screw and the barrel is reduced. This pressure

increase will then support the load acting on the screw. However if the polymer slips over the barrel wall the polymer will not be sheared and the support pressure will not be generated. This is a rather simplified view of the possible mechanism but it illustrates the general principles. A more complete picture is given in Fig. 2.29. The screw position for each δ/D used in the experimental runs is shown. The inner circle represents the outer surface of the screw flight, the outer circle the barrel. The view is looking axially down the barrel. The problem with the simple explanation above is that it assumes the clearance and hence the shear stress is such that the polymer either slips or does not slip. Obviously, with a high screw eccentricity and the right nominal clearance the shear stresses produced over a flight section may cover a range of shear stresses from sub-critical to super-critical values. In Fig. 2.29 the dotted lines represent the start and end of a flight at 1/6 turn. These discrete points are connected by an infinite number of flight slices rotating round the helix. Each slice will have a load bearing capacity and the full load bearing capacity is derived by integrating these pressure loads round the helix. Apparent total slip was found at nominal δ/D of .002 for the polymer conditions and screw speeds used in these experiments, i.e. at clearance ratios less than or equal to .002 the polymer shear stress became critical over the flight. The diagrams show the screw section just before it touches the barrel. In each case the slip region, defined by $\delta/D = .002$, is shaded.

If the slip condition is encountered after polymer has been dragged over the flight, i.e. in 3 at δ/D of .005 and .008 (Fig. 2.29) the pressure of the polymer dragged behind it forces it through the clearance. In sections 1 and 2 there is complete drag flow and the pressure increases as expected due to the reduced clearance between the

screw flight and the barrel.

This model explains why the apparent hydrodynamic lubrication behaviour seen with δ/D = .008 was not supported by the simple oil lubrication theory. The crucial flight sections, i.e. these where eccentricity is greatest and hence potential pressure generating capacity largest, have their effective flight width reduced by the polymer slipping. Obviously the flight width e, should be replaced by an effective flight width. At δ/D =.005 the effect of flight width is negligible i.e. the clearance has been reduced to produce a nominal shear stress over the flight which produces a constant effective flight width. The other problem is modelling the complex slip/no slip situation as the flight rotates round one turn of the helix.

At nominal shear stresses above the critical value not only is there no hydrodynamic lubrication but there is only the final limited boundary lubrication condition.

2.9 Conclusions

A critical shear stress criterion determines whether or not good polymer lubrication is possible. This critical shear stress is about 10^5 N/m^2 which is a figure previously linked to polymer slip in dies. At shear stresses below this value a hydrodynamic lubrication/slip mechanism exists. The complexity of this mechanism makes it difficult to calculate what load a screw will support if its geometry and operating conditions are known.

After this polymer film has been broken down there is a limited amount of boundary lubrication if the nominal shear stress is below the critical value. If it is above the slip value very limited boundary lubrication will exist. The load required to go from first contact to the final limited boundary lubrication between the screw and the barrel

is probably never greater than 30% of the load the screw will support with no contact whatsoever. This boundary lubrication is obviously useful but the only condition when no wear will occur is when there is a hydrodynamic lubrication/slip situation. Obviously the hydrodynamic lubrication/slip mechanism should be encouraged to produce no wear.

The nominal shear rate over the flight is $\pi nD/\delta$. Screw designers usually set δ/D at .001. In the screw sections used in these tests the minimum value of δ/D was .002, therefore at a particular screw speed, n, the shear rates in a new screw are higher than those encountered in these runs. Even at 30 RPM, which is lower than a usual commercially viable screw speed, no lubricating capacity was found for δ/D equal to .002. This implies that for a lot of new screws extruding commercial polymers the nominal shear stress over the flights will be above the critical shear stress of the polymer and hence the screw will only be lubricated by the final and very limited boundary lubrication previously described and the screw will wear. The lubrication situation will only become favourable when the flight has worn down so that the polymer shear stress is below the critical value. It does not seem sensible to harden the flight tip, then have to wear this hardened tip until the polymer film does not slip over the flight, to produce a situation where the loads acting on the screw are completely supported by the polymer. The critical shear stress of the polymer should be established using a rheometer and noting the shear stress when melt instability is seen at output from the capillary. This is the critical shear stress of the polymer. If the screw size and required screw speed range is known the maximum shear stress can then be calculated. By increasing the clearance until this shear stress is below the critical value lubrication can be encouraged. Unfortunately, if the clearance is made too large the throughput may be unduly affected. Maddock (Ref. 1) suggested that the

economic limit is reached when the radial clearance reaches 15% of the metering section channel depth. Therefore the screw designer has to use judgement to specify the optimum radial clearance between the screw flight tip and the barrel.

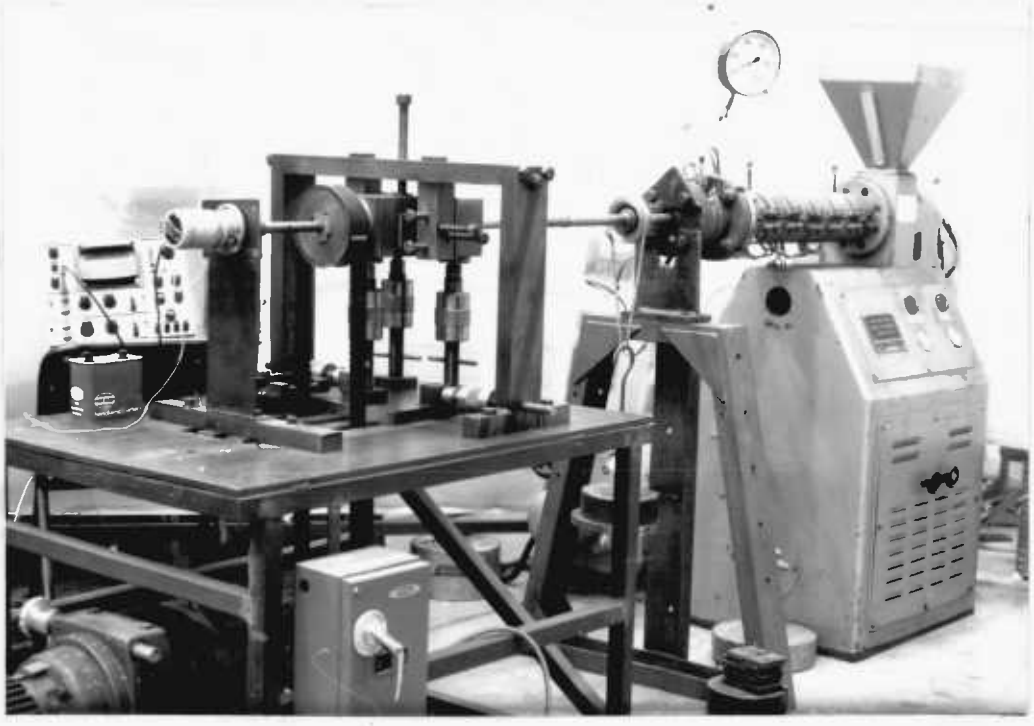

FIG. 2.1 GENERAL VIEW OF THE RIG

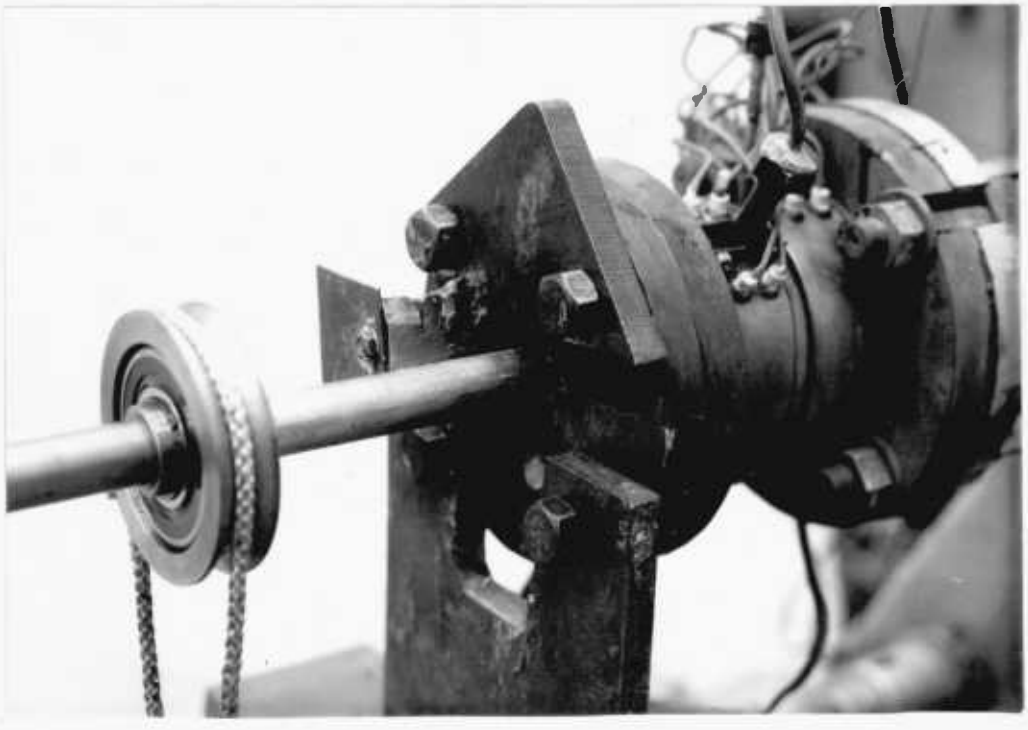

FIG. 2.2 WORKING SECTION ASSEMBLED FOR RUN

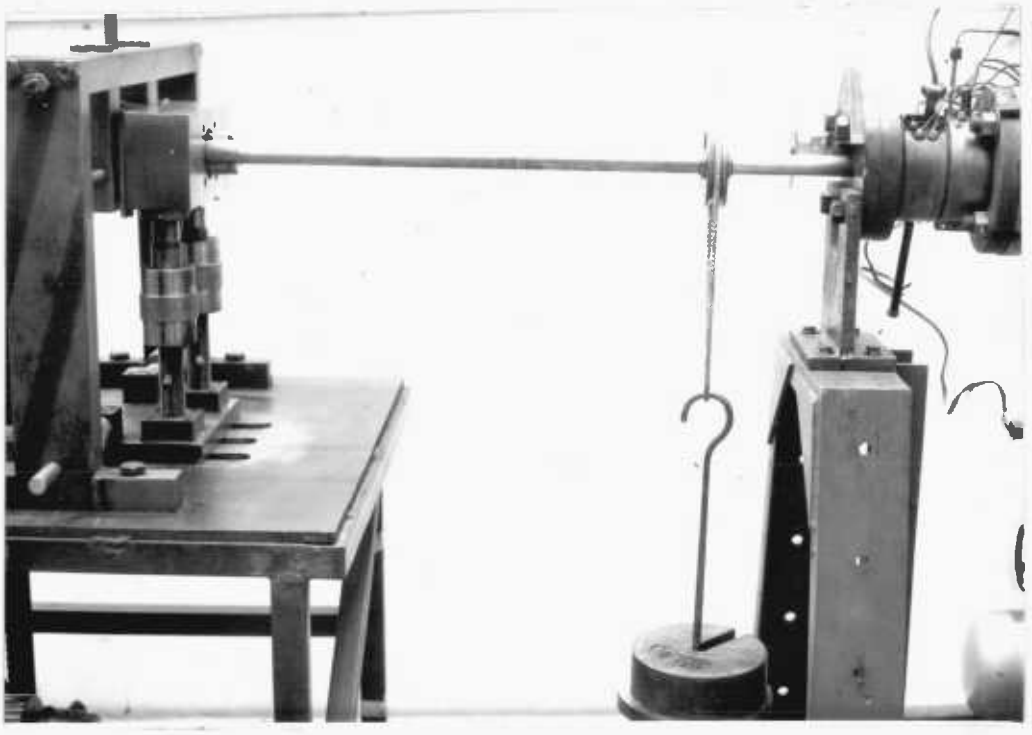

FIG. 2.3 LOAD APPLIED VIA SHAFT TO SCREW SECTION

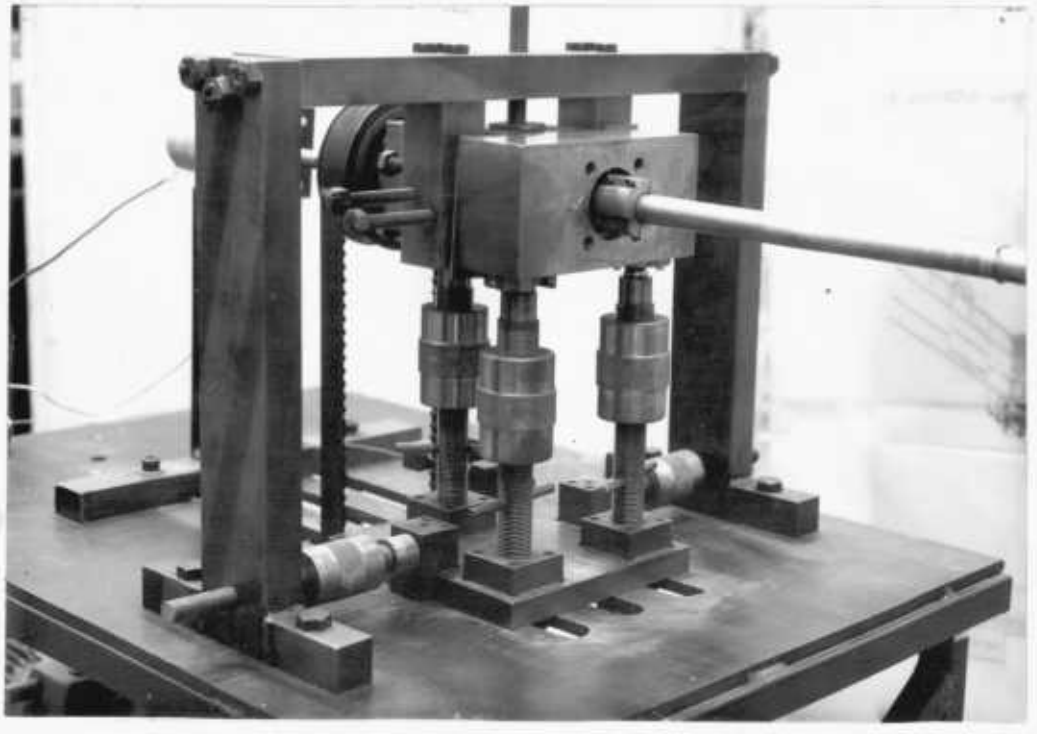

FIG. 2.4 BEARING HOUSING

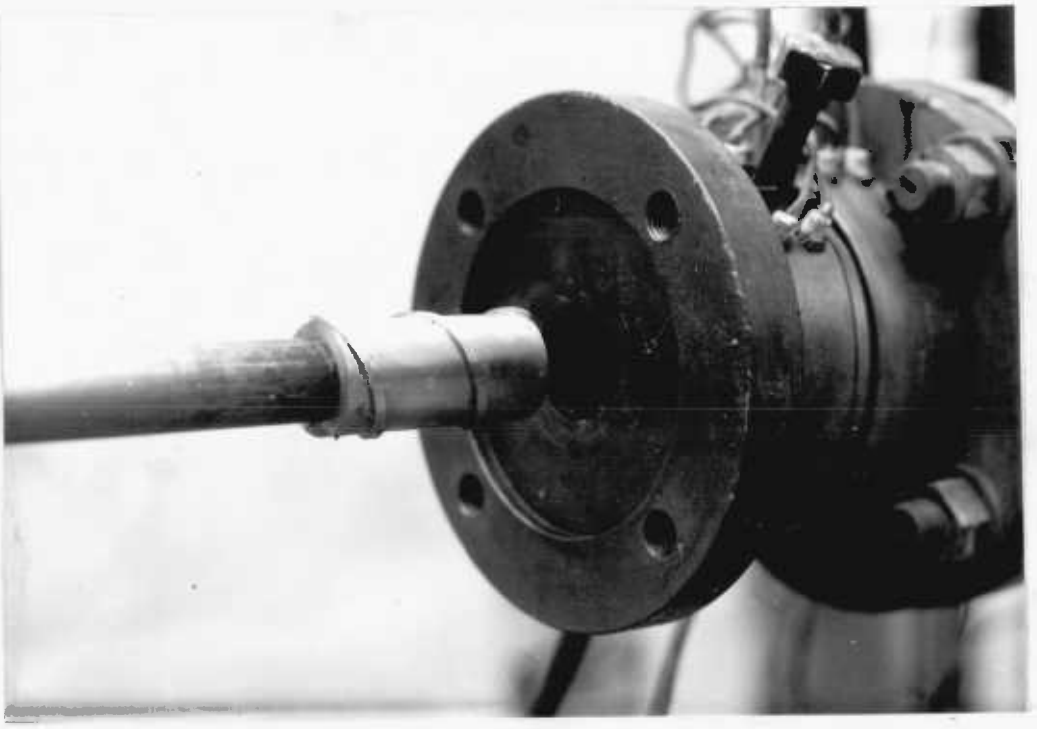

FIG. 2.5 SCREW SECTION AND OPEN WORKING SECTION BARREL

FIG. 2.6 ELECTRICAL CIRCUIT

FIG. 2.7 HYDRODYNAMIC LUBRICATION IN JOURNAL BEARING

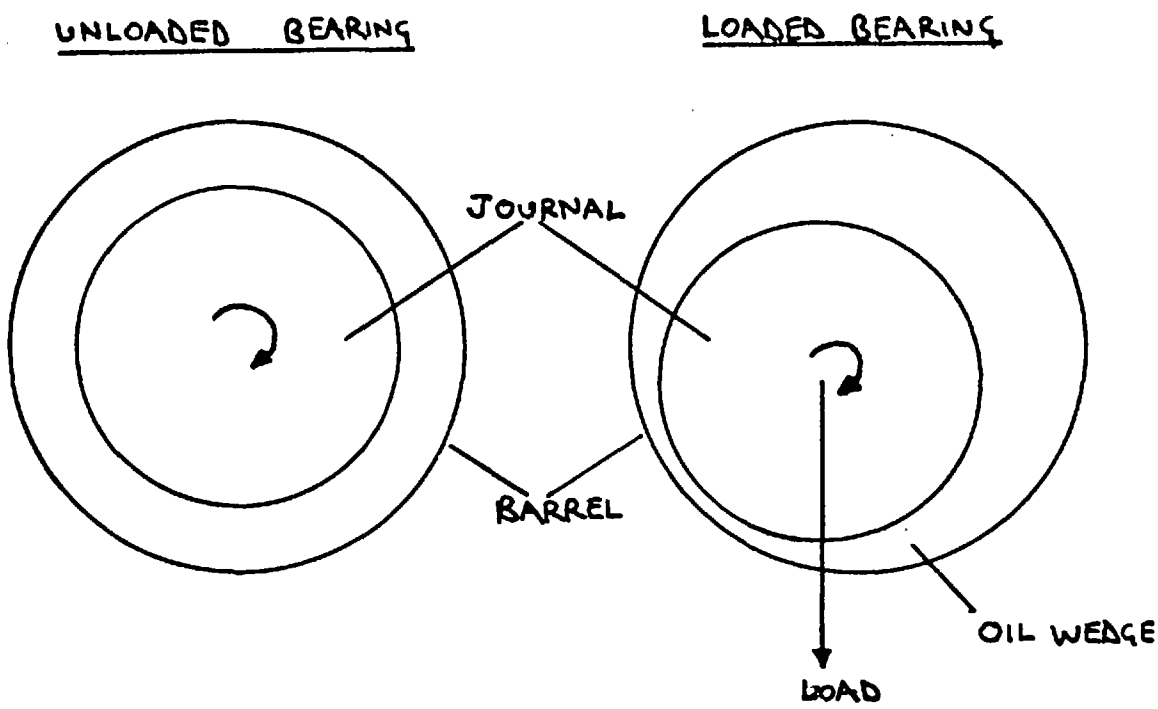

FIG. 2.8 FUREY'S CIRCUIT

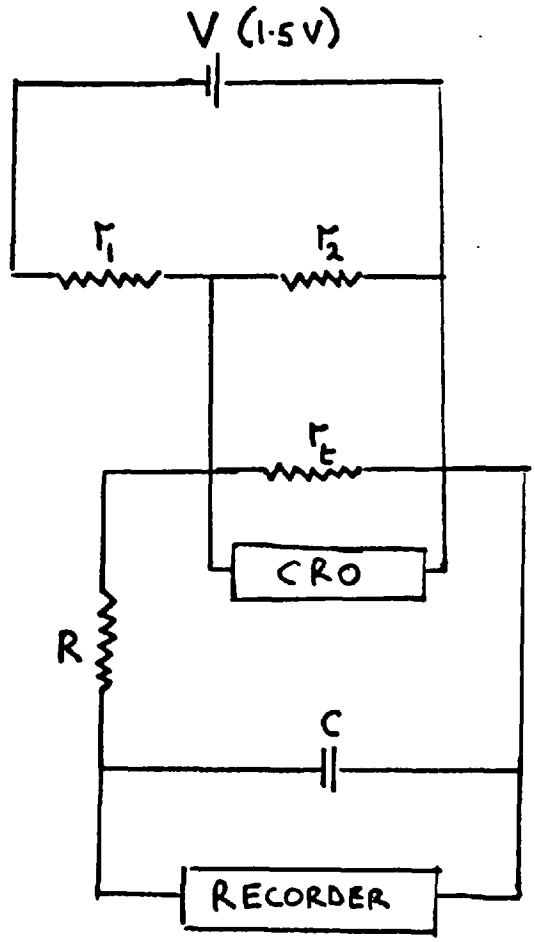

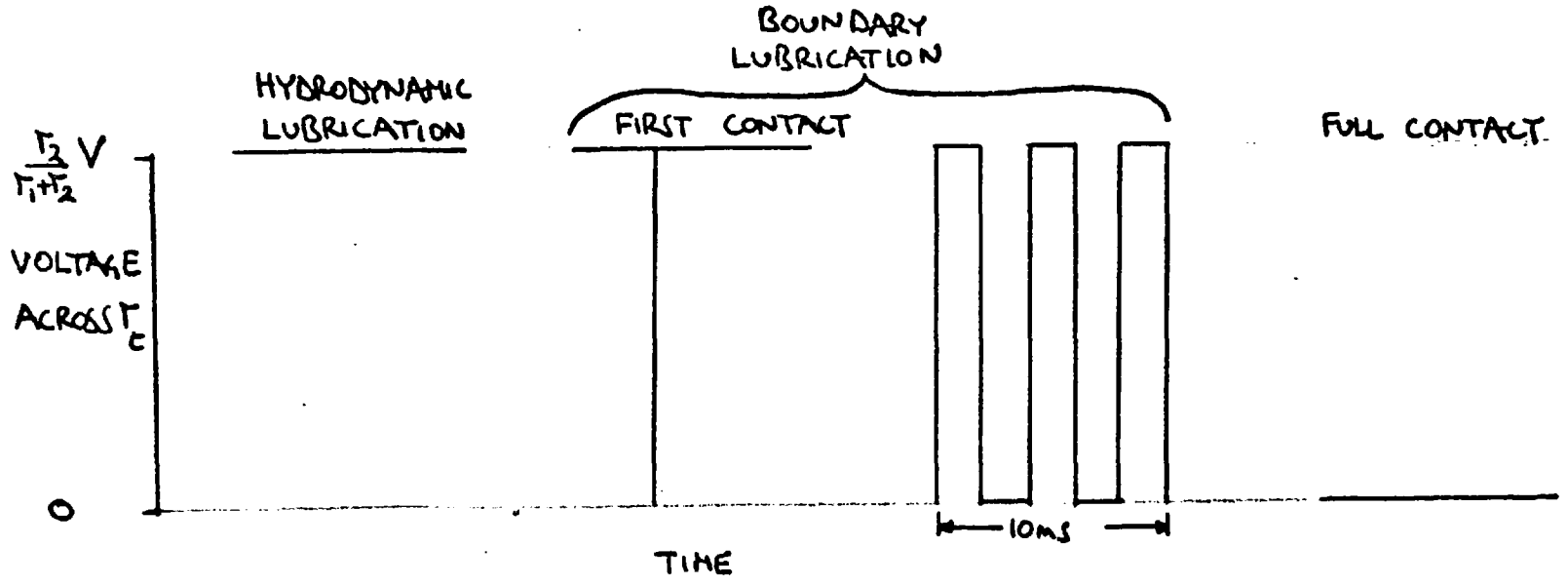

FIG. 2.9 VOLTAGE VERSUS TIME TRACE ON OSCILLOSCOPE

FIG. 2.10 TALLIAN'S CIRCUIT

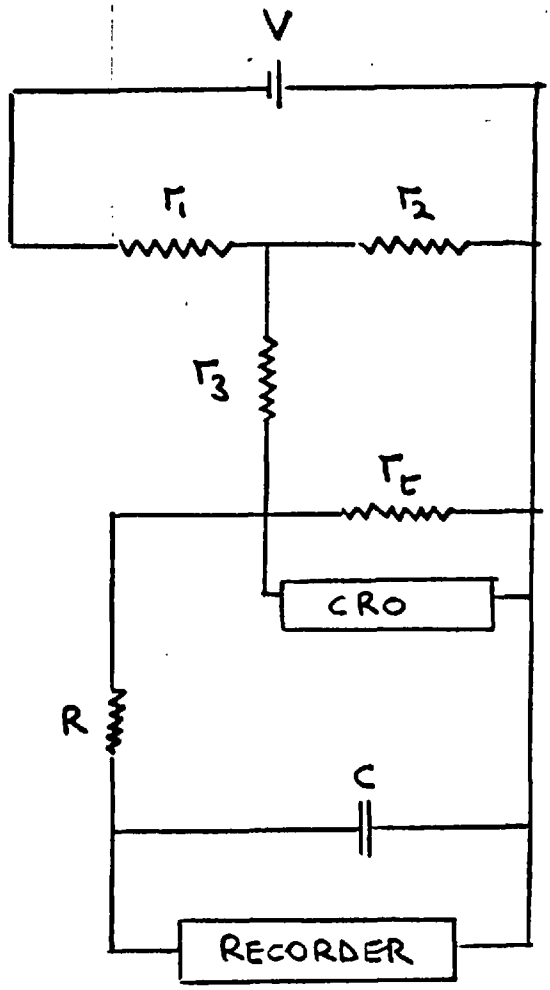

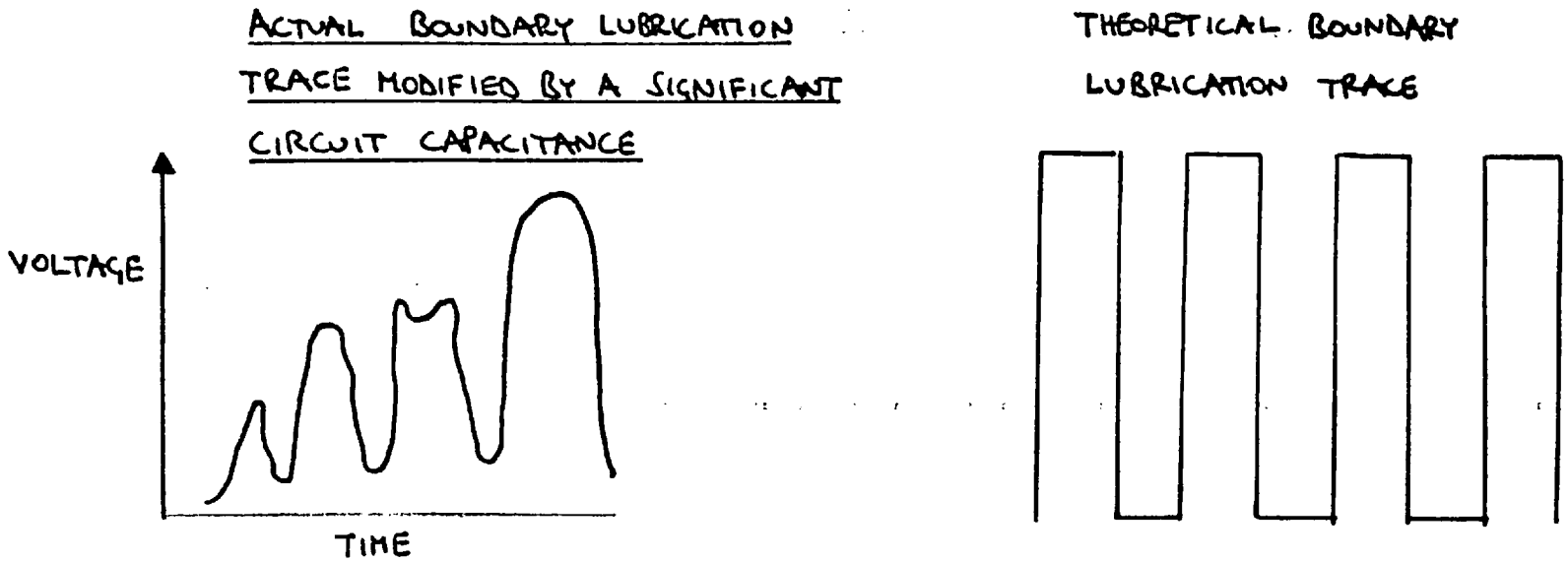

FIG. 2.11 THE EFFECT OF A SIGNIFICANT CIRCUIT TIME CONSTANT ON THE VOLTAGE TRACE

FIG. 2.12 THE RIG CIRCUIT

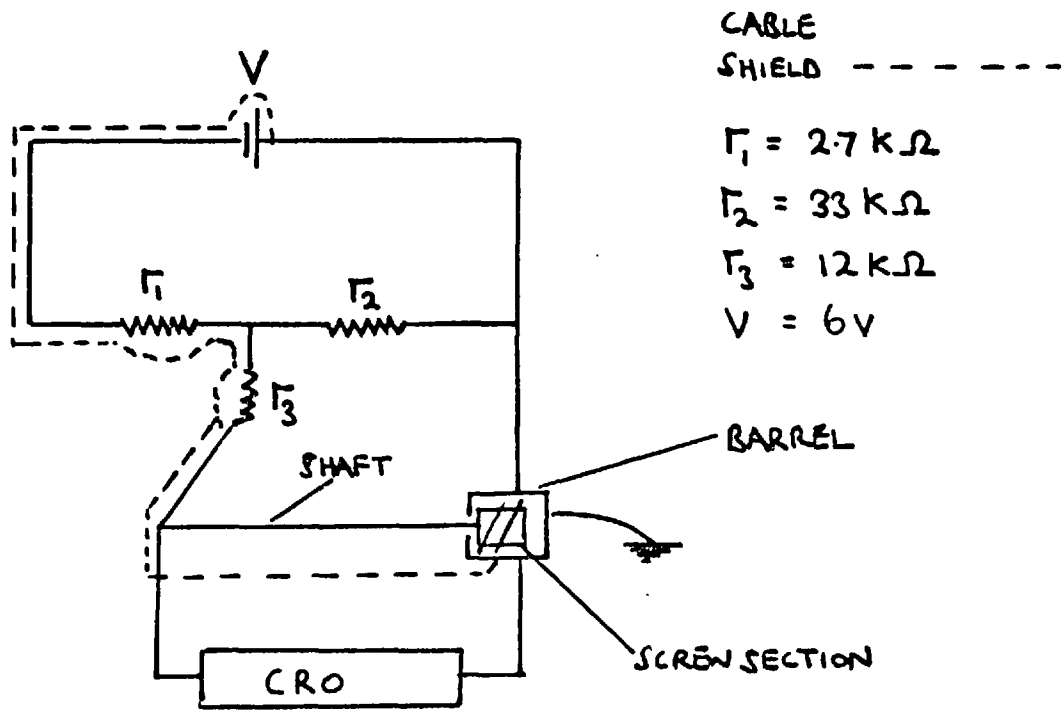

FIG. 2.13 SHAFT STIFFNESS CALIBRATION

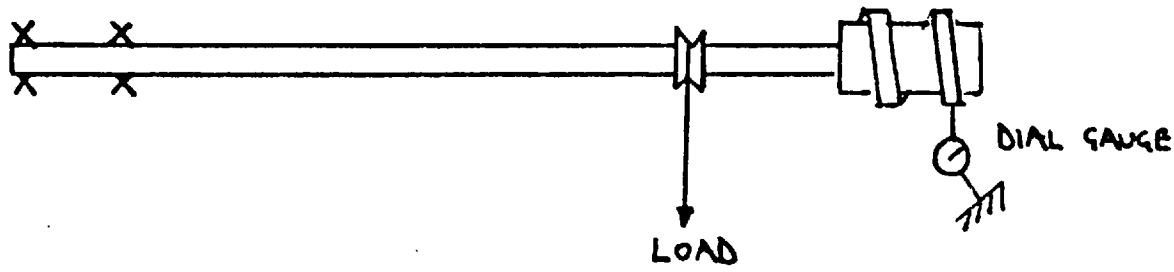

FIG. 2.14 SCREW LOAD CALIBRATION

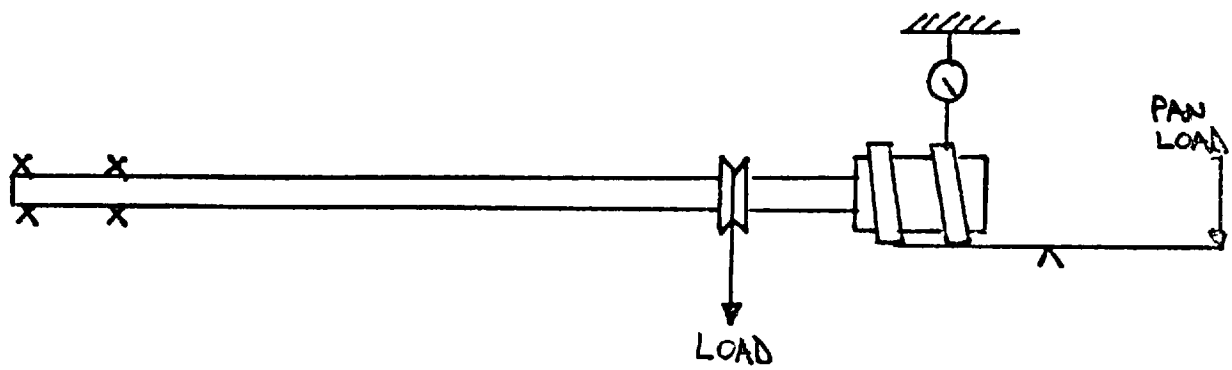

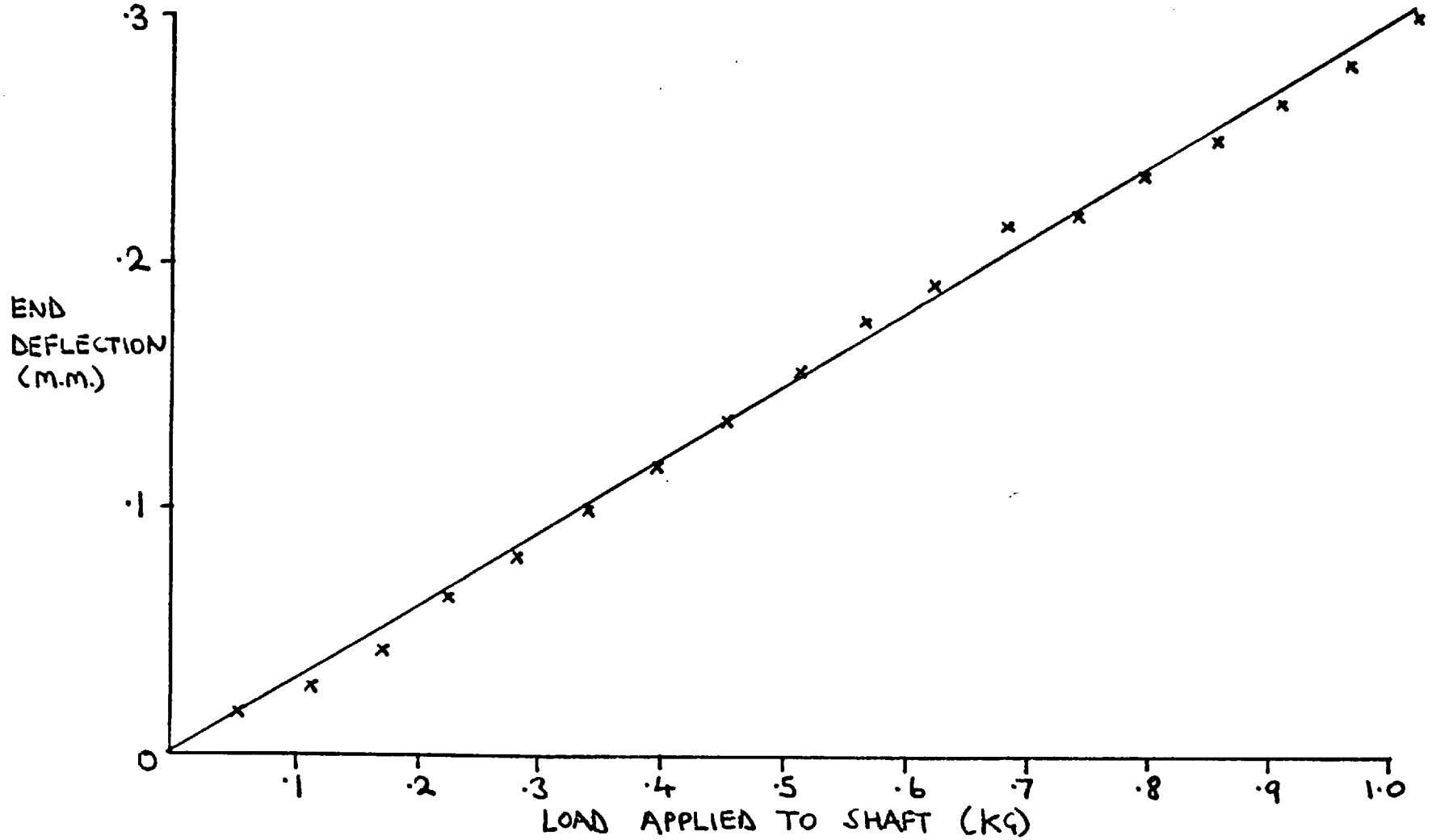

FIG. 2.15 SHAFT STIFFNESS CALIBRATION GRAPH

FIG. 2.16 THE LOAD ACTING AT THE CENTRE OF THE SCREW SECTION VERSUS THE LOAD APPLIED TO THE SHAFT

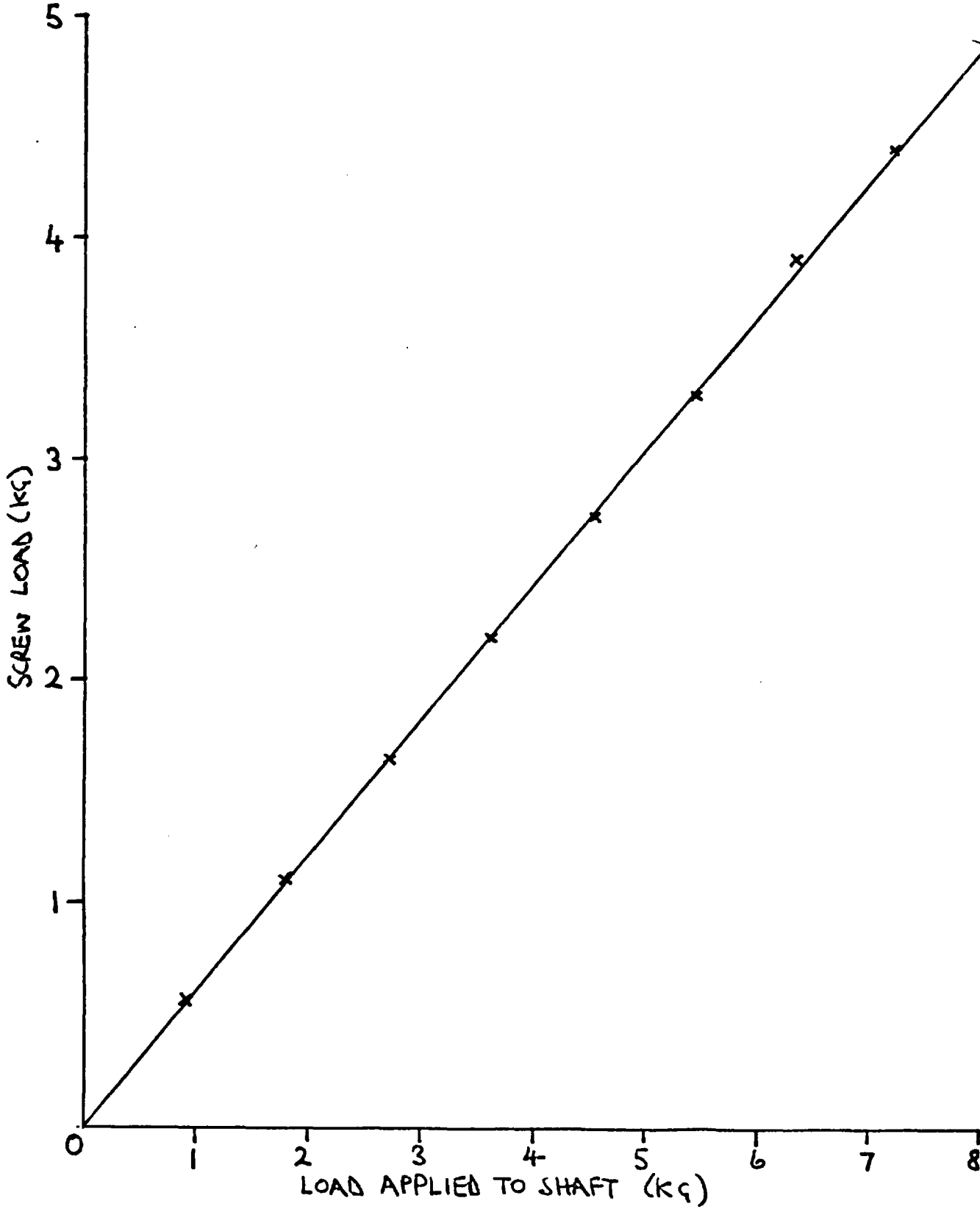

FIG. 2.17 THE EFFECT ON CONTACT LOADS OF VARYING EXTRUDER SPEED AT A CONSTANT SCREW SECTION SPEED OF 50 RPM

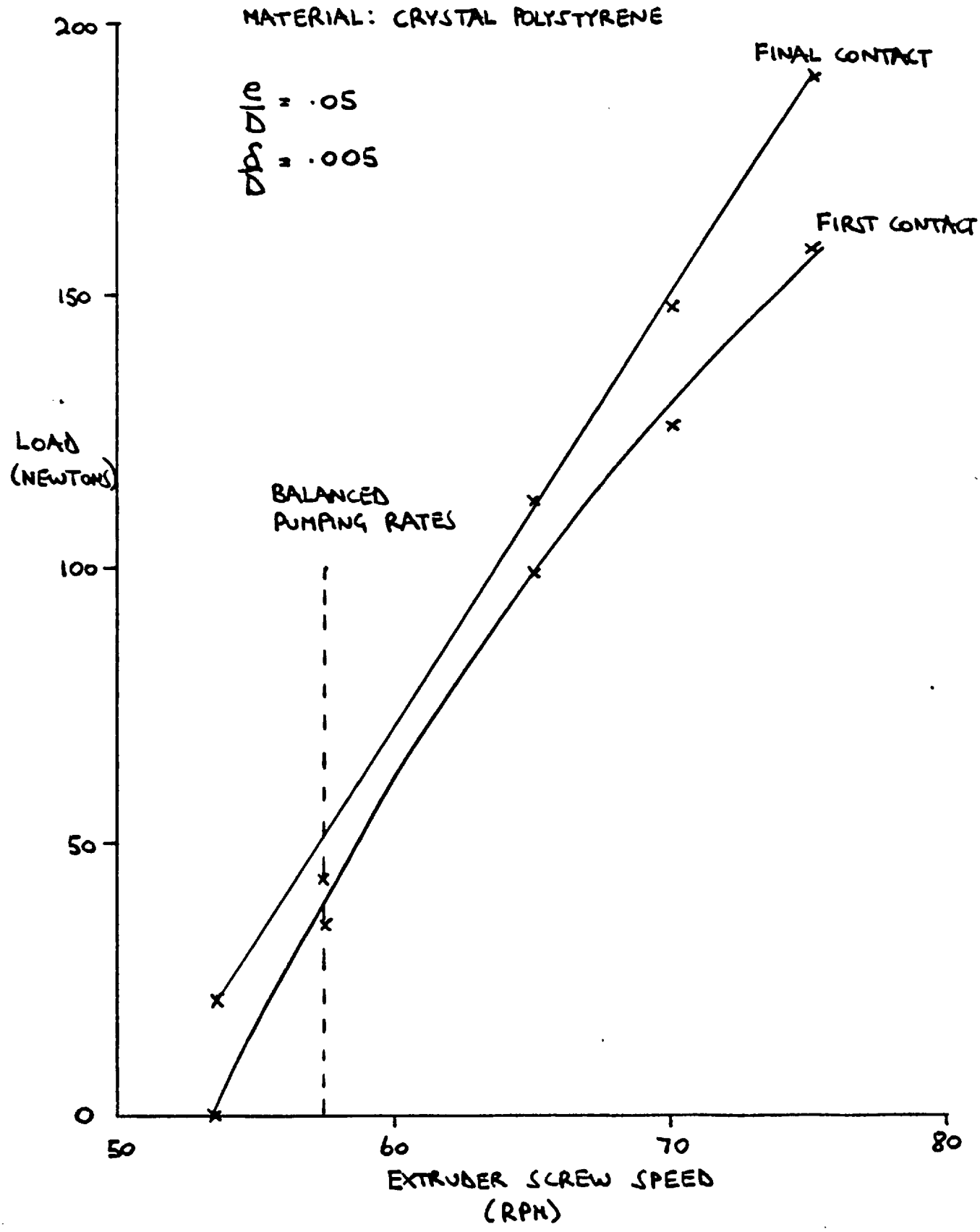

FIG. 2.18 FIRST CONTACT LOAD VERSUS SCREW SECTION SPEED FOR LOW DENSITY POLYETHYLENE PROCESSED AT 155°C

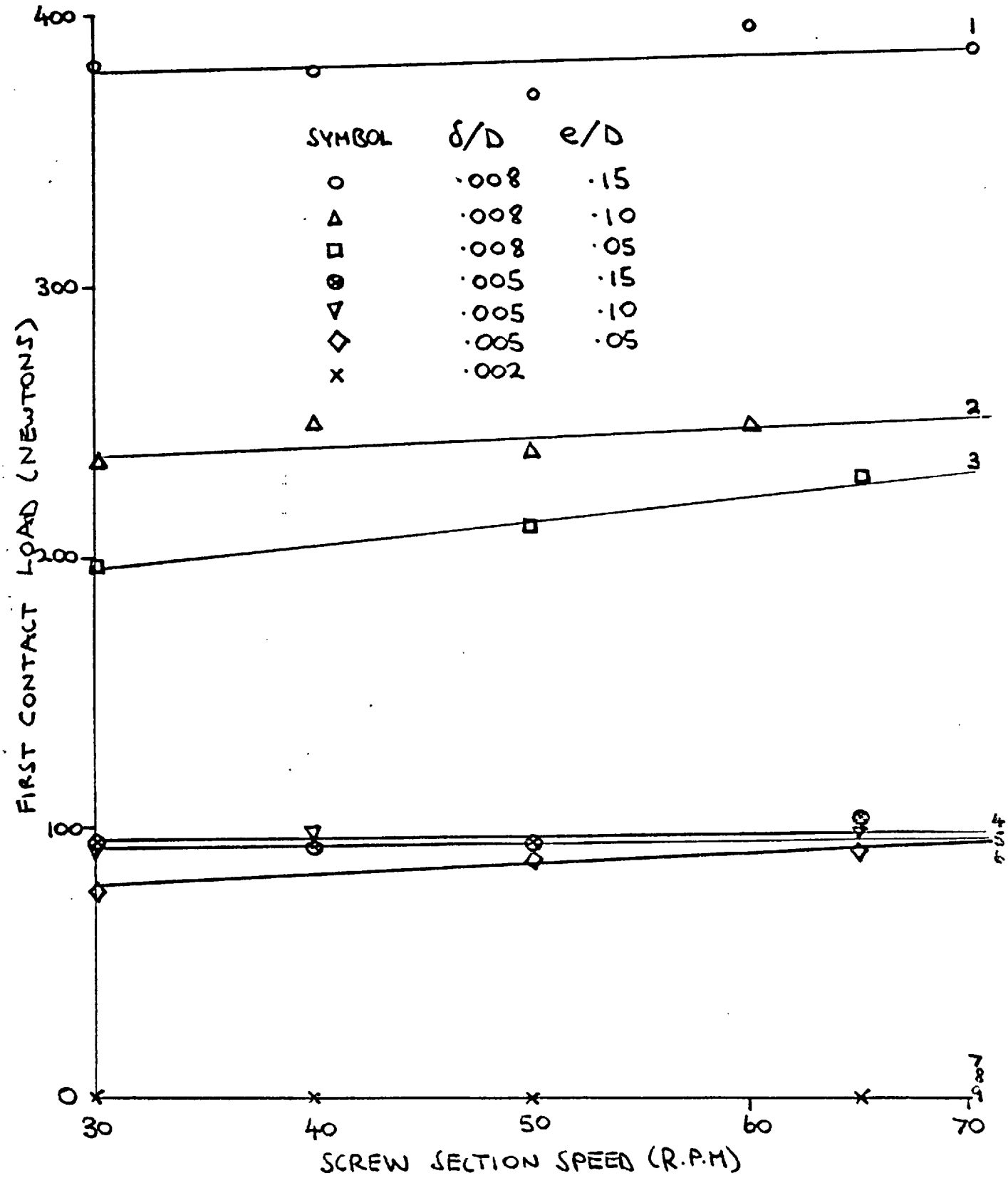

FIG 2.19 FIRST CONTACT LOAD VERSUS SCREW SECTION SPEED FOR LOW DENSITY POLYETHYLENE PROCESSED AT 220°C

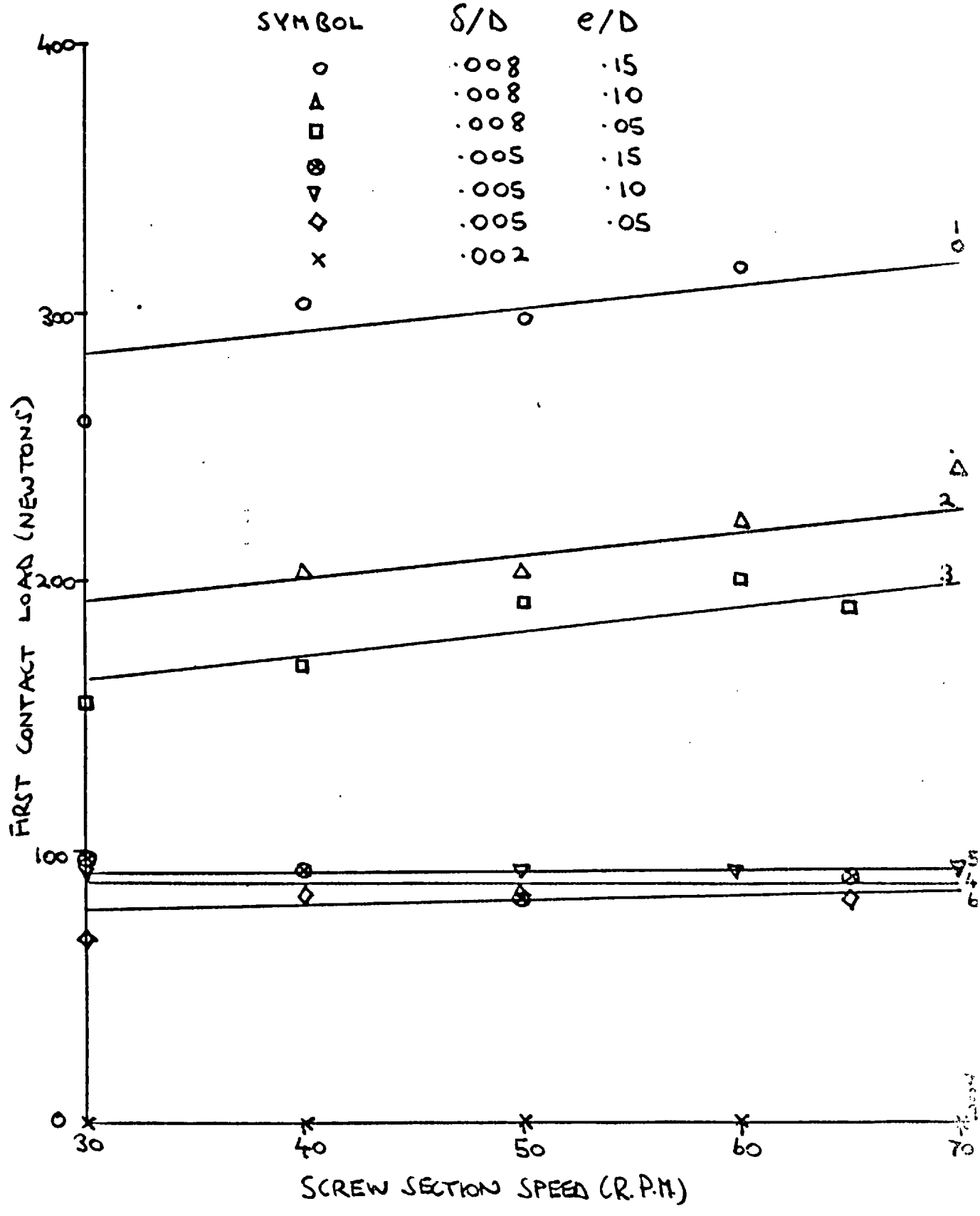

FIG. 2.20 FIRST CONTACT LOAD VERSUS SCREW SECTION SPEED FOR POLYSTYRENE PROCESSED AT 205°C

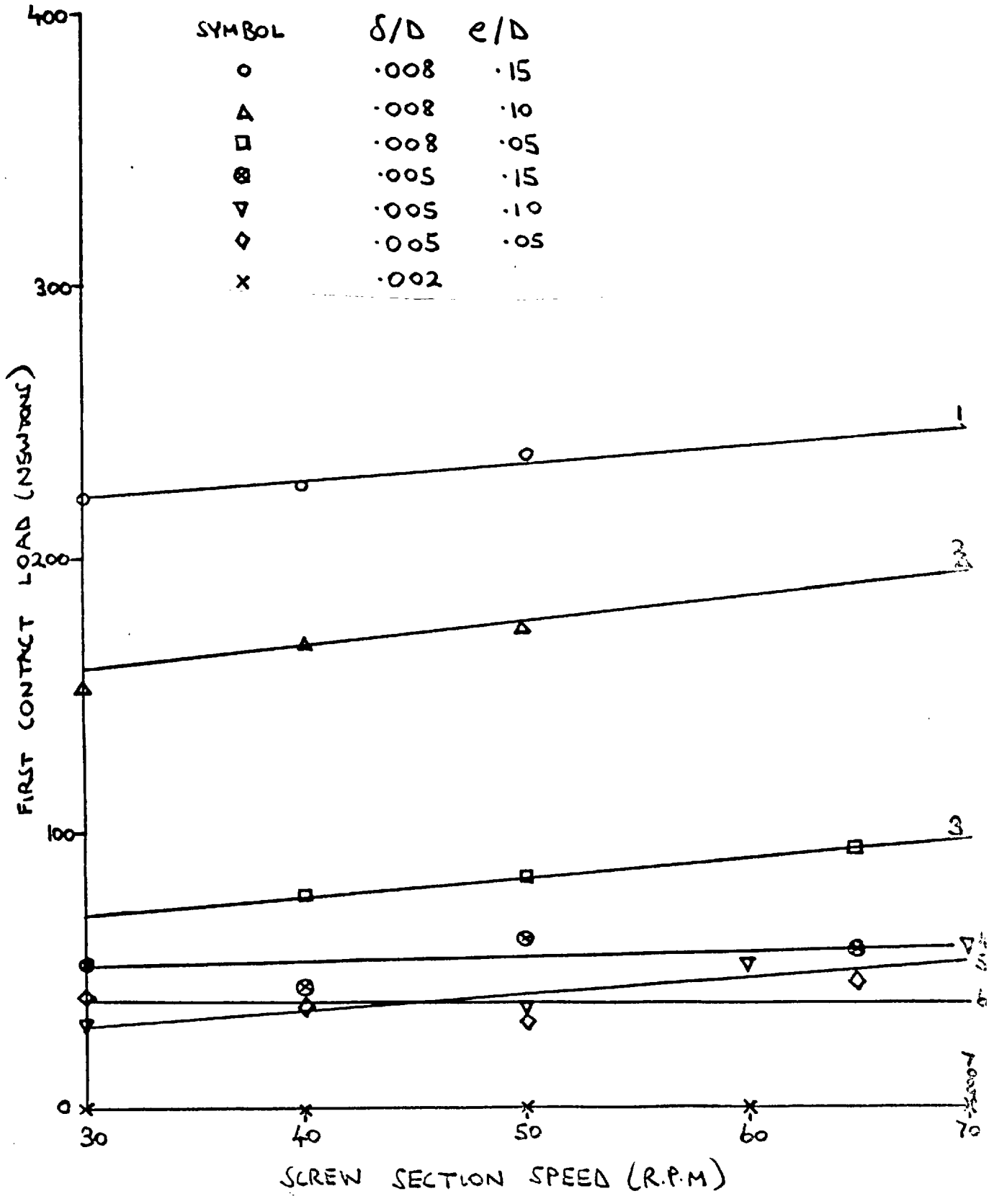

FIG. 2.21 RATIO OF FINAL CONTACT LOAD TO FIRST CONTACT LOAD VERSUS SCREW SECTION SPEED FOR LOW DENSITY POLYETHYLENE PROCESSED AT 155°C

SYMBOL	δ/D	e/D
o	·008	·15
Δ	·008	·10
□	·008	·05
⊗	·005	·15
▽	·005	·10
◇	·005	·05

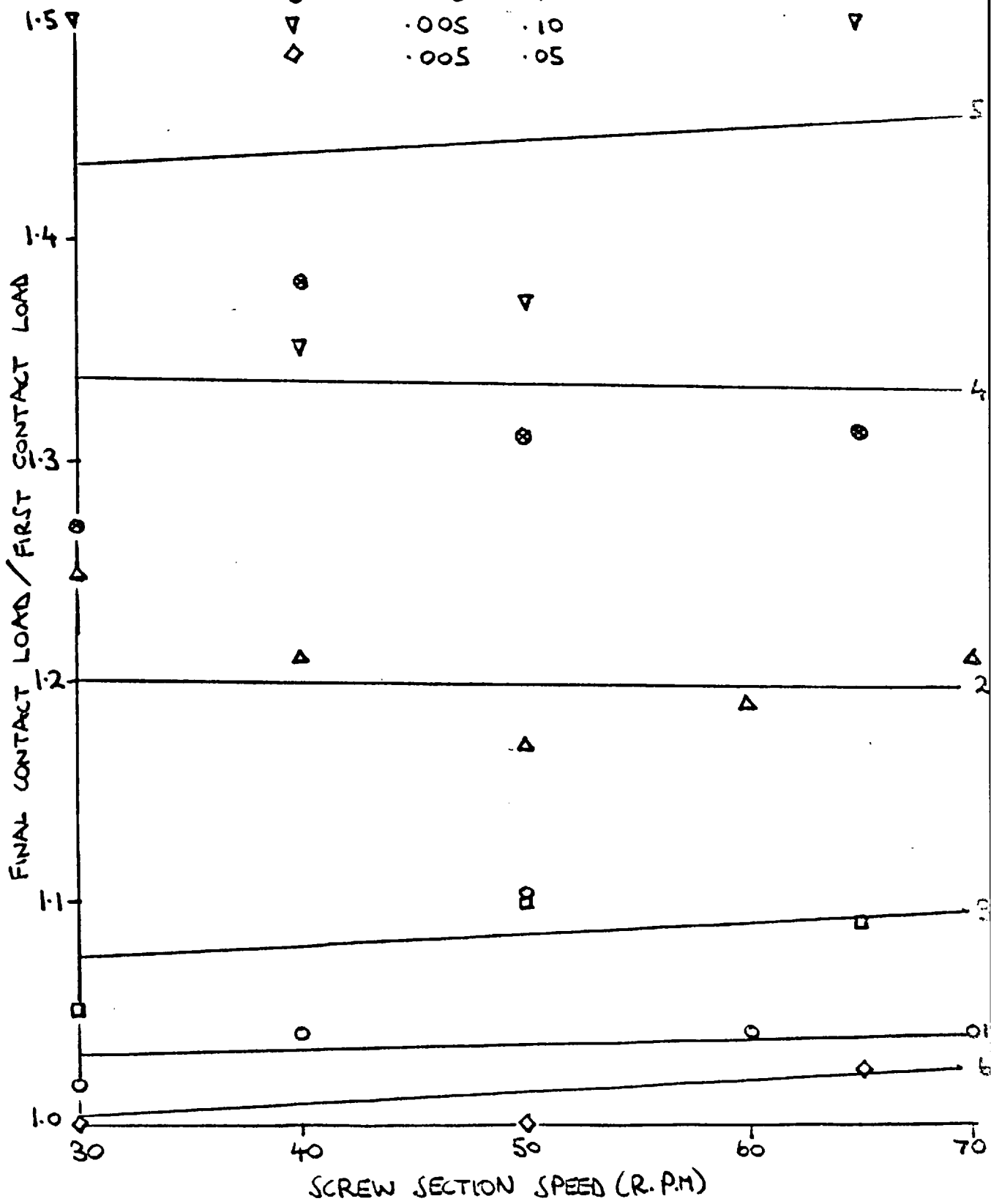

FIG. 2.22 RATIO OF FINAL CONTACT LOAD TO FIRST CONTACT LOAD VERSUS SCREW SECTION SPEED FOR LOW DENSITY POLYETHYLENE PROCESSED AT 220°C

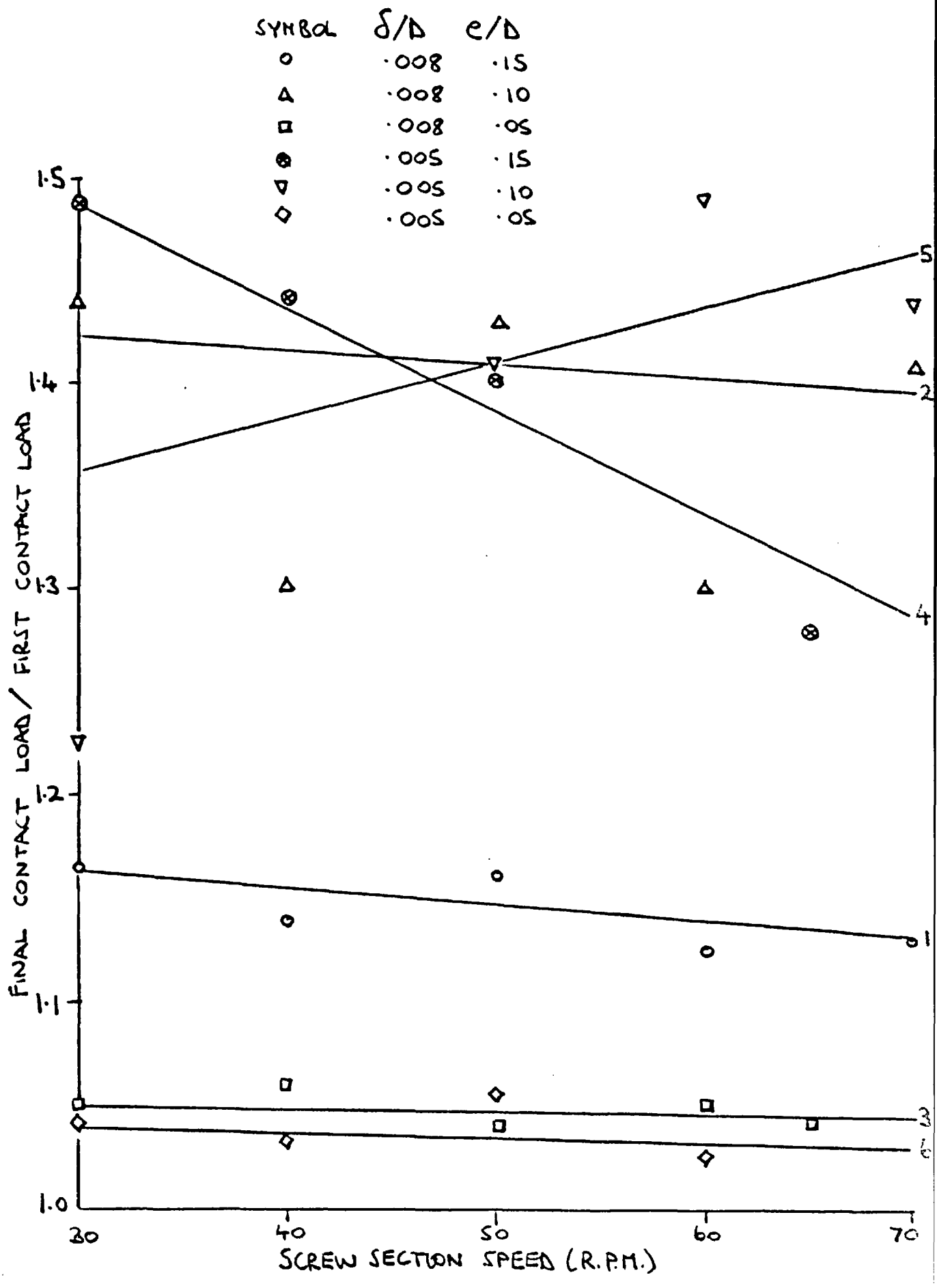

FIG. 2.23 RATIO OF FINAL CONTACT LOAD TO FIRST CONTACT LOAD VERSUS SCREW SECTION SPEED FOR POLYSTYRENE PROCESSED AT 205°C

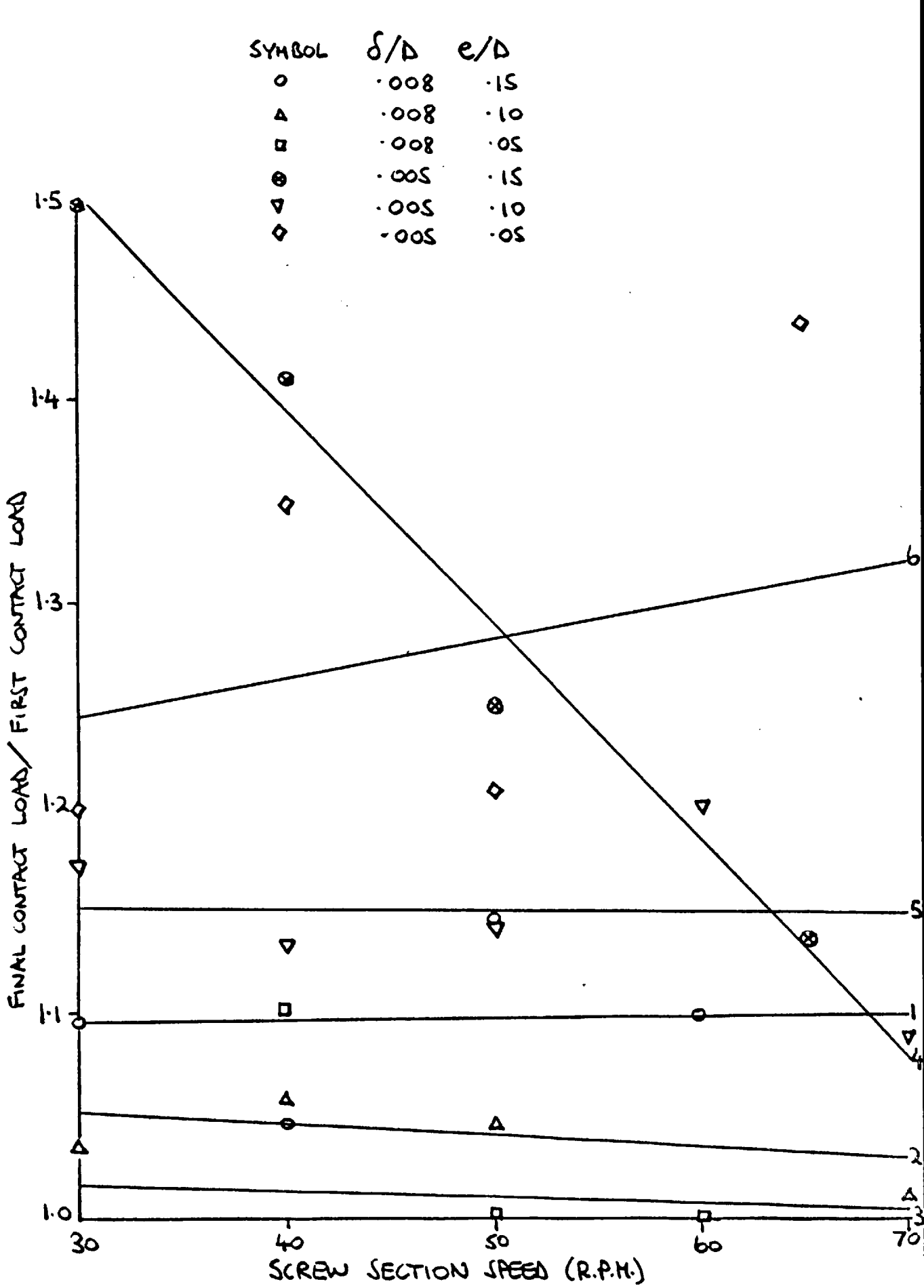

FIG. 2.24 FIRST CONTACT LOAD VERSUS FLIGHT WIDTH AT AVERAGE SCREW SECTION SPEED OF 50 RPM

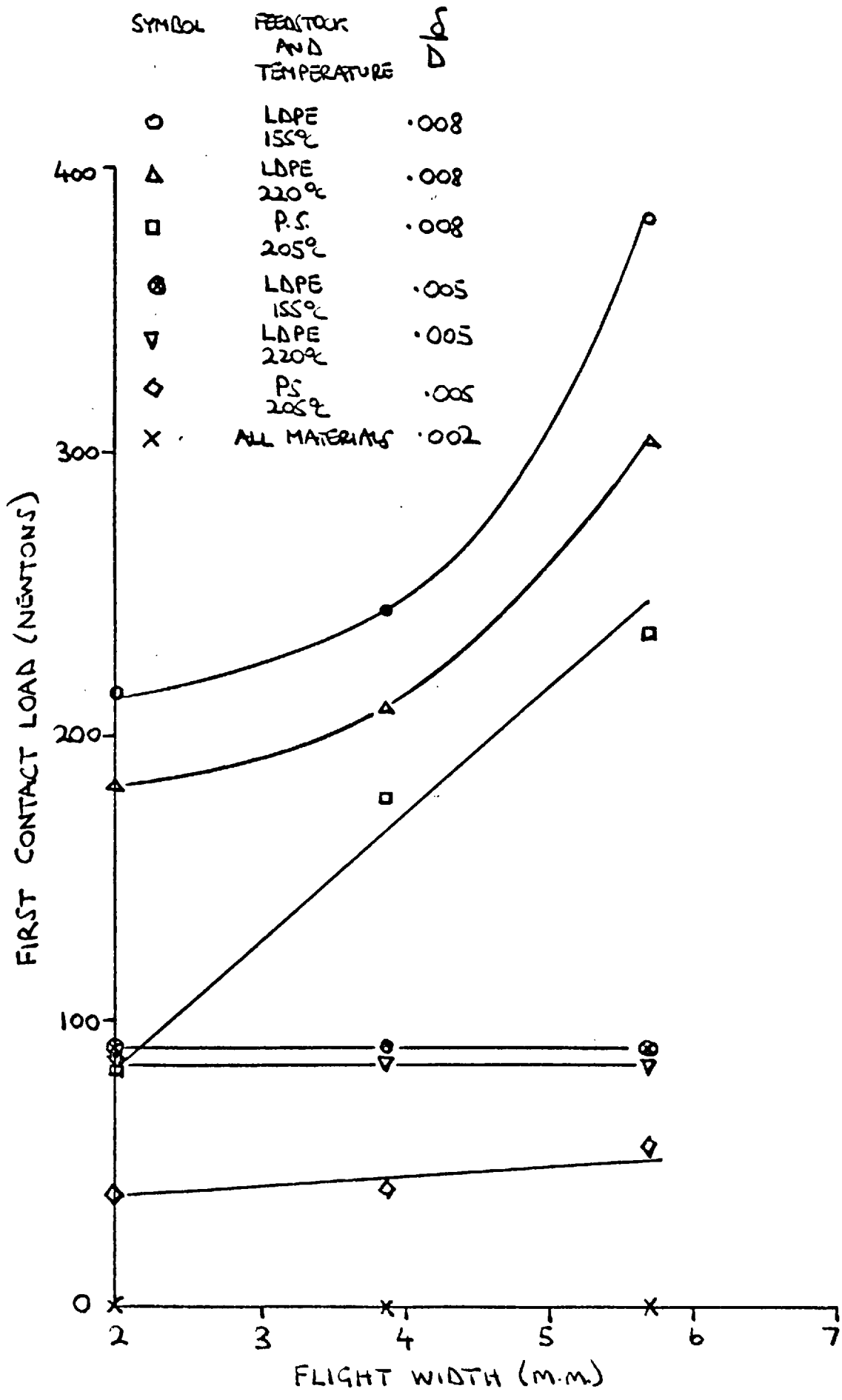

FIG. 2.25 EQUIVALENT BEARING MODEL

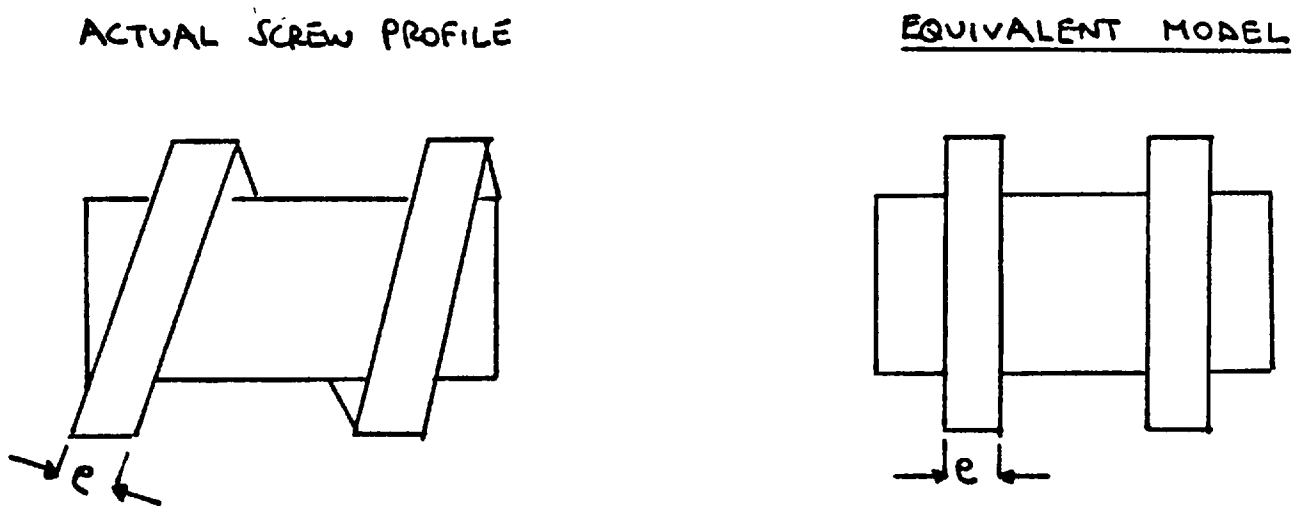

FIG. 2.26 FIRST CONTACT LOAD VERSUS NOMINAL POLYMER SHEAR STRESS IN CLEARANCE FOR LOW DENSITY POLYETHYLENE PROCESSED AT 155°C

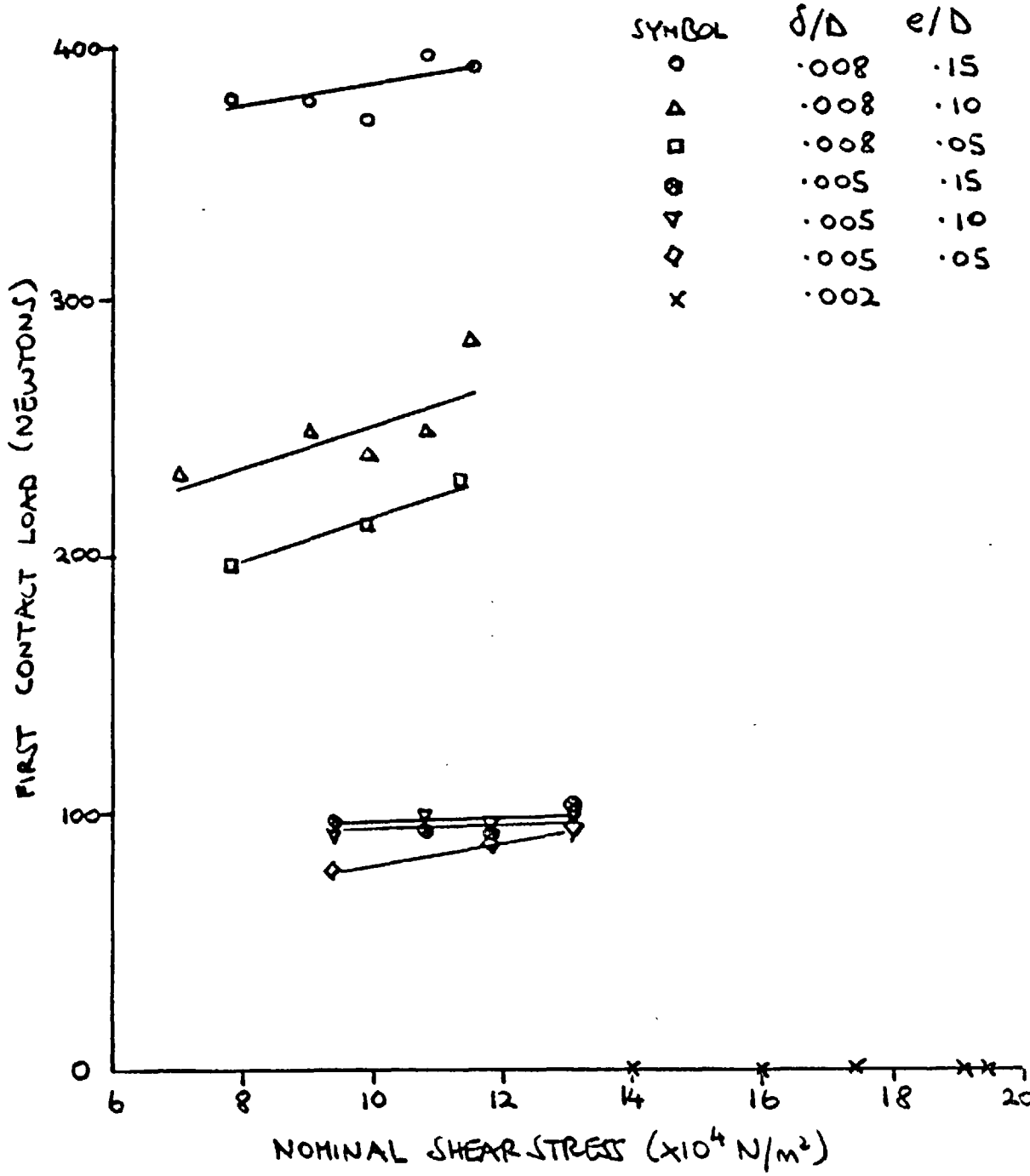

FIG. 2.27 FIRST CONTACT LOAD VERSUS NOMINAL POLYMER SHEAR STRESS IN CLEARANCE FOR LOW DENSITY POLYETHYLENE PROCESSED AT 220°C

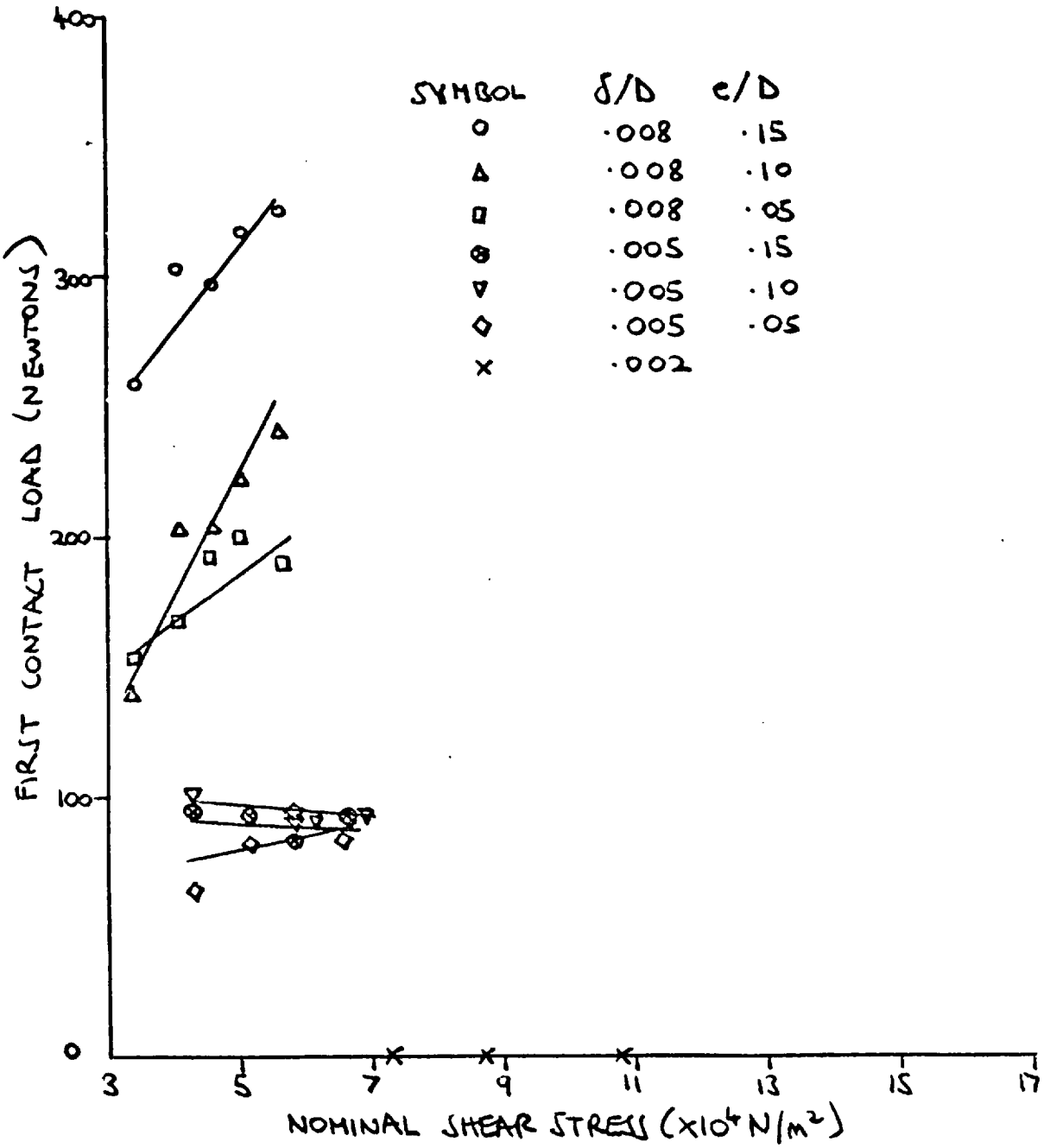

FIG. 2.28 FIRST CONTACT LOAD VERSUS NOMINAL POLYMER SHEAR STRESS IN CLEARANCE FOR POLYSTYRENE PROCESSED AT 205°C

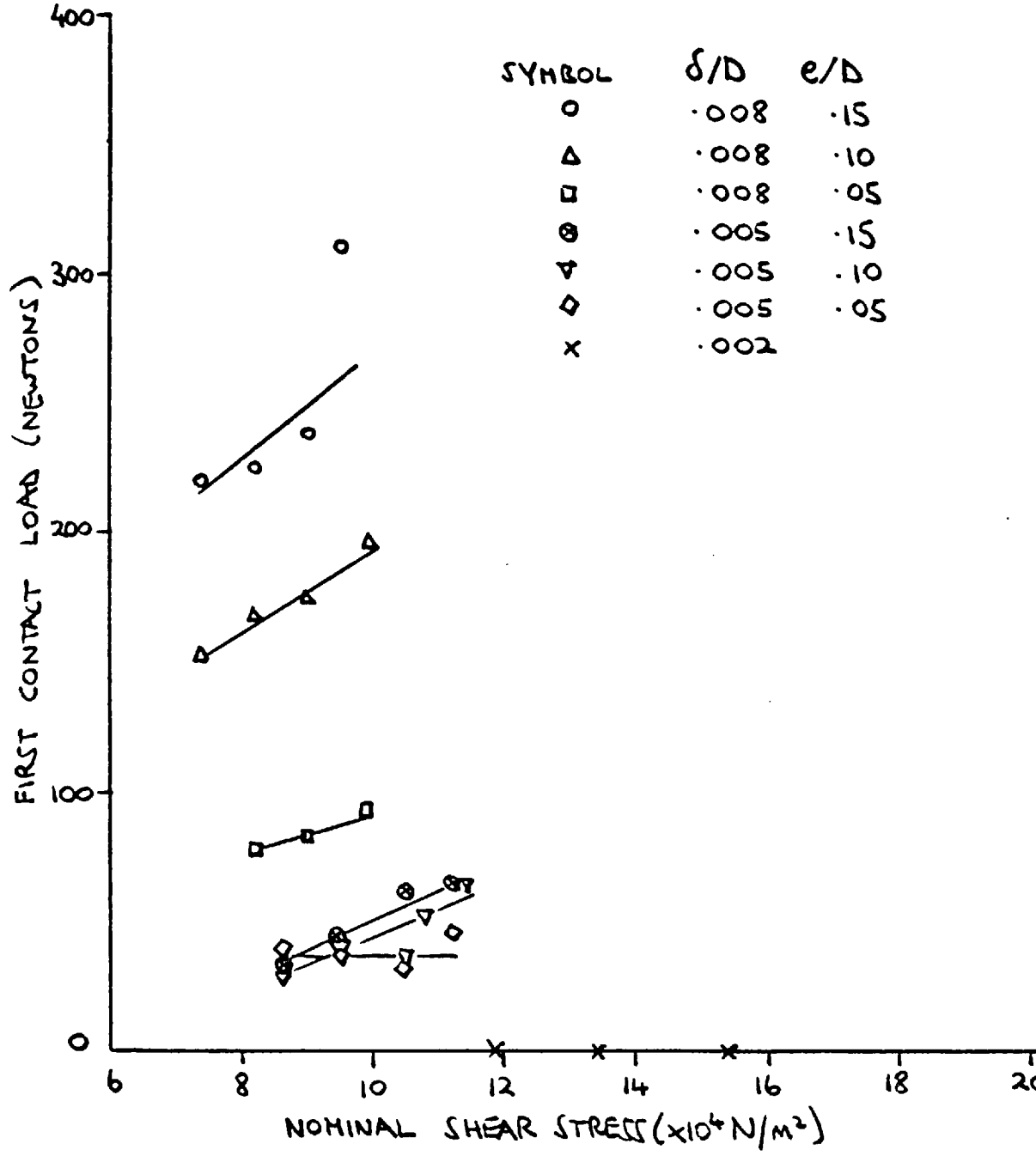

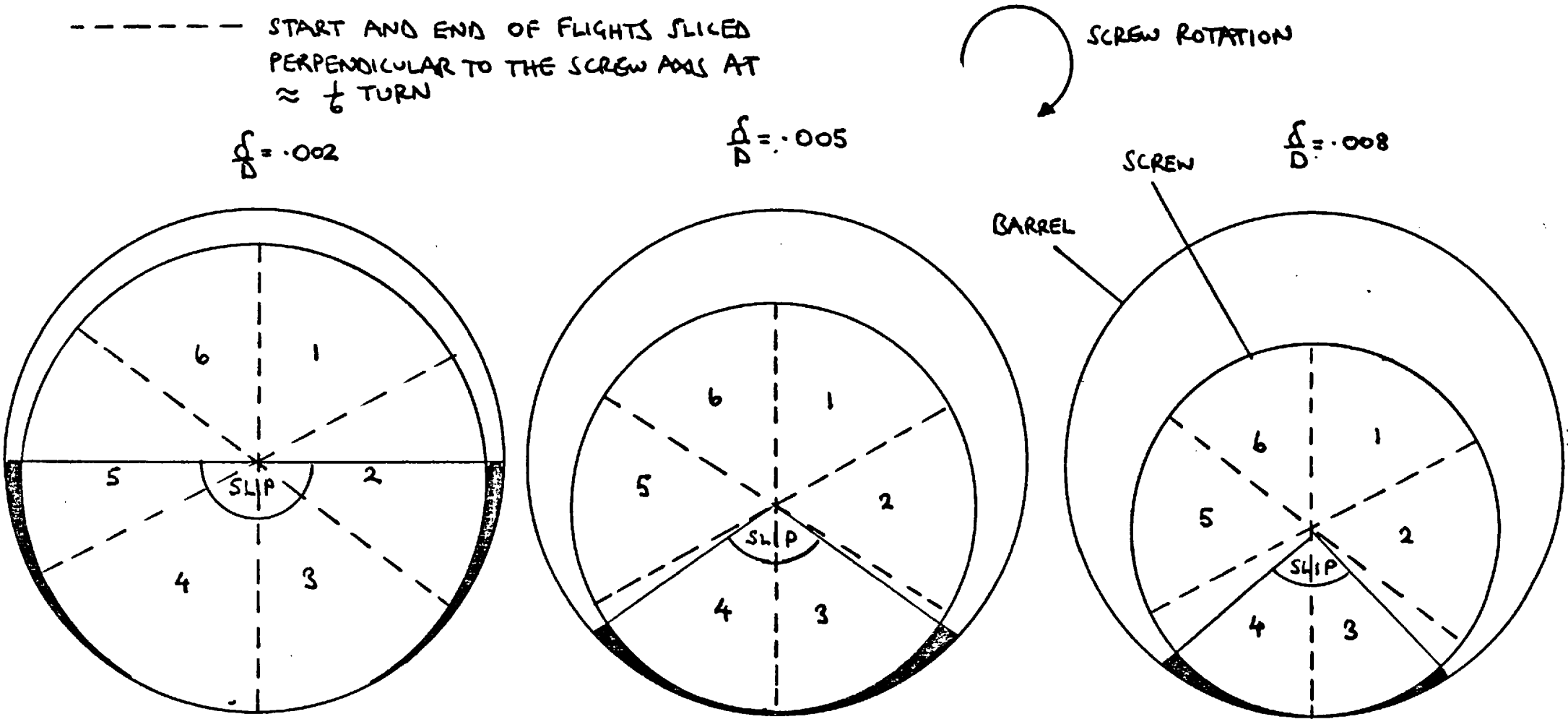

FIG. 2.29 POLYMER SLIP FOR DIFFERENT RADIAL SCREW CLEARANCES

TABLE 2.1 SCREW SECTION DIMENSIONS

Reference Number	Nominal e/D	Nominal δ/D	Radial Clearance (mm)	Flight Width (mm)	Channel Depth (mm)	Length (mm)
1	.15	.008	.315	5.715	1.899	76.2
2	.10	.008	.315	3.856	1.880	76.2
3	.05	.008	.310	1.946	1.897	76.2
4	.15	.005	.211	5.809	1.862	76.2
5	.10	.005	.213	3.858	1.857	76.2
6	.05	.005	.206	2.004	2.004	76.4
7	.15	.002	.084	5.756	1.908	76.4
8	.10	.002	.081	3.937	1.946	76.2
9	.05	.002	.076	2.004	2.004	76.2

Barrel bore diameter = 38.824 mm

CHAPTER 3

FORCE AND DEFLECTION ANALYSIS

3.1 Introduction

In the first part of this work the polymer's ability to support the self-generated screw forces has been examined. It has been shown that for the usual screw clearances (radial clearance/screw diameter of .001) there will be no hydrodynamic lubricating film between the screw and barrel. However as the screw wears, and the polymer shear stress between the screw flight and the barrel drops below a nominal critical shear stress of $10^5 N/m^2$ then substantial forces can be supported by the polymer.

In both these regimes, above and below the critical polymer shear stress, wear caused by the screw rubbing against the barrel can occur. When there is little or no polymer lubrication then this wear will be potentially severe. A measure of the severity of this wear will be the magnitude of the screw's deflections when the constraint of the barrel is removed. The larger the potential deflection, the higher the force between the screw and barrel, when present, and hence the higher the potential wear. When the polymer shear stress is below the critical value there could still be less severe wear if the force acting on the screw is higher than the polymer film can withstand.

In this part of the investigation the analysis is described which leads to computer program calculations of both the screw deflection without the barrel and also the polymer force required to restrain this deflection so that metal-to-metal contact between the screw and barrel is avoided. Experimental data from a 38.1 mm (1.5 inch) extruder processing

a range of polymers is used to calculate the deflections and forces described above. This was the only sufficiently detailed experimental data available. A wider range of data for larger extruders could have been used if the pressure profiles in a plasticating extruder had been calculated. However the accuracy of calculated pressure profiles using computer programs simulating the extrusion process is still open to question. It was therefore thought preferable to use experimental data and then scale-up the results when information on larger extruders was required.

3.2 Previous Work

Previous work has concentrated on the potential instability of the extruder screw. A simplified pressure field has been used to yield results. Fenner and Williams (Ref. 17) considered buckling of an extruder screw under the influence of the delivery pressure applied at its free end and whirling due to screw rotation. They came to the conclusion that if mechanical instability occurs it is likely to be a predominantly buckling mechanism. They presented a case for limiting screw L/D ratios to about 20:1 or for fitting a support bearing at the delivery end.

Newland (Ref. 18) considered a simplified pressure field acting along the screw. He derived a static buckling equation for this situation (equation 4) and an energy equation (equation 18) for the natural frequency of transverse vibrations in the presence of an external pressure field. He came to the conclusion that the pressure distribution along the screw, rather than the pressure at the delivery end affects the screw's stability. No previous work has considered the complete polymer forces acting on the screw, nor has previous work considered deflections that occur before screw instability is reached. This part

of the investigation extends the previous work to consider these two areas of interest.

3.3 Experimental Data

Sixteen sets of experimental data are used. This data was obtained by Edmondson (Ref. 19). The pressure data was collected using Dynisco pressure transducers whose signals, after amplification were traced on a U.V. recorder. Hence the circumferential pressure profile was taken for each experimental run at 6 positions along the screw. The assumed atmospheric pressure under the feedpocket gave 7 2-D pressure recordings along the screw. Unfortunately only 16 out of his 30 sets of operating conditions produced pressure traces with the resolution necessary for this work. The basic operating conditions are given in Table 3.1.

Two screws both of 38.1 mm diameter were used (Table 3.2) to generate the data. Screw A was only used to extrude PVC. Screw B was used in all the other experimental runs.

3.4 Forces Acting on the Screw

The forces acting on the screw can be classified into seven types:

1. Lateral pressure forces
2. An axial force due to the back pressure acting on the end of the screw.
3. Axial pressure forces due to
   (a) the pressure difference across the screw flight.
   (b) the polymer pressure acting on the screw's changing root area in the compression section.

} Pressure forces

4. Centrifugal forces.
5. The weight of the screw.
6. Stresses caused by temperature gradients in the screw.
7. Forces caused by the torque required to shear the polymer.

Edmondson (Ref. 19) did not use thermocouples set in the screw during his experimental runs. Therefore no screw temperature data were available. Even if he had used them it is doubtful if they could have given a realistic picture of temperature gradients in the screw because they would have been set at the surface of the screw. Also the necessarily restricted number used may not have indicated local hot spots. Therefore internal screw stresses caused by temperature gradients are ignored in this analysis.

Again no data were available for the torques acting on the screw. If available, they would have taken the form of a single value with no indication of the torque distribution along the screw. Therefore these stresses are ignored in this analysis.

It is obvious how centrifugal and weight forces are derived from the density, geometry and rotational speed of the screw. However, the derivation of the essentially 3-D pressure field acting on the screw from the limited number of circumferential pressure profiles taken down the screw is not immediately self-evident. This 3-D pressure field is required to derive the three previously mentioned types of pressure force acting on the screw. To obtain the true 3-D pressure field acting on the screw an infinite number of circumferential pressure profiles, and hence transducers would be required. Therefore some form of curve fit technique is required to expand the limited information from the pressure transducers into an approximation to the real 3-D pressure field.

A number of points are taken along each recorded pressure profile. The value of the pressure at the start of the flight is given the reference

number 1 (Fig. 3.1). The second value over the flight is given the reference number 2 and so on until the last value in the channel has the number j. A curve is fitted to all the data from pressure points 1 along the screw, another to pressure points 2 etc. Hence, we have j curves fitted round the screw helix giving a continuous profile for the j points. Also a curve is fitted to the average pressure recordings from each transducer to obtain the average pressure curve along the screw.

The average polymer pressure as a function of axial position was plotted for all 16 experimental runs. Six representative traces were selected to find a suitable curve fit. Initially a least squares polynomial fit was tried. The fit was good in the compression section, reasonable in the metering section but very inaccurate in the feed section. Consequently the traces were divided into the three sections and the best fit found in each. The pressure profile is of an exponential form in the feed section (Ref. 20). Therefore, not surprisingly a good fit in this section was obtained using an exponential curve. A third order polynomial fitted the data in the compression section and a straight line fitted the data in the metering section.

As shown later in section 3.12.1.2 26 steps give an accurate integration round the pressure profile. Therefore there are 27 pressure curves for each of the 16 sets of experimental data. The accuracy of using 3 separate curve fits to the pressure transducer data was further checked by plotting each of the 27 curves for every one of the 16 experiments. In each case the curves satisfactorily passed through the experimental data points.

3.5 Screw Geometry

The geometry of the screw has to be defined in mathematical expressions.

An arbitrary datum line is taken as the vertical line through the start of the feed section, looking down the screw. The Z axis is in the axial direction down the screw and the X and Y axes are the lateral ones shown in Fig. 3.2. The deflection of the screw at axial position z is x in the X-direction and y in the Y-direction. The flight rotates clockwise round the screw. γ is the angle between the datum line and the start of the flight at axial position z. θ_f is the angle subtended by the flight at the centre of the screw. The value of γ at the start of the feed section changes as the screw rotates and this initial value, γ_i, will have an effect on the deflections along the screw. Therefore a range of values of γ_i is considered.

$$\gamma = \gamma_i + \frac{2\pi z}{L_p} \qquad 3.1$$

Where L_p is the screw pitch.

θ_f depends on the flight width, e, and the helix angle, θ_h. Therefore from Figs. 3.3(a) and 3.3(b)

$$e_1 = R_o\theta_f$$

and $$e = e_1 \sin\theta_h$$

$$\therefore \quad e = R_o\theta_f \sin\theta_h$$

$$\therefore \quad \theta_f = \frac{e}{R_o} \frac{1}{\sin\theta_h} \qquad 3.2$$

3.6 Possible Screw Deflection Prediction Methods

A knowledge of the forces acting on the screw, the screw's stiffness and boundary conditions will enable screw deflections to be

calculated. A 3-D Finite Element analysis would probably give the most accurate solution. However the computer core storage required for the stiffness matrix is immense when modelling a shape as complex as an extruder screw. Economic storage methods were considered, particularly the substructure method (Ref. 21), where the screw is divided into sections which are treated as complicated elements interconnected at external nodes to form the overall screw. The stiffness matrix for each section, or substructure, is determined by eliminating the internal degrees of freedom which do not participate in the interconnection. The analysis is then carried out by adding the substructure stiffnesses to form the overall stiffness matrix and then solving for the screw deflections. If the minimum number of sections of the screw to be considered is fixed at 10, i.e. every 2 turns for the 19.83 turn screw used to generate the pressure data then the maximum number of interconnecting nodal points for 45 K storage is only 17. It is impossible to even make a fair representation of the screw shape with only 17 connecting nodal points and the available turnround time for a computer program using 45K storage was very long.

In the previous section it has been explained why only pressure, centrifugal and weight forces are considered in this analysis. The 3-D pressure field is necessarily derived from only 6 circumferential pressure traces and one assumed pressure along the screw. The accuracy of the refined data, the accuracy of the solution procedure using available facilities, the high core storage requirements leading to slow turnround time and consequent slow development of the program suggests that a 3-D Finite Element analysis is not justified in this case.

A simplified approach was therefore taken using the Principle of Superposition. The axial screw displacement is not of interest. It is the lateral screw displacements that will cause metal-to-metal contact

between the screw and the barrel and consequent wear. Therefore the lateral pressure, weight and centrifugal forces acting on the screw are resolved into forces in two directions (X and Y) perpendicular to the screw axis (Z). The forces acting in the X-direction are then considered to act on the screw in conjunction with all the axial forces. The deflections x, caused by the resulting bending moments are then calculated in the X-direction. Similarly, the forces acting in the Y-direction are considered to act on the screw in conjunction with all the axial forces. Then the deflections y, caused by the bending moments are separately calculated in the Y-direction. The deflections and forces in the X-Z and Y-Z planes are combined by the Principle of Superposition into the complete lateral deflections and force fields. The stiffness of the flight is ignored to keep the bending analysis relatively simple, i.e. the neutral axis of the screw is taken through the centre of the screw's root not as it truly does, rotating in a spiral round the centre of the screw. However, the flight is not ignored when calculating the forces acting on the screw. Therefore, within the limits of the data, an accurate force field is applied to a screw whose stiffness has been reduced by ignoring the stiffness of the flight. Hence the resulting deflections will be slightly pessimistic.

3.7 Elemental Axial Slice of the Screw

Eventually, from analysing an elemental axial slice of the screw, differential equations will be derived which enable screw deflections to be calculated. To derive these equations, expressions are required to define the various forces acting on an elemental slice of the screw. The shape of the slice must be decided to obtain these expressions.

When the screw bends under the action of the generated forces there will be a deflection at an axial point z, and a very small curvature of the screw from z to z + Δz. This situation is shown in an exaggerated form in Figs. 3.4(a) and (b). The only difference between the two is that in Fig. 3.4(a) the slice has been cut perpendicular to the local axis. In Fig. 3.4(b) the slice has been cut perpendicular to the original axis. The slice in Fig. 3.4(a) is selected for ease of use because the axial forces acting on the screw act along the local not the original axis. The differential equations are derived from a force and moment balance on this elemental axial slice. The forces are resolved perpendicular to the local axis of the screw (Fig. 3.5). Moments are taken about point o, the point where the neutral axis intersects the end of the elemental axial slice. The direction of resolution and positive moment direction used in the force and moment balances are shown in Fig. 3.5. The contribution of each force acting on the screw to the elemental force and moment balance will now be found. The resulting differential equations will be solved using a digital computer to yield the screw deflections under the action of the forces generated in each experiment. The computer program

(i) calculates the forces acting on the screw from the raw input data.

(ii) calculates the resulting deflections along the screw.

(iii) calculates the polymer forces to prevent the screw touching the barrel from the previously calculated values in (i) and (ii).

3.8 Forces Acting on the Screw

3.8.1 Lateral Pressure Forces

An elemental axial slice of the screw is shown in two views. Fig. 3.6 is a view of the slice perpendicular to the local screw axis. The view is given in the X-Z plane (Fig. 3.6(a)) and also in the Y-Z plane (Fig. 3.6(b)). In each case the datum line, defined in Fig. 3.2 is shown. The original length of the slice was Δz at axial position z. The rotation and curvature of the slice due to forces acting on the screw has been exaggerated for ease of illustration. The slice has rotated through an angle θ_g and the length of the slice at rotational position ω in the cross section, originally Δz, has now changed to Δs. Δs can either be greater than, equal to, or less than Δz depending on the value of ω the angle between the datum line and this position. The length along the neutral axis is still Δz. In this analysis the neutral axis passes through the centre of the screw's root, not in a helical path round the centre as it would in reality. This is because the flight, as explained earlier, will be ignored in the analysis. Therefore the bending cross-section is the root of the screw. The radius of curvature of the neutral axis is R_n and the distance between the centre of curvature and the length Δs is R_a. The angle of curvature is θ_a.

Fig. 3.7 shows a view of the elemental slice's cross-section. A typical elemental section ω from the datum line is shown. The section is subtended by an angle $\Delta\omega$ at the centre of the screw. The radius, R of the screw to this section can either be R_o, the radius of the screw, or R_r the radius of the screw's root depending on the value of ω.

The lateral pressure force/unit length acting on the slice is found by integrating all the forces/unit length acting on the elemental

sections round the slice. The resulting force/unit length is then resolved into an X and Y-component.

The force acting on the representative section in Fig. 3.7 is the pressure multiplied by the area of the section. Both the area and the pressure acting on this section have changed due to the curvature and rotation of the elemental axial slice. The area of the section is $R\Delta\omega\ \Delta s$ where R is either R_o or R_r. The X-component of the lateral pressure force/unit length at ω is (the pressure at ω) x $R\Delta\omega\frac{\Delta s}{\Delta z}\sin\omega$. The Y-component of the lateral pressure force/unit length at ω is (the pressure at ω) x $R\Delta\omega\ \frac{\Delta s}{\Delta z}\cos\omega$. The slice has rotated through an angle θ_g. Because θ_g is very small it will effectively equal the deflection gradient, i.e. $\frac{dx}{dz}$ in the X-Z plane and $\frac{dy}{dz}$ in the Y-Z plane. The axial movement depends on the value of ω. In the X-Z plane (Fig. 3.6(a)) the axial movement is zero at $\omega = 0$ and π, $R\frac{dx}{dz}$ at $\omega = \frac{\pi}{2}$ and $-R\frac{dx}{dz}$ at $\omega = \frac{3\pi}{2}$. Therefore the X-component of the lateral pressure force/unit length at ω,

$$\Delta F_{\ell,x} = (p_{\omega,z} + R\frac{dx}{dz}\frac{dp_z}{dz}\sin\omega)\ R\Delta\omega\ \frac{\Delta s}{\Delta z}\ \sin\omega$$

where $p_{\omega,z}$ is the pressure ω from the datum line in the cross-section at axial position z and p_z is the average pressure at axial position z. In the Y-Z plane (Fig. 3.6(b)) the axial movement is $R\frac{dy}{dz}$ at $\omega = 0$, $-R\frac{dy}{dz}$ at $\omega = \pi$ and zero at $\omega = \frac{\pi}{2}$ and $\frac{3\pi}{2}$. Therefore the Y-component of the lateral force/unit length at ω,

$$\Delta F_{\ell,y} = (p_{\omega,z} + R\frac{dy}{dz}\frac{dp_z}{dz}\cos\omega)\ R\Delta\omega\ \frac{\Delta s}{\Delta z}\cos\omega$$

Δs must now be found in the X-Z and Y-Z planes. In the X-Z plane from Fig. 3.6(a)

$$\Delta s = R_a \theta_a$$

$$\Delta z = R_n \theta_a$$

$$\therefore \quad \theta_a = \frac{\Delta z}{R_n}$$

$$R_a = R_n + R \sin\omega$$

$$\therefore \quad \Delta s = (R_n + R \sin\omega) \frac{\Delta z}{R_n}$$

$$= (1 + \frac{R}{R_n} \sin\omega) \Delta z$$

From simple bending theory $R_n = 1/\frac{d^2x}{dz^2}$

$$\therefore \quad \Delta s = (1 + R \sin\omega \frac{d^2x}{dz^2}) \Delta z$$

Similarly in the Y-Z plane

$$\Delta s = (1 + R \cos\omega \frac{d^2y}{dz^2}) \Delta z$$

$$\therefore \quad \Delta F_{\ell,x} = (p_{\omega,z} + R \frac{dx}{dz} \frac{dp_z}{dz} \sin\omega) \, R\Delta\omega \quad (1 + R \sin\omega \frac{d^2x}{dz^2}) \frac{\Delta z}{\Delta z} \sin\omega$$

$$= p_{\omega,z} \, R\Delta\omega \, \sin\omega + p_{\omega,z} \, R\Delta\omega \quad R \sin\omega \frac{d^2x}{dz^2} \sin\omega$$

$$+ R \frac{dx}{dz} \frac{dp_z}{dz} \sin\omega \quad R\Delta\omega \quad \sin\omega$$

$$+ R \frac{dx}{dz} \frac{dp_z}{dz} \sin\omega \quad R\Delta\omega \quad R \sin\omega \frac{d^2x}{dz^2} \sin\omega$$

The last term has the product $\frac{dx}{dz} \frac{d^2x}{dz^2}$ in it and it will be small compared with other terms in the expression.

$$\therefore \quad \Delta F_{\ell,x} = Rp_{\omega,z} \sin\omega \, \Delta\omega + R^2 \frac{d^2x}{dz^2} p_{\omega,z} \sin^2\omega \, \Delta\omega$$

$$+ R^2 \frac{dp_z}{dz} \frac{dx}{dz} \sin^2\omega \, \Delta\omega$$

This force/unit length acting on the section at ω is now integrated round the screw. The limits of the integration will be from γ to $\gamma+\theta_f$ over the flight, radius R_o, and from $\gamma+\theta_f$ to $2\pi+\gamma$ in the screw root, radius R_r (Fig. 3.7). In addition to this summation the effect of the nett pressure force on the side of the flight is considered.

$$\therefore \quad F_{\ell,x} = (R_o - R_r)(p_{\gamma+\theta_f,z} \cos(\gamma+\theta_f) - p_{\gamma,z} \cos\gamma) +$$

$$R_o \int_{\gamma}^{\gamma+\theta_f} p_{\omega,z} \sin\omega \, d\omega + R_r \int_{\gamma+\theta_f}^{2\pi+\gamma} p_{\omega,z} \sin\omega \, d\omega$$

$$+ R_o^2 \frac{d^2x}{dz^2} \int_{\gamma}^{\gamma+\theta_f} p_{\omega,z} \sin^2\omega d\omega + R_r^2 \frac{d^2x}{dz^2} \int_{\gamma+\theta_f}^{2\pi+\gamma} p_{\omega,z} \sin^2\omega d\omega$$

$$+ R_o^2 \frac{dp_z}{dz} \frac{dx}{dz} \int_{\gamma}^{\gamma+\theta_f} \sin^2\omega d\omega + R_r^2 \frac{dp_z}{dz} \frac{dx}{dz} \int_{\gamma+\theta_f}^{2\pi+\gamma} \sin^2\omega d\omega$$

The last two terms in the equation have explicit integrals in them.

Now $\int \sin^2\omega \, d\omega = \frac{1}{2}\omega - \frac{1}{4}\sin 2\omega$

$$\therefore \quad R_o^2 \frac{dp_z}{dz} \frac{dx}{dz} \int_{\gamma}^{\gamma+\theta_f} \sin^2\omega d\omega + R_r^2 \frac{dp_z}{dz} \frac{dx}{dz} \int_{\gamma+\theta_f}^{2\pi+\gamma} \sin^2\omega \, d\omega$$

$$= R_o^2 \frac{dp_z}{dz}\frac{dx}{dz}\left[\frac{1}{2}\omega - \frac{1}{4}\sin 2\omega\right]_{\gamma}^{\gamma+\theta_f} + R_r^2 \frac{dp_z}{dz}\frac{dx}{dz}\left[\frac{1}{2}\omega - \frac{1}{4}\sin 2\omega\right]_{\gamma+\theta_f}^{2\pi+\gamma}$$

$$= \frac{dp_z}{dz}\frac{dx}{dz}\left(\left(\frac{R_o^2}{2}\theta_f + \frac{R_r^2}{2}(2\pi-\theta_f)\right) + \left(\frac{R_o^2-R_r^2}{4}\right)(\sin 2\gamma - \sin 2(\gamma+\theta_f))\right)$$

The magnitude of the second term is of the order of $\frac{1}{10}$th of that of the first term and is therefore ignored. The removal of the second term is further justified later when it is seen the contribution of the modified term to the calculated deflection is small.

$$\therefore \quad F_{\ell,x} = R_o \int_{\gamma}^{\gamma+\theta_f} p_{\omega,z} \sin\omega d\omega + R_r \int_{\gamma+\theta_f}^{2\pi+\gamma} p_{\omega,z} \sin\omega d\omega$$

$$+ (R_o - R_r)(p_{\gamma+\theta_f,z}\cos(\gamma+\theta_f) - p_{\gamma,z}\cos\gamma)$$

$$+ \frac{1}{2}\frac{dp_z}{dz}(R_o^2\theta_f + R_r^2(2\pi-\theta_f))\frac{dx}{dz}$$

$$+ \left(R_o^2 \int_{\gamma}^{\gamma+\theta_f} p_{\omega,z}\sin^2\omega\, d\omega + R_r^2 \int_{\gamma+\theta_f}^{2\pi+\gamma} p_{\omega,z}\sin^2\omega d\omega\right)\frac{d^2x}{dz^2} \qquad 3.3$$

i.e. substituting symbols for the above coefficients

$$F_{\ell,x} = F^*_{\ell,x} + F^{**}_{\ell,x}\frac{dx}{dz} + F^{***}_{\ell,x}\frac{d^2x}{dz^2}$$

Similarly in the Y-Z plane

$$F_{\ell,y} = R_o \int_{\gamma}^{\gamma+\theta_f} p_{\omega,z}\cos\omega\, d\omega + R_r \int_{\gamma+\theta_f}^{2\pi+\gamma} p_{\omega,z}\cos\omega\, d\omega$$

$$+ (R_o - R_r)(p_{\gamma,z}\sin\gamma - p_{\gamma+\theta_f,z}\sin(\gamma+\theta_f))$$

$$+ \frac{1}{2}\frac{dp_z}{dz}(R_o^2\theta_f + R_r^2(2\pi - \theta))\frac{dy}{dz}$$

$$+ (R_o^2 \int_{\gamma}^{\gamma+\theta_f} p_{\omega,z}\cos^2\omega d\omega + R_r^2 \int_{\gamma+\theta_f}^{2\pi+\gamma} p_{\omega,z}\cos^2\omega\, d\omega)\frac{d^2y}{dz^2} \qquad 3.4$$

i.e. $F_{\ell,y} = F^*_{\ell,y} + F^{**}_{\ell,y}\frac{dy}{dz} + F^{***}_{\ell,y}\frac{d^2y}{dz^2}$

Contribution to Force Balance (see Fig. 3.5)

In the X-Z plane the contribution is $F_{\ell,x}\Delta z$ which equals $(F^*_{\ell,x} + F^{**}_{\ell,x}\frac{dx}{dz} + F^{***}_{\ell,x}\frac{d^2x}{dz^2})\Delta z$.

In the Y-Z plane the contribution is $F_{\ell,y}\Delta z$ which equals $(F^*_{\ell,y} + F^{**}_{\ell,y}\frac{dy}{dz} + F^{***}_{\ell,y}\frac{d^2y}{dz^2})\Delta z$.

Contribution to Moment Balance (see Fig. 3.5)

In the X-Z plane the contribution is $F_{\ell,x}\frac{\Delta z^2}{2}$ which equals $(F^*_{\ell,x} + F^{**}_{\ell,x}\frac{dx}{dz} + F^{***}_{\ell,x}\frac{d^2x}{dz^2})\frac{\Delta z^2}{2}$.

In the Y-Z plane the contribution is $F_{\ell,y}\frac{\Delta z^2}{2}$ which equals $(F^*_{\ell,y} + F^{**}_{\ell,y}\frac{dy}{dz} + F^{***}_{\ell,y}\frac{d^2y}{dz^2})\frac{\Delta z^2}{2}$.

3.8.2 Axial Pressure Forces

There are two axial forces acting on an elemental slice of the screw:

(i) The force caused by pressure acting on the changing root area in the compression section.

(ii) The force transmitted through the flight due to the pressure difference across it.

3.8.2.1 Axial Force from Polymer Pressure Acting on a Changing Screw Root Area

An elemental axial slice of the screw's compression section is shown in Fig. 3.8. The root radius changes from R_i to R_e over an axial length Δz, with a root taper angle of θ_r. The length of the surface of the root is ΔL_r over the elemental slice considered.

At an angular position ω from the datum line in the cross-section the elemental axial force/unit length,

$$\Delta F_r = p_{\omega,z} \sin\theta_r \times \text{surface area}/\Delta z$$

The surface area from ω to $\omega + \Delta\omega$ is

$$\frac{\Delta\omega}{2\pi} \pi (R_i + R_e)\Delta L_r$$

$$\therefore \quad \Delta F_r = p_{\omega,z} \sin\theta_r \frac{\Delta\omega}{2} (R_i + R_e)\Delta L_r/\Delta z$$

Now $\sin\theta_r = \dfrac{(R_e - R_i)}{\Delta L_r}$

$$\therefore \quad \Delta F_r = p_{\omega,z} \frac{\Delta\omega}{2} \frac{(R_e^2 - R_i^2)}{\Delta z}$$

The change in the area of the root's cross-section,

$$\Delta A_r = \pi(R_e^2 - R_i^2)$$

$$\therefore \quad \Delta F_r = p_{\omega,z} \frac{\Delta\omega}{2} \frac{\Delta A_r}{\Delta z \pi}$$

Integrating round the screw's root with limits $\gamma+\theta_f$ to $2\pi+\gamma$

$$F_r = \frac{1}{2\pi}\frac{dA_r}{dz}\int_{\gamma+\theta_f}^{2\pi+\gamma} p_{\omega,z}\, d\omega \qquad 3.5$$

Contribution to Force Balance

F_r makes a contribution to the local axial force P, evaluated in section 3.8.5.

Contribution to Moment Balance (see Fig. 3.5)

The momentum contributions are summed up round the channel. Therefore the moment in the X-Z plane $M_{r,x}\,\Delta z$

$$= -\frac{R_r}{2\pi}\frac{dA_r}{dz}\int_{\gamma+\theta_f}^{2\pi+\gamma} p_{\omega,z}\,\sin\omega\, d\omega\Delta z$$

The moment in the Y-Z plane

$$M_{r,y}\Delta z = -\frac{R_r}{2\pi}\frac{dA_r}{dz}\int_{\gamma+\theta_f}^{2\pi+\gamma} p_{\omega,z}\,\cos\omega\, d\omega\,\Delta z$$

3.8.2.2 Axial Force due to the Pressure Difference across the Flight

At axial position z there will be an axial force acting on the flight due to the pressure difference across it. The situation is shown in Fig. 3.9. S_f is the force acting on the flight at axial position z. The pressure difference is the difference between the average pressure at $z-\hat{e}$ and the average pressure at $z+\hat{e}$, i.e. $(p_{z-\hat{e}} - p_{z+\hat{e}})$. This pressure acts through the centre of the area of length L_f represented by

the shaded area in Fig. 3.10.

$$\therefore \quad S_f = (p_{z-\hat{e}} - p_{z+\hat{e}}) \frac{L_f}{R_o} \frac{\pi}{2\pi} (R_o^2 - R_r^2)$$

Now from Fig. 3.9

$$\frac{2\hat{e}}{e} = \cos\theta_h$$

$$\hat{e} = \frac{e}{2} \cos\theta_h \qquad 3.6$$

S_f can be resolved into two components, one making a contribution to the torque, which is ignored in this analysis, and the other making a contribution to the axial force.

$\therefore$ the axial force/unit length acting at axial position z,

$$F_f = (p_{z-\hat{e}} - p_{z+\hat{e}}) \frac{L_f}{R_o} \frac{(R_o^2 - R_r^2)}{2L_f} \frac{\cos\theta_h}{\sin\theta_h}$$

$$\therefore \quad F_f = (p_{z-\hat{e}} - p_{z+\hat{e}}) \frac{(R_o^2 - R_r^2)}{2R_o} \cot\theta_h \qquad 3.7$$

Contribution to Force Balance

This axial force makes a contribution to the local axial force P, evaluated in section 3.8.5.

Contribution to Moment Balance (see Fig. 3.5)

The contribution to the moment balance can be seen from Fig. 3.11.

The X-component of the moment,

$$\Delta z M_{f,x} = - F_f \frac{(R_r + R_o)}{2} \sin(\gamma + \frac{\theta_f}{2}) \Delta z$$

The Y-component of the moment,

$$\Delta z M_{f,y} = - F_f \frac{(R_r+R_o)}{2} \cos(\gamma + \frac{\theta_f}{2})\Delta z$$

3.8.3 Centrifugal Forces

Two screw eccentricities produce inertia or centrifugal forces. They are

(i) the unbalanced flight

(ii) the displaced centre of gravity of the circular cross-section from the centre of rotation.

Although the centrifugal force is really a D'Alembert force and should not strictly be represented as shown in Figs. 3.12 and 3.13, this has been done to ease the evaluation of the X and Y components of the centrifugal forces. The forces/unit length due to these two eccentricities are now evaluated.

3.8.3.1 Centrifugal Force caused by the Screw Flight

A diagram of the situation is given in Fig. 3.12. Two components of centrifugal force/unit length, $F_{c,x}$ in the X-direction and $F_{c,y}$ in the Y-direction act through the centre of the flight when the screw has deflected-x in the X-direction and-y in the Y-direction. m_f is the mass/unit length of the flight and ρ is the density of the screw.

$$\therefore \quad m_f = \rho \times \frac{\theta_f}{2\pi} \pi (R_o^2 - R_r^2)$$

$$= \frac{\rho}{2} \theta_f (R_o^2 - R_r^2)$$

The force/unit length in the X-direction, $F_{c,x}$

$$= - m_f R_f \frac{n^2}{g_o} \cos\theta_d$$

$$R_f \cos\theta_d = \frac{(R_r + R_o)}{2} \sin(\gamma + \frac{\theta_f}{2}) - x$$

$$\therefore F_{c,x} = - \frac{\rho\theta_f}{2g_o} (R_o^2 - R_r^2)(\frac{(R_r + R_o)}{2} \sin(\gamma + \frac{\theta_f}{2}) - x)n^2$$

$$\therefore F_{c,x} = - \frac{\rho\dot{\theta}_f}{4g_o} n^2(R_o^2 - R_r^2)(R_r + R_o) \sin(\gamma + \frac{\theta_f}{2})$$

$$+ \frac{\rho\theta_f}{2g_o} n^2(R_o^2 - R_r^2)x \qquad 3.8$$

Substituting symbols for the above coefficients

$$F_{c,x} = F^*_{c,x} + F^{**}_{c,x} x$$

The force/unit length in the Y-direction, $F_{c,y}$

$$= - m_f R_f \frac{n^2}{g_o} \sin\theta_d$$

$$R_f \sin\theta_d = \frac{(R_r + R_o)}{2} \cos(\gamma + \frac{\theta_f}{2}) - y$$

$$\therefore F_{c,y} = - \frac{\rho\theta_f}{2} (R_o^2 - R_r^2) \frac{n^2}{g_o}(\frac{(R_r + R_o)}{2} \cos(\gamma + \frac{\theta_f}{2}) - y)$$

$$\therefore F_{c,y} = - \frac{\rho\theta_f}{4g_o} n^2(R_o^2 - R_r^2)(R_r + R_o) \cos(\gamma + \frac{\theta_f}{2})$$

$$+ \frac{\rho\theta_f}{2g_o}(R_o^2 - R_r^2)n^2 y \qquad 3.9$$

i.e. $$F_{c,y} = F^*_{c,y} + F^{**}_{c,y}\, y$$

3.8.3.2 Centrifugal Force caused by the Screw's Displaced Centre of Gravity

The situation is shown in Fig. 3.13. $\hat{F}_{c,x}$ is the coefficient of the X-component of the force/unit length, $\hat{F}_{c,y}$ is the coefficient of the Y-component of the force/unit length. m_r is the mass/unit length of the screw root.

$$\therefore \quad x\hat{F}_{c,x} = - m_r \sqrt{x^2+y^2}\, \frac{n^2}{g_o} \cos\theta_c$$

$$= - m_r \sqrt{x^2+y^2}\, \frac{n^2}{g_o} - \frac{x}{\sqrt{x^2+y^2}}$$

$$\therefore \quad \hat{F}_{c,x} = \rho\pi R_r^2 \frac{n^2}{g_o} \qquad 3.10$$

$$y\hat{F}_{c,y} = - m_r \sqrt{x^2+y^2}\, \frac{n^2}{g_o} \sin\theta_c$$

$$= - m_r \sqrt{x^2+y^2}\, \frac{n^2}{g_o} - \frac{y}{\sqrt{x^2+y^2}}$$

$$\therefore \quad \hat{F}_{c,y} = \rho\pi R_r^2 \frac{n^2}{g_o} \qquad 3.11$$

Contribution to Force Balance (see Fig. 3.5)

In the X-Z plane the contribution is

$$(F^*_{c,x} + F^{**}_{c,x} x + \hat{F}_{c,x}\, x)\Delta z$$

In the Y-Z plane the contribution is

$$(F^*_{c,y} + F^{**}_{c,y}\, y + \hat{F}_{c,y}\, y)\Delta z$$

Contribution to Moment Balance (see Fig. 3.5)

In the X-Z plane the contribution is

$$(F^{*}_{c,x} + F^{**}_{c,x}x + \hat{F}_{c,x}\,x)\,\frac{\Delta z^2}{2}$$

In the Y-Z plane the contribution is

$$(F^{*}_{c,y} + F^{**}_{c,y}y + \hat{F}_{c,y}y)\,\frac{\Delta z^2}{2}$$

3.8.4 Weight of the Screw

There are two contributions to the weight/unit length of the screw (Fig. 3.14):

(i) The weight/unit length of the root = $\rho\pi R_r^2 \frac{g}{g_o}$

(ii) The weight/unit length of the flight = $\frac{\rho\theta_f}{2\pi}\,\pi(R_o^2-R_r^2)\frac{g}{g_o}$

$$= \frac{\rho\theta_f}{2}(R_o^2-R_r^2)\frac{g}{g_o}$$

$\therefore$ the weight/unit length, $F_W = \frac{\rho}{2}(2\pi R_r^2 + \theta_f(R_o^2-R_r^2))\,\frac{g}{g_o}$ 3.12

Contribution to Force Balance (see Fig. 3.5)

In the X-Z plane there is no contribution.

In the Y-Z plane the contribution is $F_W\Delta z$.

Contribution to Moment Balance (see Fig. 3.5)

In the X-Z plane there is no contribution.

In the Y-Z plane the contribution is $F_W\frac{\Delta z^2}{2}$

3.8.5 Axial Force Acting at any Point Along the Screw

The internal axial force acting on the screw, z along the axis is P (Fig. 3.15). This force is simply the back pressure force acting on the end of the screw, P_e, minus the summed contributions of the axial pressure force due to pressure acting on the flight and on the changing root area in the compression section.

From Fig. 3.15 $$P = P_e - \int_z^L (F_r+F_f)d\eta$$

$$\therefore \quad P = P_e - \int_z^L \left(\frac{1}{2\pi} \frac{dA_r}{dz} \int_{\gamma+\theta_f}^{2\pi+\gamma} p_{\omega,\eta}\, d\omega\right)d\eta$$

$$- \int_z^L \left((p_{\eta-\hat{e}} - p_{\eta+\hat{e}}) \frac{(R_o^2-R_r^2)}{2R_o} \cot\theta_h\right)d\eta \qquad 3.13$$

The end of the screw is conical in shape.

$P_e = p_L$ x projected area of the end of the screw.

The area of the end of screw = cross sectional area of the screw in the metering section

$$= \frac{1}{2}(R_r^2(2\pi - \theta_f) + \theta_f R_o^2)$$

$$\therefore \quad P_e = \frac{p_L}{2}(R_r^2(2\pi-\theta_f) + \theta_f R_o^2)$$

3.9 Deflection Equations

3.9.1 Simple Bending Theory

This bending analysis, as explained previously, ignores the stiffness of the flight therefore from simple bending theory

$$M = EI \frac{d^2x}{dz^2} \text{ in the X-Z plane}$$

3.14

$$M = EI \frac{d^2y}{dz^2} \text{ in the Y-Z plane}$$

where I is the second moment of area of the screw root cross-section about its neutral axis and E is Young's modulus.

3.9.2 Force Balance

Individual contributions to the force balance have been derived. These are now summed together with the internal forces shown in Fig. 3.16. Fig. 3.16 is simply Fig. 3.4(a) with additions necessary for the force balance.

Resolving perpendicular to the local axis in the X-Z plane

$$S + \Delta S - S - (P + \Delta P)\Delta z \frac{d^2x}{dz^2}$$

$$+(F^*_{\ell,x} + F^{**}_{\ell,x} \frac{dx}{dz} + F^{***}_{\ell,x} \frac{d^2x}{dz^2} + F^*_{c,x} + F^{**}_{c,x}x + \hat{F}_{c,x}x)\Delta z = 0$$

$$\therefore \quad \frac{\Delta S}{\Delta z} = - F^*_{\ell,x} - F^{**}_{\ell,x} \frac{dx}{dz} - F^{***}_{\ell,x} \frac{d^2x}{dz^2} - F^*_{c,x} - F^{**}_{c,x}\, x - \hat{F}_{c,x}x$$

$$+ (P + \Delta P)\frac{d^2x}{dz^2}$$

in the limit as $\Delta z \to 0$, $\Delta P \to 0$

The bending moment, M at axial position z is used as a variable instead of $\frac{d^2x}{dz^2}$ to enable explicit use of the zero bending moment boundary condition at the end of the screw. From simple bending theory $\frac{d^2x}{dz^2} = \frac{M}{EI}$. Therefore simplifying the force equation

$$\frac{dS}{dz} = C_1 + C_2x + C_3 \frac{dx}{dz} + C_4M \qquad 3.15$$

where $C_1 = - (F^*_{\ell,x} + F^*_{c,x})$

$C_2 = - (F^{**}_{c,x} + \hat{F}_{c,x})$

$C_3 = - F^{**}_{\ell,x}$

$C_4 = (P - F^{***}_{\ell,x})/EI$

Similarly in the Y-Z plane with the added contribution of the screw's weight.

$$\therefore \quad \frac{dS}{dz} = C_1 + C_2y + C_3 \frac{dy}{dz} + C_4M \qquad 3.16$$

where $C_1 = - (F^*_{\ell,y} + F^*_{c,y} + F_W)$

$C_2 = - (F^{**}_{c,y} + \hat{F}_{c,y})$

$C_3 = - F^{**}_{\ell,y}$

$C_4 = (P - F^{***}_{\ell,y})/EI$

3.9.3 Moment Balance

Again, referring to Fig. 3.16 and to the previously derived contributions to the moment balance. In the X-Z plane

$$- S\Delta z - M - \Delta M + M + (F^*_{\ell,x} + F^{**}_{\ell,x} \frac{dx}{dz} + F^{***}_{\ell,x} \frac{d^2x}{dz^2}) \frac{\Delta z^2}{2}$$

$$+ (F^*_{c,x} + F^{**}_{c,x}x + \hat{F}_{c,x}x)\frac{\Delta z^2}{2} + M_{r,x}\,\Delta z + M_{f,x}\,\Delta z = 0$$

$$\therefore \quad \frac{\Delta M}{\Delta z} = - S + M_{r,x} + M_{f,x} + (F^{*}_{\ell,x} + F^{**}_{\ell,x} \frac{dx}{dz} + F^{***}_{\ell,x} \frac{d^2x}{dz}) \frac{\Delta z}{2}$$

$$+ (F^{*}_{c,x} + F^{**}_{c,x}\, x + \hat{F}_{c,x} x) \frac{\Delta z}{2}$$

in the limit $\Delta z \to 0$

$$\therefore \quad \frac{dM}{dz} = - S + M_{r,x} + M_{f,x} \qquad 3.17$$

Similarly in the Y-Z plane

$$\frac{dM}{dz} = - S + M_{r,y} + M_{f,y} \qquad 3.18$$

3.9.4 Comparison of Deflection Equations with Previously Derived Equations

Newland (Ref. 18) derived a static buckling equation for a shaft of variable cross-section (equation 4 in Ref. 18). The shaft was subjected to a pressure which was a function of the axial position. The shaft's weight was ignored. This equation was differentiated twice to obtain equation 8 in Ref. 22. His analysis was carried out in one plane. Therefore the deflection equations in the X-Z plane, derived in the last section, are simplified using the conditions specified in Newland's papers and the resulting deflection equation is compared with equation 8 in Ref. 22. The deflection equations just derived in the X-Z plane are

$$M = EI \frac{d^2x}{dz^2} \qquad 3.14$$

$$\frac{dS}{dz} = C_1 + C_2 x + C_3 \frac{dx}{dz} + C_4 M \qquad 3.15$$

$$\frac{dM}{dz} = - S + M_{r,x} + M_{f,x} \qquad 3.17$$

Each coefficient is now examined in the light of the conditions specified in Refs. 18 and 22. There is no flight therefore $R_o = R_r = R$ and the limits of integrals round the screw are from 0 to 2π. The pressure is only a function of z therefore $p_{\omega,z} = p_z$. The shaft is static therefore the rotational speed n is zero.

$$C_1 = - R_o \int_{\gamma}^{\gamma+\theta_f} p_{\omega,z} \sin\omega d\omega - R_r \int_{\gamma+\theta_f}^{2\pi+\gamma} p_{\omega,z} \sin\omega d\omega$$

$$- (R_o - R_r)(p_{\gamma+\theta_f,z} \cos(\gamma+\theta_f) - p_{\gamma,z} \cos\gamma)$$

$$+ \frac{\rho\theta_f}{4g_o} n^2 (R_o^2 - R_r^2)(R_r + R_o) \sin(\gamma + \frac{\theta_f}{2})$$

$$= 0$$

$$C_2 = 0$$

$$C_3 = - \frac{1}{2} \frac{dp_z}{dz} (R_o^2 \theta_f + R_r^2 (2\pi - \theta_f))$$

$$= - \pi R^2 \frac{dp_z}{dz}$$

$$= - A \frac{dp_z}{dz} \quad \text{where A is the area of the shaft.}$$

$$C_4 = (P - R_o^2 \int_{\gamma}^{\gamma+\theta_f} p_{\omega,z} \sin^2\omega d\omega - R_r^2 \int_{\gamma+\theta_f}^{2\pi+\gamma} p_{\omega,z} \sin^2\omega d\omega)/EI$$

$$= (P - R^2 p_z \int_0^{2\pi} \sin^2\omega d\omega)/EI$$

$$= (P - R^2 p_z [\frac{\omega}{2} - \frac{\sin^2\omega}{4}]_0^{2\pi})/EI$$

$$= (P - R^2 p_z \pi)/EI$$

$$= (P - Ap_z)/EI$$

$$M_{r,x} = - \frac{R_r}{2\pi} \frac{dA_r}{dz} \int_{\gamma+\theta_f}^{2\pi+\gamma} p_{\omega,z} \sin\omega d\omega$$

$$= - \frac{R_r}{2\pi} \frac{dA_r}{dz} p_z [- \cos\omega]_{2\pi+\gamma}^{2\pi+\gamma}$$

$$= 0$$

$$M_{f,x} = - (p_{z-\hat{e}} - p_{z+\hat{e}}) \frac{(R_o^2 - R_r^2)}{2R_o} \cot\theta_h \frac{(R_r+R_o)}{2} \sin(\gamma + \frac{\theta_f}{2})$$

Which is the moment caused by the pressure difference across the flight. There is no flight, $R_o = R_r$

$\therefore \quad M_{f,x} = 0$

$\therefore$ the deflection equations reduce to

$$M = EI \frac{d^2x}{dz^2}$$

$$\frac{dS}{dz} = - A \frac{dp_z}{dz} \frac{dx}{dz} + (P - Ap_z)M/EI$$

$$= - A \frac{dp_z}{dz} \frac{dx}{dz} + (P - Ap_z) \frac{d^2x}{dz^2}$$

$$\frac{dM}{dz} = - S$$

$$\therefore \quad \frac{dS}{dz} = - \frac{d^2M}{dz^2} = - \frac{d^2}{dz^2}(EI \frac{d^2x}{dz^2})$$

$$= - A \frac{dp_z}{dz} \frac{dx}{dz} + (P - Ap_z) \frac{d^2x}{dz^2}$$

$$\text{i.e.} \quad \frac{d^2}{dz^2}(EI \frac{d^2x}{dz^2}) + (P - Ap_z)\frac{d^2x}{dz^2} - A \frac{dp_z}{dz} \frac{dx}{dz} = 0 \qquad 3.19$$

This is equation 8 in Ref. 22. Therefore the relatively complex deflection equations derived in this work reduce to an equation derived from a simpler analysis of the situation.

3.10 Numerical Analysis

3.10.1 Boundary Conditions

The pressure data to be used are taken from an extruder whose screw is held by two separated bearings at the feed end, i.e. the screw is assumed built in with initial boundary conditions of zero deflection and zero deflection gradient.

For convenient insertion of pressure profiles the computer program was written with the start of the screw at the start of the flighted section of the screw, not at the end of the bearing section where the deflection and deflection gradient are both zero (Fig. 3.17). Therefore the unknown boundary conditions at the start of the screw have to be related to the required boundary conditions at the start of the flighted section of the screw. Simple bending theory is used to derive these relationships which

are inserted into the computer program.

The screw is free at its delivery end and the end moment and shear force are both zero. Hence there are two pairs of split boundary conditions.

	X-Z PLANE	Y-Z PLANE
$z = -(L_{b,1} + L_{b,2})$	$x = \frac{dx}{dz} = 0$	$y = \frac{dy}{dz} = 0$
$z = L$	$M = S = 0$	$M = S = 0$

$L_{b,1}$ and $L_{b,2}$ are shown in Fig. 3.17.

3.10.2 Equation Solution Procedure

The deflection equations derived in the X-Z plane are 3.14, 3.15 and 3.17. Similar equations have been derived in the Y-Z plane. The solution procedure will be the same for both sets of equations therefore only the equations in the X-Z plane are considered.

Now $\frac{d}{dz}(x) = \frac{dx}{dz}$

equation 3.14 $\rightarrow$ $\frac{d}{dz}(\frac{dx}{dz}) = \frac{M}{EI}$

equation 3.17 $\rightarrow$ $\frac{d}{dz}(M) = -S + M_{r,x} + M_{f,x}$

equation 3.15 $\rightarrow$ $\frac{d}{dz}(S) = C_1 + C_2x + C_3\frac{dx}{dz} + C_4M$

i.e. four simultaneous first order equations of the form

$$\frac{dX}{dz} = F(X,z).$$

A predictor-corrector solution procedure was initially used to solve the four above equations for x, the deflections. Out of the numerous predictor-corrector methods available a simple Adams Bashforth type, truncated after the second term of the series, was used. This is an initial value solution procedure and the boundary conditions are split. Two initial values are known and the other two, moment (M) and shear force (S), are derived using the following procedure. A linear relationship is assumed between the known zero end values of shear force and moment and the unknown initial values of shear force and moment.

$$M_e = \alpha_0 + \alpha_1 M_i + \alpha_2 S_i \qquad 3.20$$

$$S_e = \beta_0 + \beta_1 M_i + \beta_2 S_i \qquad 3.21$$

The values of α's and β's are found with three integrations using arbitrary values of M_i and S_i and the actual values of the deflection equations' coefficients. The end values of moment and shear force are noted from each integration. Thus six equations are set up to derive the six values of the coefficients in equations 3.20 and 3.21. In the real integration M_e and S_e are both zero and when these values are inserted into equations 3.20 and 3.21 the values of M_i and S_i are found from the two equations:

$$M_i = \frac{\alpha_0\beta_2 - \alpha_2\beta_0}{\alpha_2\beta_1 - \alpha_1\beta_2} \qquad 3.22$$

$$S_i = \frac{\alpha_1\beta_0 - \alpha_0\beta_1}{\alpha_2\beta_1 - \alpha_1\beta_2} \qquad 3.23$$

A fourth integration is now carried out to find the screw deflection. A check is made on the original linear assumption by comparing the end values of the shear force and moment with average values of shear force and moment along the screw. If the original assumption is correct these

ratios are very small i.e. they approach their true zero values. If both ratios are less than 10^{-6} the end moment and shear force are effectively regarded as zero and the deflections from the integration are taken as the calculated deflections. If, however, either ratio is greater than 10^{-6} then the calculated end boundary conditions are used in equations 3.20 and 3.21 to find new values of S_i and M_i. The integration is then carried out along the screw. This loop continues until both ratios are less than 10^{-6}. A maximum of 10 loops was specified in the program. Unfortunately, with some of the input data the Adams Bashforth method failed to satisfy the conditions that both ratios should be less than 10^{-6} within 10 integration loops. Another initial value solution procedure, the Runge-Kutta fourth order method was substituted for the Adams-Bashforth solution procedure and produced, with the same formulae for estimating initial values of moment and shear force, moment and shear force ratios of less than 10^{-8}, usually in the first loop and never taking more than two loops.

3.11 Computer Program

The computer program flow chart is given in Fig. 3.18.

3.12 Computer Program Tests

Four types of program tests were carried out:

(i) Tests to check integrals in expressions for calculating pressure forces acting on the screw. Summations are made either round the circumference of the screw or along its axis.

(ii) Tests to check the ability of the program to calculate screw deflections caused by the different types of force acting on it. 19.83 L/D screws were used to generate the experimental data used in this work (Table 3.2). 119 integration steps were used along the screw, i.e. 6 steps per screw pitch over the flighted length of 19.75 L/D.

(iii) Tests to check the sensitivity of the screw end deflection to the assumed initial value of polymer pressure.

(iv) Deflection convergence tests as a function of integration step length.

The pressure data in experiments 5, 6, 21 and 22 is used in tests (iii) and (iv). Experiments 5 and 21 have positive pressure gradients in the metering section and experiments 6 and 22 have negative pressure gradients in the metering section, i.e. both broad types of pressure profiles are considered.

3.12.1 Integral Tests

3.12.1.1 Axial Integration Tests

P, the axial force acting on the screw, equals $P_e - \int_z^L (F_r+F_f)d\eta$. P_e is set to zero and the integral checked. The term (F_r+F_f) is set to the continuous function $\eta^3+\eta^2$ and the integration carried out using the Trapezoidal Rule from z = 0 to z = L. The maximum error was 10^{-3}%.

3.12.1.2 Circumferential Integration Tests

Seven integrals are tested using Simpson's Rule with 26 steps. The integrations are carried out in the cross-section at 119 axial positions. The integrals are all functions of $p_{\omega,z}$ the circumferential pressure profile at axial position z. $p_{\omega,z}$ is set to $(35 + 7\omega)KG_f/cm^2$

for these tests. This typically simulates circumferential pressure profiles encountered in the input pressure data. The integrals checked, and the errors are listed in Table 3.3.

3.12.2 Deflection Analysis Tests

Comparisons are made of deflections resulting from numerical analyses using the computer program and known analytical solutions. The program considers the variable cross-section of the screw and the various forces acting on the screw. Tests are split into two types. The first type tested the ability of the program to consider the variable screw root cross-section. To enable a simple analytical solution the only force considered is an evenly distributed load W/unit length. A typical value of W is 40 KN/m. The maximum error was 2.5×10^{-7}%. The second type tests the ability of the program to calculate screw deflections resulting from the applied forces. The full deflection equations are:

$$M = EI \frac{d^2x}{dz^2} \qquad 3.14$$

$$\frac{dM}{dz} = - S + M_{r,x} + M_{f,x} \qquad 3.17$$

$$\frac{dS}{dz} = C_1 + C_2x + C_3 \frac{dx}{dz} + C_4M \qquad 3.15$$

In this test I is taken to be constant, i.e. a beam of constant cross-section is considered. The full fourth order differential equation is checked with atypical coefficient values. Then all except convenient combinations of the coefficients are set to zero and typical values are inserted for these coefficients and the resulting analytical deflection values are compared with the numerical values.

3.12.2.1 Full Equation Test

Combining equations 3.14, 3.15 and 3.17

$$\frac{d^2M}{dz^2} = EI\,\frac{d^4x}{dz^4} = -C_1 - C_2x - C_3\frac{dx}{dz} - C_4M + \frac{d}{dz}(M_{r,x} + M_{f,x})$$

$$\therefore \quad \frac{d^4x}{dz^4} + C_4\frac{d^2x}{dz^2} + \frac{C_3}{EI}\frac{dx}{dz} + \frac{C_2}{EI}x = -\frac{C_1}{EI}$$

$$+ \frac{1}{EI}\frac{d}{dz}(M_{r,x} + M_{f,x})$$

Typical values of C_1, $M_{r,x}$ and $M_{f,x}$ were inserted with values of C_2, C_3 and C_4 chosen to enable easy solution of the equation i.e.

$$C_4 = -\frac{9}{8}a^2,\ C_3 = -\frac{3}{8}a^3EI,\ C_2 = -\frac{a^4}{32}EI$$

where a is an arbitrary constant set to .01. The maximim errors in x and y deflections were .0013%.

3.12.2.2 Separate Equation Term Tests

C_1 and C_2 non-zero:

$$\frac{d^2M}{dz^2} = EI\,\frac{d^4x}{dz^4} = -C_1 - C_2x$$

$$\therefore \quad \frac{d^4x}{dz^4} + \frac{C_2}{EI}x = -\frac{C_1}{EI}$$

C_1 is set to 200 and C_2 to -.01.

The maximum errors in both the X and Y directions were 9×10^{-5}%.

C_1 and C_3 non-zero:

$$\frac{d^2M}{dz^2} = EI\,\frac{d^4x}{dz^4} = -\,C_1 - C_3\,\frac{dx}{dz}$$

$$\therefore \quad \frac{d^4x}{dz^4} + \frac{C_3}{EI}\,\frac{dx}{dz} = -\,\frac{C_1}{EI}$$

C_1 is set to 200 and C_3 to -200.

The maximum errors in both the X and Y directions were $7 \times 10^{-7}\%$

C_1 and C_4 non-zero:

$$\frac{d^2M}{dz^2} = EI\,\frac{d^4x}{dz^4} = -\,C_1 - C_4M$$

$$\therefore \quad \frac{d^4x}{dz^4} + C_4\,\frac{d^2x}{dz^2} = -\,\frac{C_1}{EI}$$

C_1 is set to 200 and C_4 to .001.

The maximum errors in both the X and Y directions were $5 \times 10^{-6}\%$

$M_{r,x}$ and $M_{f,x}$ non-zero:

$$\frac{d^2M}{dz^2} = EI\,\frac{d^4x}{dz^4} = \frac{d}{dz}(M_{r,x} + M_{f,x})$$

$M_{r,x}$ is set to $5z^2 + 20z$.

$M_{f,x}$ is set to $8z^2 + 30z$

$$\therefore \quad \frac{d}{dz}(M_{r,x} + M_{f,x}) = 26z + 50$$

$$\text{i.e.} \quad \frac{d^4x}{dz^4} = \frac{26}{EI}\,z + \frac{50}{EI}$$

The maximum deflection errors in the X and Y directions were $10^{-6}\%$.

3.12.3 Test of the Screw's End Deflection as a Function of the Assumed Pressure at the Start of the Screw

In the analysis the pressure at the start of the screw (z=0) is assumed. This assumption will affect the axial pressure profile fitted between this assumed value and the first measured circumferential pressure profile. This may in turn affect the screw deflections of which the end deflection will be the largest.

The probable initial pressure is around atmospheric, say in the range 70 to 140 KN/m^2. The effect of using different values of initial pressure is shown in Figs. 3.19 to 3.22 for experimental runs 5, 6, 21 and 22. The effect of varying initial pressure in the range 70 to 140 KN/m^2 is small therefore the initial pressure is set at 100 KN/m^2.

3.12.4 Convergence of Deflection Integration as a Function of Integration Step Length

The same data were used for this test as in the initial pressure test. The readily available computer storage capacity limited the maximum number of steps to 357. Any increase in the number of steps would have limited the turnround time between program runs. The convergence of the solution shown in Figs. 3.23 to 3.26 does not suggest that increasing the number of steps above 357 would be worthwhile. This gives 18 steps/pitch of the screw.

3.13 Equation Instability

Extremely high screw end deflections were initially calculated for some of the sets of experimental operating conditions. The three deflection equations are given below for the X-Z plane.

$$M = EI \frac{d^2x}{dz^2} \qquad 3.14$$

$$\frac{dM}{dz} = -S + M_{r,x} + M_{f,x} \qquad 3.17$$

$$\frac{dS}{dz} = C_1 + C_2x + C_3 \frac{dx}{dz} + C_4M \qquad 3.15$$

$$\therefore \quad \frac{d^2M}{dz^2} = \frac{d^2}{dz^2}(EI \frac{d^2x}{dz^2}) = - C_1 - C_2x - C_3 \frac{dx}{dz} - C_4M + \frac{d}{dz}(M_{r,x} + M_{f,x})$$

The equation is similar for the Y-Z plane except y is substituted for x.

The program was run five times using data from experiments 5, 6, 21 and 22. In each run some of the equation coefficients were set to zero. The effect of C_1, the lateral pressure force/unit length caused by the centrifugal force of the flight about the centre of rotation and the lateral pressure force, and C_1 combined with other non-zero coefficients is shown in Table 3.4. The deflections are large in experiments 5 and 21 when C_1 and C_3 are both non-zero. C_3 is the lateral pressure force coefficient due to the local deflection and pressure gradients. The major difference between the pressure data in experiments 5 and 21 and experiments 6 and 22 is that in the former two the axial pressure gradient is positive in the metering section and in the latter two experiments the pressure gradient is negative. This behaviour can be usefully examined if the equations are viewed in the simplified form used by Newland (Ref. 22). This equation has already been derived in section 3.9.4 i.e.

$$\frac{d^2}{dz^2}(EI \frac{d^2x}{dz^2}) + (P - p_zA) \frac{d^2x}{dz^2} - A \frac{dp_z}{dz} \frac{dx}{dz} = 0$$

The axial pressure gradient is constant in the metering section. In Timoshenko and Gere (Ref. 23) the deflection equation of a flagpole is given by

$$EI \frac{d^3x}{dz^3} + q\,(L - z) \frac{dx}{dz} = 0$$

where L is the flagpole length. Differentiating with respect to z

$$EI \frac{d^4x}{dz^4} - q \frac{dx}{dz} + q(L - z) \frac{d^2x}{dz^2} = 0 \qquad 3.24$$

To yield an analytical solution the axial pressure gradient is assumed to be constant and equal to that in the metering section.

$$\therefore \quad P = L \frac{dp_z}{dz} A \quad \text{and} \quad p_z = z \frac{dp_z}{dz}$$

$\therefore$ Newland's equation becomes

$$EI \frac{d^2x}{dz^4} + A \frac{dp_z}{dz} (L - z) \frac{d^2x}{dz^2} - A \frac{dp_z}{dz} \frac{dx}{dz} = 0$$

which is the same as equation 3.24 with q equal to $A \frac{dp_z}{dz}$.

The flagpole buckles when $qL = 7.837EI/L^2$ i.e. a positive value. Therefore the simplified screw buckles when $A \frac{dp_z}{dz}$ is positive. Which is true in experiments 5 and 21 but not in experiments 6 and 22.

$$A \frac{dp_z}{dz} = 7.837\ EI/L^2$$

The critical value of $\frac{dp_z}{dz}$ is therefore 2.72×10^5 KN/m^3.

In experiment 5 the axial pressure gradient in the metering section is 4.2×10^4 KN/m^3 and in experiment 21 the gradient is 2.91×10^4 KN/m^3.

Buckling will only occur when there is no constraint to lateral deflections. In the real case of course the barrel will constrain the deflection to the radial clearance. The constraint of the barrel has been removed in this analysis to calculate screw deflections when the barrel is absent as a measure of consequent wear of the screw and/or barrel. Therefore the C_3 force gives a false picture and is removed from the analysis by setting C_3 equal to zero.

3.14 The Effect of Individual Terms in the Deflection Equations on the Full Screw Deflection

The three deflection equations, with C_3 set to zero, are

$$M = EI \frac{d^2x}{dz^2} \qquad 3.14$$

$$\frac{dM}{dz} = - S + M_{r,x} + M_{f,x} \qquad 3.17$$

$$\frac{dS}{dz} = C_1 + C_2x + C_4M$$

i.e. $$\frac{d^2}{dz^2}(EI \frac{d^2x}{dz^2}) = - C_1 - C_2x - C_4M + \frac{d}{dz}(M_{f,x} + M_{r,x})$$

The typical values along the screw in the X-Z and Y-Z plane of all the above coefficients for experiment 5 are given below:

	X-Z plane	Y-Z plane
C_1 (N/m)	35,000	17,500
C_2 (N/m^2)	70	
C_4 (m^{-2})	5	5
$\frac{d}{dz}(M_{f,x} + M_{r,x})$	-2100 to -3500	-2100 to -3500

The maximum real deflection of the screw is .13mm (the clearance between the screw and barrel).

the maximum value of $|C_2x| = 70 \times .13 \times 10^{-3}$ N/m

$= .0091$ N/m

the maximum value of $\left|\frac{d^2x}{dz^2}\right| = 1.39 \times 10^{-5}$

$\therefore$ the maximum value of $|C_4M| = \left|C_4 EI \frac{d^2x}{dz^2}\right|$

$= 12.6$ N/m

Comparing the magnitude of C_1 with the other terms in the equation:

$C_1 = 17500$ to 35000 N/m $\quad C_2x = .0091$ N/m

$|C_4M| = 12.6$ N/m $\quad \frac{d}{dz}(M_{r,x} + M_{f,x}) = 3500$ N/m

$|C_2x|$ and $|C_4M|$ are insignificant c.f. C_1 and $\frac{d}{dz}(M_{f,x} + M_{r,x})$.

C_2x is the centrifugal force/unit length caused by the screw's deflection

from its original axis. C_4M is the axial force/unit length which makes a contribution to the lateral deflections.

3.15 The Final Equations with Insignificant Terms Removed

The reduced equations are:

$$M = EI \frac{d^2x}{dz^2} \qquad 3.14$$

$$\frac{dM}{dz} = - S + M_{r,x} + M_{f,x} \qquad 3.17$$

$$\frac{dS}{dz} = C_1 \qquad 3.25$$

3.16 The Polymer Force Required to Limit the Maximum Screw Deflection to the Radial Clearance between the Screw and the Barrel

There is no unique force system which when applied to the screw in opposition to the self-generated forces would reduce the screw deflection to the magnitude of the radial clearance. If we calculate the simple distributed load required to deflect the screw a maximum distance equal to the clearance, and subtract this from the original force system we have the nett force system which is required to limit the deflection to the size of the clearance, i.e. the polymer lubrication force required to prevent contact and hence wear of the screw and barrel. For any combination of screw and loading system there will be components of the end deflection in the X and Y directions, x_e

and y_e. The maximum deflection of the screw calculated with the constraint of the barrel removed is at the end of the screw. As there is no unique polymer force system which will reduce this unconstrained deflection to the magnitude of the clearance it is sensible to choose a combination of constraining polymer X and Y forces along the screw to reduce the full end deflection. Therefore the simply distributed load acting on the screw which will give an end deflection of magnitude of the clearance in the direction of the original deflections has to be calculated. In reality any point along the screw could be in contact with the barrel. This arbitrary point is chosen to be the end of screw, i.e. the point of first contact of an unconstrained screw.

There are two conditions to be satisfied:

(i) The end deflection is equal to the radial clearance between the screw and barrel.

(ii) The ratio of X and Y end deflections, i.e. the full deflection direction, equals the ratio and hence direction of the unconstrained screw's end deflection.

If x_δ is the X-component and y_δ the Y-component of the end deflection caused by the simply distributed load then to satisfy condition (i):

$$\sqrt{x_\delta^2 + y_\delta^2} = \delta$$

To satisfy condition (ii):

$$\frac{x_\delta}{y_\delta} = \frac{x_e}{y_e}$$

where x_e and y_e are the components of the end deflection of the unconstrained screw.

i.e. $$\frac{x_\delta^2}{y_\delta^2} = \frac{x_e^2}{y_e}$$

$$\therefore \quad x_\delta^2 = \frac{x_e^2}{y_e^2}\, y_\delta^2 = \delta^2 - y_\delta^2$$

$$\therefore \quad y_\delta^2\left(1 + \frac{x_e^2}{y_e^2}\right) = \delta^2$$

$$\therefore \quad y_\delta = \pm \frac{\delta}{\left(1 + \frac{x_e^2}{y_e^2}\right)^{\frac{1}{2}}} \qquad 3.26$$

and $$x_\delta = \frac{x_e}{y_e}\, y_\delta \qquad 3.27$$

The simple distributed loads in the X-Z and Y-Z planes are then calculated using simple bending theory, the calculated values of y_δ and x_δ and the stiffness of the screw. These evenly distributed loads are then subtracted from the self-generated loads along the screw to give the required polymer force to prevent contact between and hence wear of the screw and barrel. The force at one point is rather meaningless as it will be opposed by another force ½ turn round the screw. Therefore the polymer bearing load is calculated over each turn of the screw. The summation of the force/turn is started from the feed end. There is no reason why it should not start from the end of the screw. This would lead to a different force profile as there is not an integer number of screw turns, i.e. the last section of the screw has an unbalanced force situation (less than 1 turn). Thus the force on the last section may be large c.f. other forces. Therefore the summation is started at .83 turns along the screw, i.e. the effective length of the screw is

an integer (19) number of turns.

In a working extruder granules are conveyed a distance down the screw before a pressure build-up occurs. The point down the screw at which this occurs is difficult to calculate but may be of the order of .83 turns.

3.17 Results

3.17.1 Screw Deflection Graphs

Calculations are carried out using the 16 sets of data. As explained in section 3.1. two types of calculated values are of interest:

(i) The end deflection of the unconstrained screw.

(ii) The polymer force required to restrict the screw deflection to the magnitude of the clearance.

The first will give an idea of the wear rate when the barrel is present to constrain the screw. The second will give an idea of how large the polymer lubricating force has to be to prevent the screw touching the barrel. This will only occur when the clearance between the screw and the barrel is large enough to produce polymer shear stresses below the critical slip level. Otherwise there will always be metal-to-metal contact between the screw and barrel.

3.17.2 Unconstrained Screw End Deflection as a Function of Rotational Position (Fig. 3.27)

The deflection will change as the screw rotates. The pressure forces are assumed to remain constant relative to the screw as the screw rotates. However, the effect of the screw weight will produce

a change in the nett force. This effect is significant when deflections are low, e.g. in experiments 9, 18, 19, 22 and 26, and hence the effect of the weight is significant. It is insignificant (experiment 28) when the effect of the weight is relatively insignificant.

3.17.3 Unconstrained Screw End Deflection as a Function of Various Pressure Variance Functions (Figs. 3.28 to 3.33)

Pressure variance at any point along the screw is simply the difference between the maximum and minimum pressure round the circumference of the screw.

The dependence of the end deflection on functions of pressure variance, v, was tested by plotting the end deflection as a function of the following functions summed up over all the points at which pressures were computed. These functions were selected from a consideration of bending theory explained below:

$$\Sigma_o^L v, \quad \Sigma_o^L zv, \quad \Sigma_o^L \frac{dv}{dz}, \quad \Sigma_o^L z\frac{dv}{dz}, \quad \Sigma_o^L \left|\frac{dv}{dz}\right|, \quad \Sigma_o^L z\left|\frac{dv}{dz}\right|,$$

$$\Sigma_o^L \frac{d^2v}{dz^2}, \quad \Sigma_o^L z\frac{d^2v}{dz^2}, \quad \Sigma_o^L \left|\frac{d^2v}{dz^2}\right|, \quad \Sigma_o^L z\left|\frac{d^2v}{dz^2}\right|.$$

The end deflection is only a significant function of $\Sigma_o^L \frac{dv}{dz}$. The graphs of end deflection versus $\Sigma_o^L \frac{dv}{dz}$ are shown in Figs. 3.28 to 3.31 for values of γ_i during one rotation of the screw. Each point represents one calculated result for each of the 16 sets of experimental data. Figs. 3.32 and 3.33 show the typically random distributions obtained for unconstrained end deflections plotted against all the other functions of pressure variance.

The end deflection is a linear function of $\Sigma_o^L \frac{dv}{dz}$ except for experiment 26. Experiment 26 was the only experiment when screw A (Table 3.2) was used. If summed values of the pressure variance gradient is doubled then the unconstrained deflection will be doubled. This shows how important are the self-generated pressure forces c.f. inertia or weight forces in producing potential screw deflections and consequent wear.

It is instructive to consider a very simple beam, length L, loaded with an evenly distributed load W/unit length. This throws some light on the trends in these graphs.

$$\text{The end deflection, } x_e = \frac{WL^4}{8EI} \qquad 3.28$$

Now W is proportional to v if we assume the weight of the beam is negligible and the geometry is constant, which is the case except for experiment 26 where a different screw was used. This is why experiment 26 gives the point which deviates most from the straight line. Figs. 3.28 to 3.31 show x_e proportional to $\Sigma_o^L \frac{dv}{dz}$. This results from the more complicated practical situation where the nett pressure forces rotate round the screw in the axial direction. Obviously, if the pressure variance remains constant at v, then the nett force over one turn will be zero, i.e. all the forces will cancel out leaving a less serious moment acting on the screw. However, if v varies over one turn of the screw then the forces elemental slices will change and the nett force on one turn will be non-zero, i.e. the larger the value of $\frac{dv}{dz}$ the larger the nett force on the screw and the larger the end deflection. $|\frac{dv}{dz}|$ is not important because diametrically opposed forces which would cancel out are summed up to give a false impression.

It would be unwise to conclude that $x_e = K\Sigma_o^L \frac{dv}{dz}$ with a unique value of K for all screws. The result for experiment 26 shows that this gradient would probably change for each screw geometry. However the general observation that x_e is a significantly linear function of $\Sigma_o^L \frac{dv}{dz}$ is reasonable for all screws. It is therefore very important to reduce $\Sigma_o^L \frac{dv}{dz}$ to a minimum for all screw duties, i.e. the absolute pressure is not important, but the shape of the pressure profile round the screw should remain as nearly constant as possible over the length of the screw. The practical implications of this conclusion will be discussed in Section 3.18.

3.17.4 The Relative Importance of Each Component of Force on the Screw Deflection (Figs. 3.34 and 3.35)

Figs. 3.34 and 3.35 show the relative importance in producing the screw end deflection of

(i) lateral pressure forces

(ii) the screw's weight

(iii) axial pressure forces.

The axial pressure forces will only increase the deflection when combined with the lateral forces. Therefore the contributions of the first two forces are subtracted from the full end deflection to give the contribution of the axial pressure forces.

There are two graphs, the first for X-components of end deflection and the second for Y-components of end deflection. The results from all 16 sets of data are plotted in the graphs as a function of the end component of deflection. Each component of deflection is a percentage of the full component of deflection whether it is a positive or negative

value. Therefore some percentages are negative if the contribution by that force system produces a deflection of opposite sign to the full component of deflection. In Fig. 3.34 the X-component graph, the lateral force deflection is considerably more important than the almost negligible axial pressure force contribution. In Fig. 3.35 the contribution to the Y deflection of the axial forces is even less than in the X-direction. This is probably due to the fact that the weight makes a contribution to the deflections in the Y-direction, reducing the contribution of the axial forces even more than in the X-direction. Again the contribution of the lateral pressure forces is the most significant except when the deflection becomes relatively small at which point the deflection due to the weight of the screw takes on an equal significance. Therefore, generally the effect of the lateral pressure force is greater than any other, hence the good fit when end deflection is plotted against pressure variance gradient, a function of lateral pressure force.

3.17.5 The Effect of Increasing Screw O.D. on Screw End Deflection (Figs. 3.36 to 3.38)

The deflection results are for the screws used in the experimental work. The effect of increasing screw diameter is shown in Figs. 3.36 to 3.38 in which the ratio of end deflection to screw O.D. is plotted against screw O.D. Three experiments, 3, 28 and 26 are considered to cover the range from high to low deflection cases. The pressure profiles are taken to be the same, but stretched round the larger screw circumference, as for the 38.1 mm screw experimental results. The screw geometry has been scaled up using two methods:

(i) Geometrical similarity

(ii) Maddock's scale-up

The first scale-up method simply keeps the ratio of channel depth to screw O.D. constant. Maddock first suggested keeping the channel depth proportional to the square root of the screw O.D. as a compromise decision (Ref. 24). This is the generally used scale-up factor for plasticating extruders and more recently Pearson (Ref. 25) has suggested this, with appropriate reduction of screw speed, will keep heat transfer and generation the same in the original and scaled-up extruder. In both methods the screw length is kept proportional to the O.D. Consequently, all the forces acting on the screw are changed as the screw diamemter and hence the screw area is increased by either of these methods. The ratio of screw end deflection to O.D. is plotted against O.D. in Figs. 3.36 to 3.38 for the three experiments. The three ratios, X-component, Y-component and the full deflection to screw O.D. are all shown.

Experiments 3 and 28, where the pressure forces dominate the screw loading give similar shaped graphs. Experiment 26 where the deflection is relatively small gives a different shaped set of curves. This is because the dominant force system changes. In Figs. 3.36 and 3.37 the lateral pressure force is the dominant deflection force whereas in Fig. 3.38 the weight is the dominant deflection force.

The ratio of full deflection to O.D. reduces more with the Maddock scaled results than with the Geometrical similarity results. This is because the stiffness of the screw is reduced less when the channel depth is proportional to $\sqrt{D}$ than when it is proportional to D. The conclusion is that although absolute deflections will increase in all cases with an increase in screw O.D. the ratio of full deflection to O.D. will increase with O.D. when the pressure forces are not as significant as the weight force and decrease when the pressure forces are dominant.

As the screw clearance is normally proportional to the screw O.D. this means that the deflection to clearance ratio will decrease with an increase in O.D. when wear rates are high for a small screw and hence the wear rate will not be as severe. However if the screw weight is the largest force acting on the screw the reverse is true, i.e. wear rates will increase with an increase in screw O.D.

3.17.6 Polymer Forces Required to Prevent Metal-to-Metal Contact between the Screw and the Barrel

In Table 3.5 the maximum calculated polymer force/turn along the screw, required to restrict the screw deflection to the radial clearance for all experiments is given, i.e. the maximum magnitude of polymer lubricating force/turn required to prevent metal-to-metal contact between the screw and barrel. This force, as previously explained is summed up over each turn down the screw to give a result allowing for the cancellation of forces round the screw. In every experiment, the maximum force occurred over the compression section where the pressure variance is changing most rapidly in the axial direction.

The magnitude of the force/turn ranges from 25.2 Newtons in experiment 9 where polypropylene is extruded to 139 Newtons for the extrusion of rigid PVC in experiment 26.

3.18 Conclusions

If the range of screw speeds, die diameters and polymers used in the experimental runs considered in this section are typical then the effect of pressure forces on a screw appear to be more significant than its weight. Specifically, the lateral pressure force causes screw

deflections leading to contact and wear between the screw and barrel unless the polymer acts as a satisfactory lubricant.

This lateral pressure force can be reasonably quantified by the summation of the pressure variance gradient along the screw. If changes in extruder operating conditions lead to this summation being doubled then the unconstrained end deflection of the screw will be doubled. This summation has to be reduced to keep screw and barrel wear to a minimum, i.e. the absolute pressure profile along the screw is not important but the shape of the pressure profile round the screw should be kept as constant as possible along the screw. This assumes that the length of the screw is an interger number of turns. If it is not then each term in $\Sigma_0^L \frac{dv}{dz}$ has less chance to cancel another term.

From the scale-up results, when, as appears to be normal, the most important forces acting on the screw are the self-generated pressure forces, then the wear rate will decrease with an increase in screw diameter. The reverse is true if the effect of the weight is larger than that of the lateral pressure forces.

The average maximum force acting on one turn of the 38.1 mm diameter screw in the range of operating conditions considered is around 40 Newtons and the range is from 25.2 to 139 Newtons (Table 3.5). This will be related to the lubricating force generated by the polymer, in Section 4.0. The maximum lateral force/turn acting on the screw, for the screws considered in the analysis, was always over the very gentle compression section. As seen before, each section length along the screw should be an interger number of turns otherwise the lateral pressure forces do not have a full chance to cancel each other. It appears to be most important to do this in the compression section. The screws used to generate experimental data for the calculations have a relatively gentle root taper. Presumably, as the compression section is reduced in length

and the compression and root taper becomes more severe the pressure variance gradient in the axial direction may rapidly increase. It seems to be a good idea to use as long a compression as possible to reduce this effect.

FIG. 3.1 CIRCUMFERENTIAL PRESSURE TRACE DIVIDED INTO A FINITE NUMBER OF SECTIONS

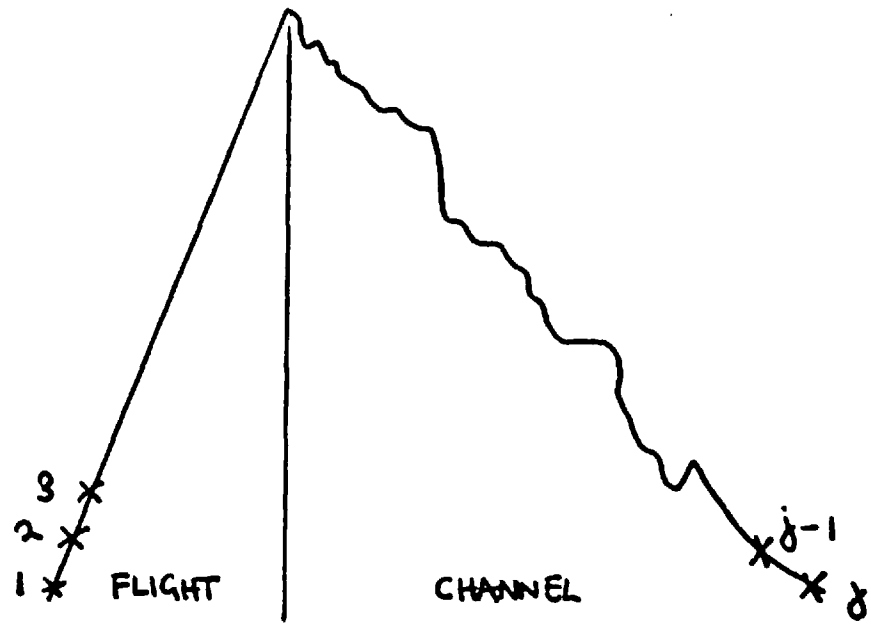

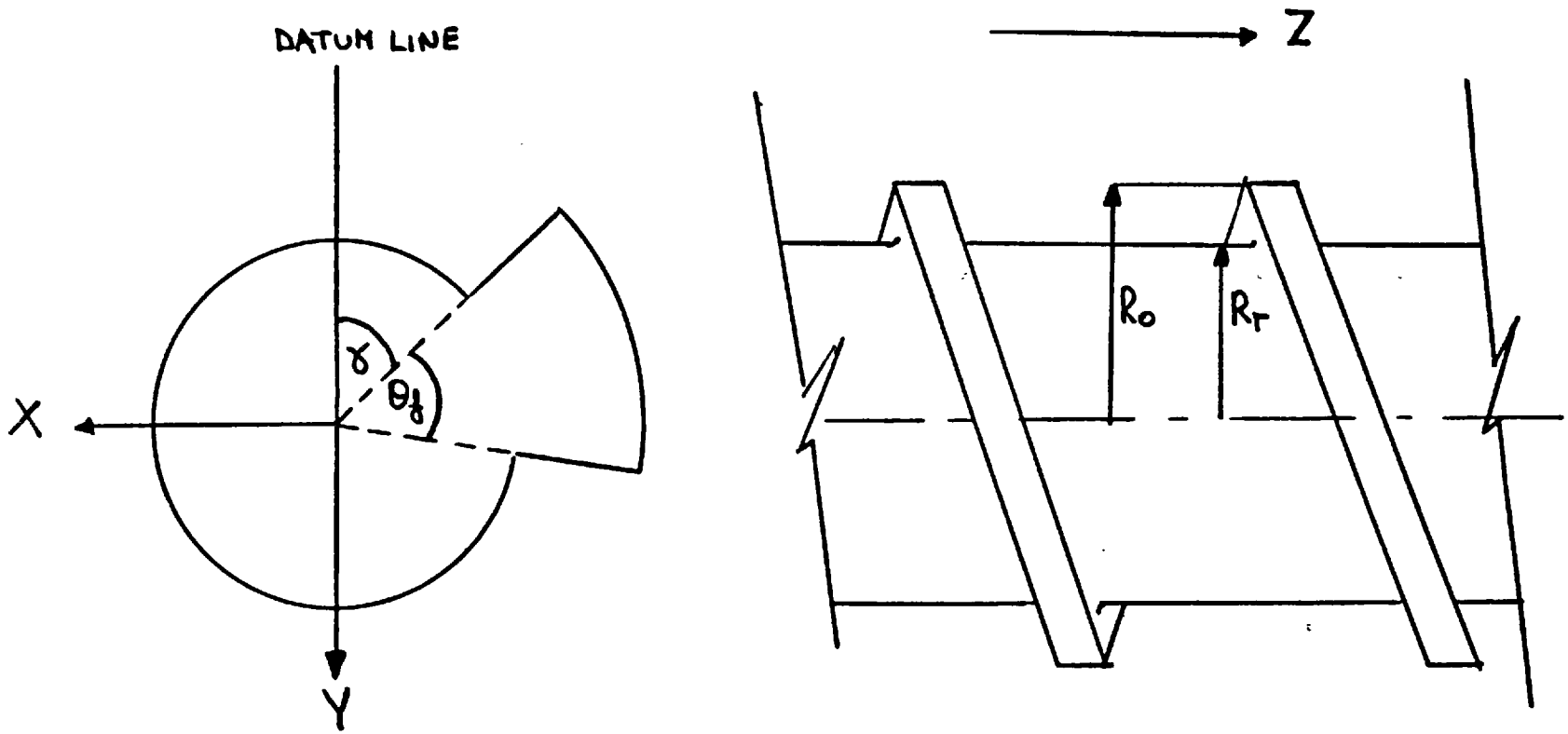

FIG. 3.2 SCREW GEOMETRY

FIG. 3.3 SCREW FLIGHT GEOMETRY

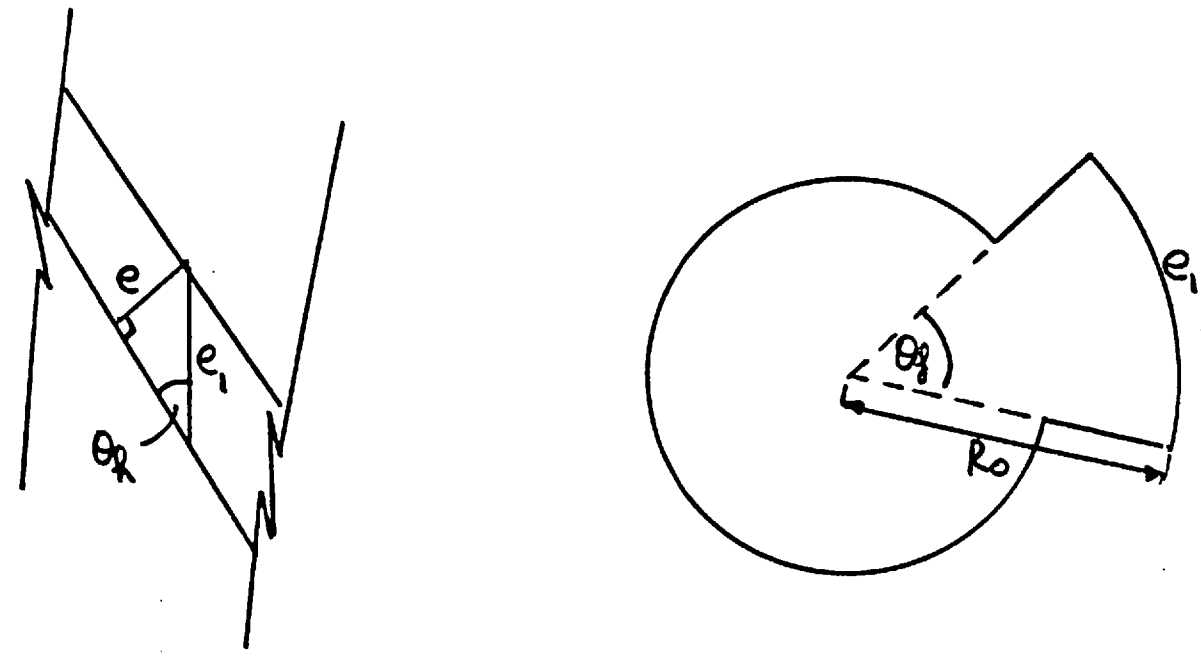

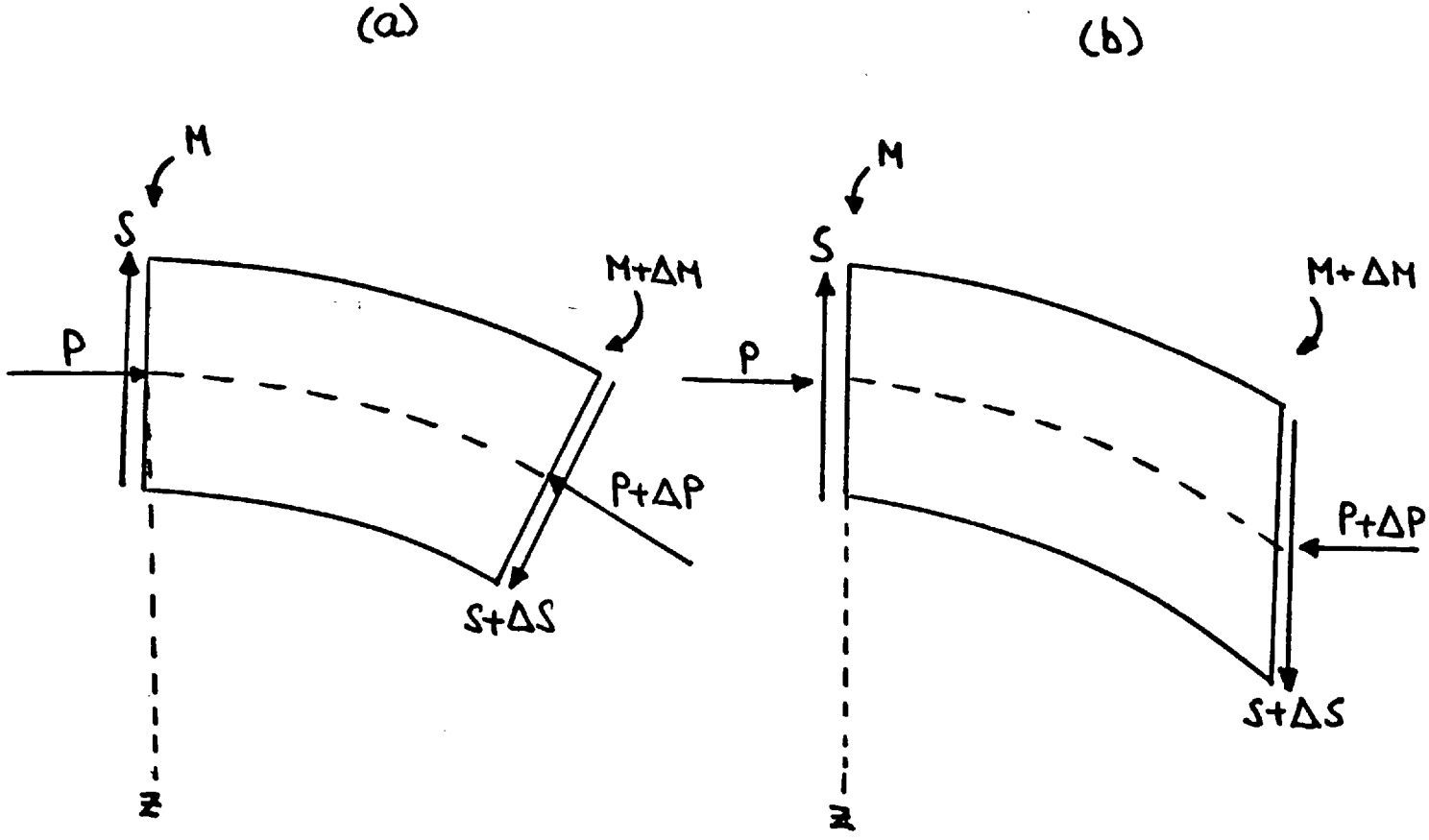

FIG. 3.4 ELEMENTAL AXIAL SLICE OF THE SCREW

FIG. 3.5 POSITIVE FORCE AND MOMENT DIRECTIONS

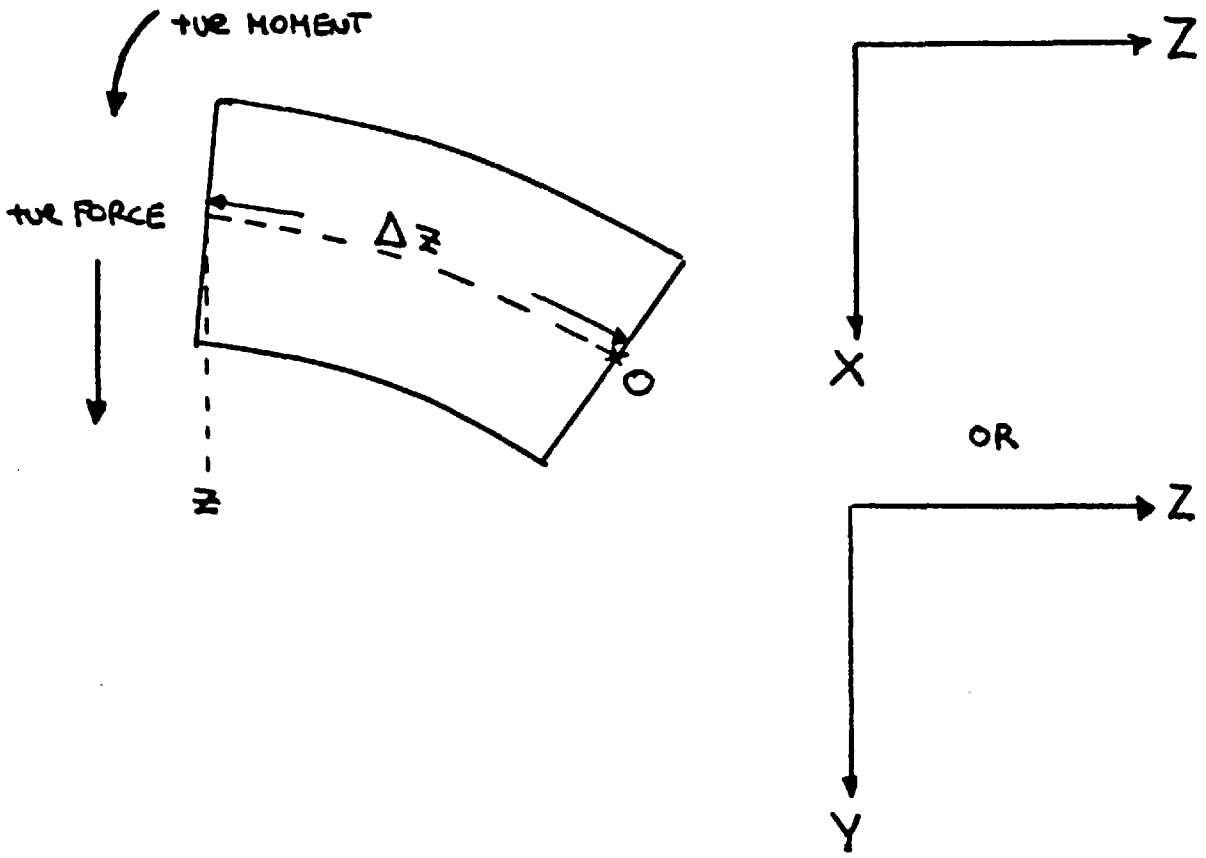

FIG. 3.6 AN ELEMENTAL AXIAL SLICE OF THE SCREW

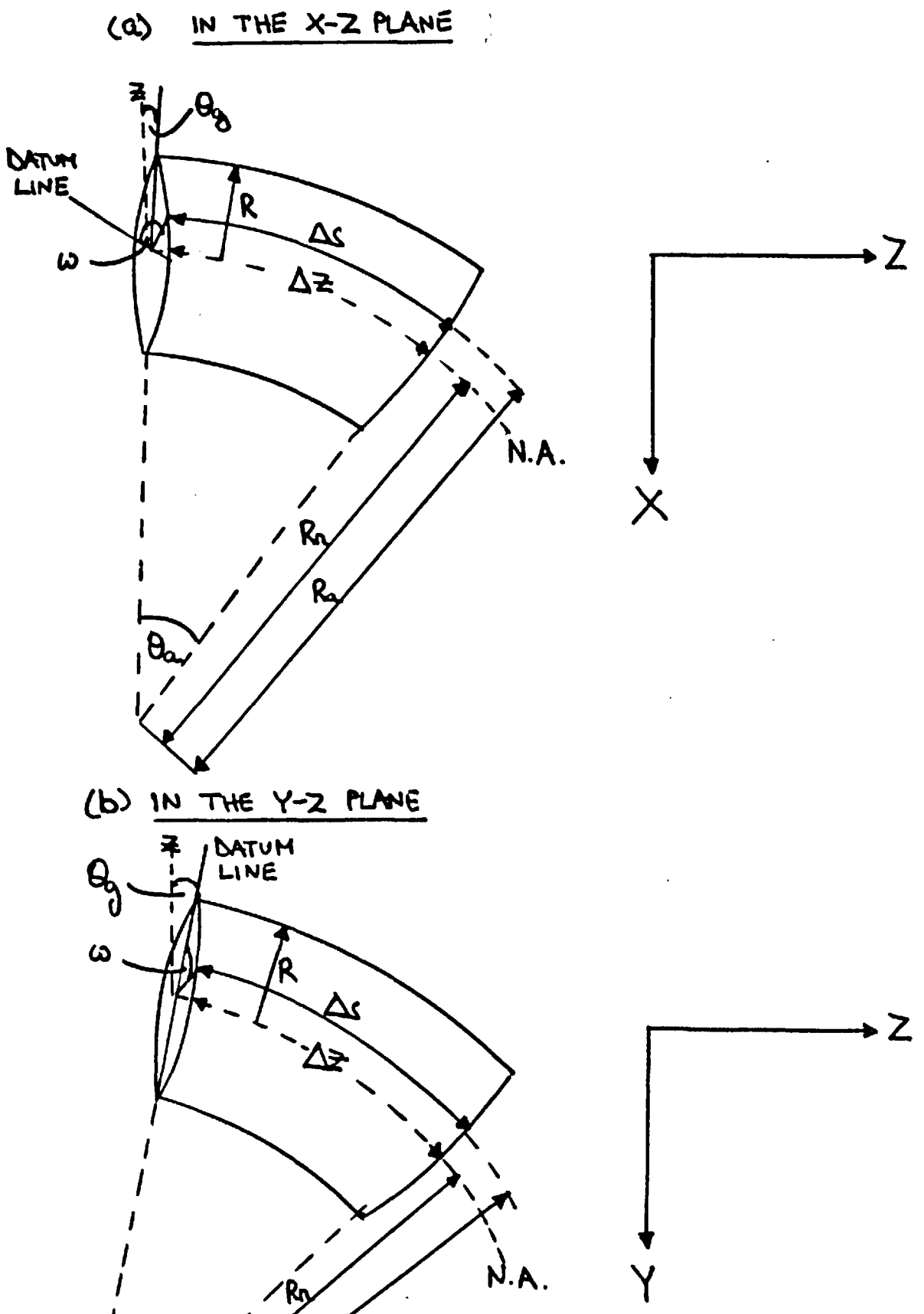

FIG. 3.7 VIEW OF THE CROSS-SECTION OF AN ELEMENTAL AXIAL SLICE OF THE SCREW

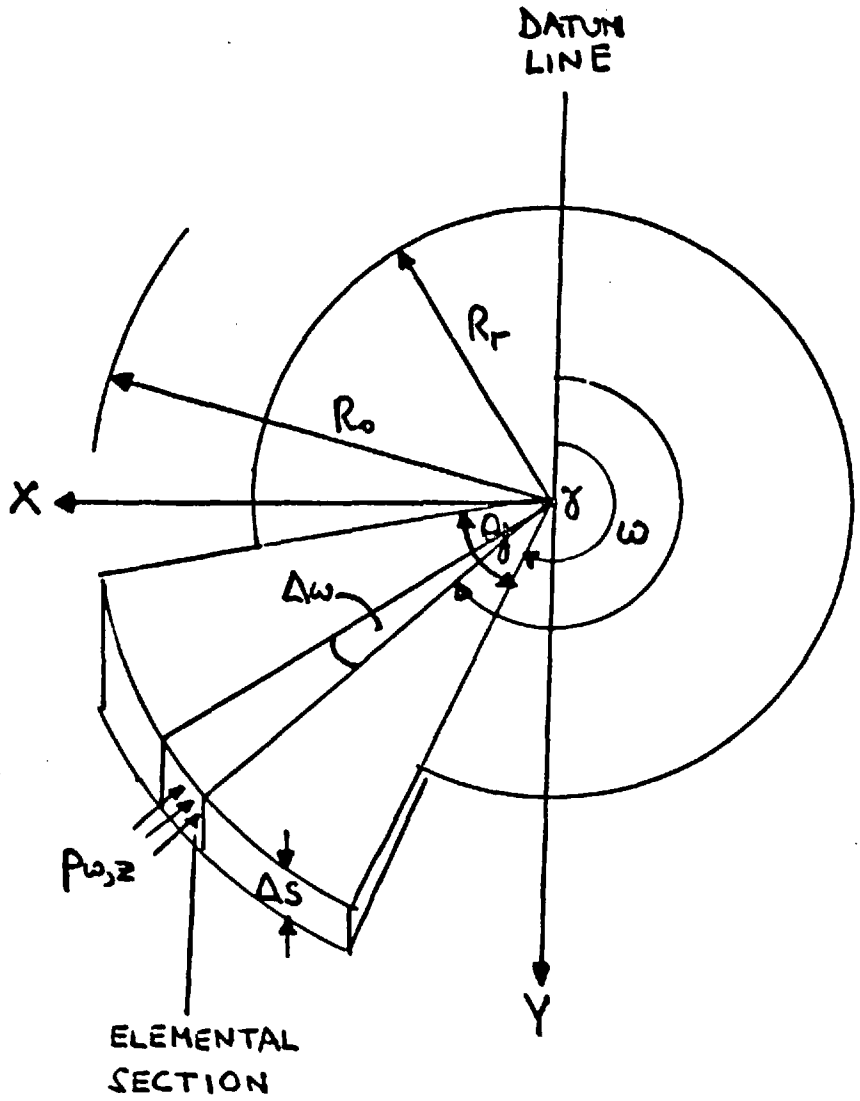

FIG. 3.8 ELEMENTAL AXIAL SLICE OF THE SCREW IN THE COMPRESSION SECTION

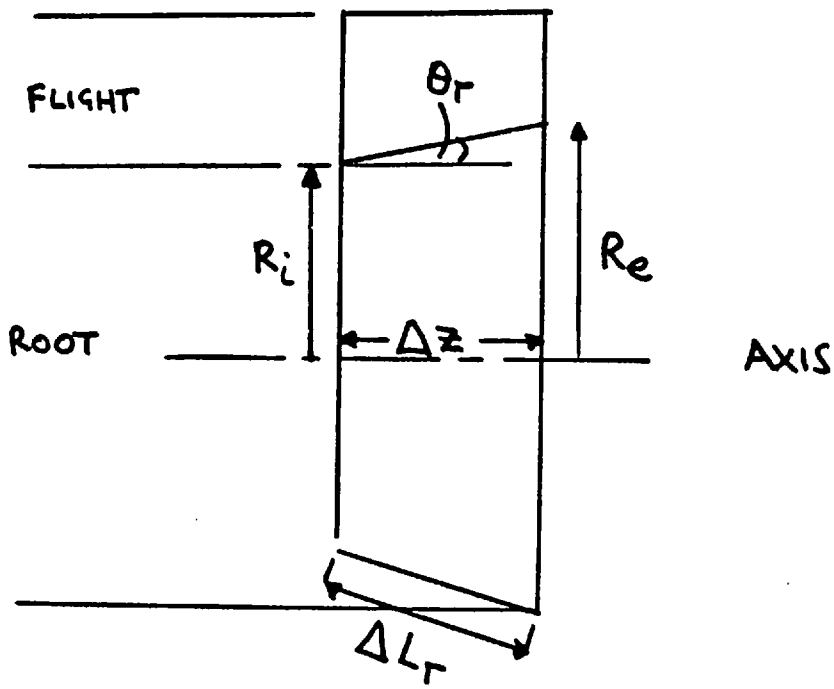

FIG. 3.9 NETT PRESSURE FORCE ACTING ON THE FLIGHT

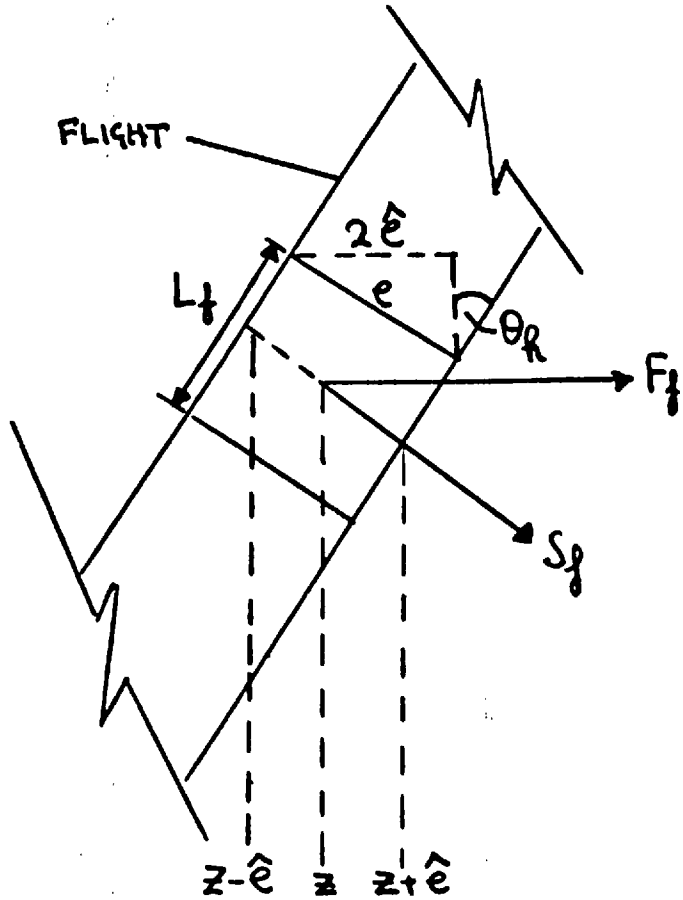

FIC. 3.10 SECTION OF FLIGHT CUT PERPENDICULAR TO THE SCREW AXIS

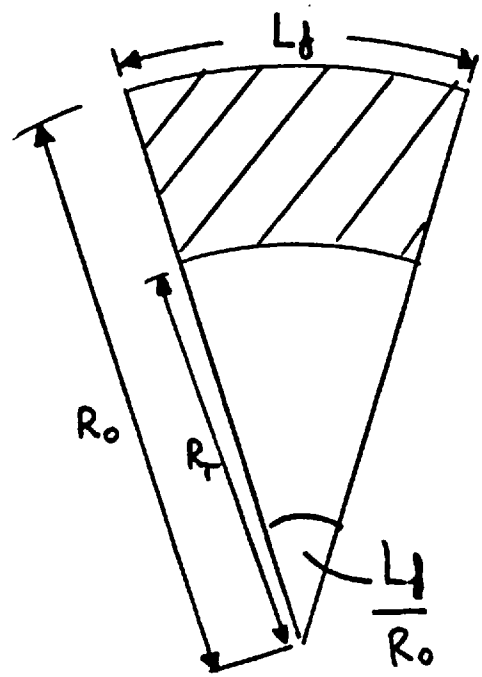

FIG. 3.11 NETT PRESSURE FORCE ACTING ON THE FLIGHT

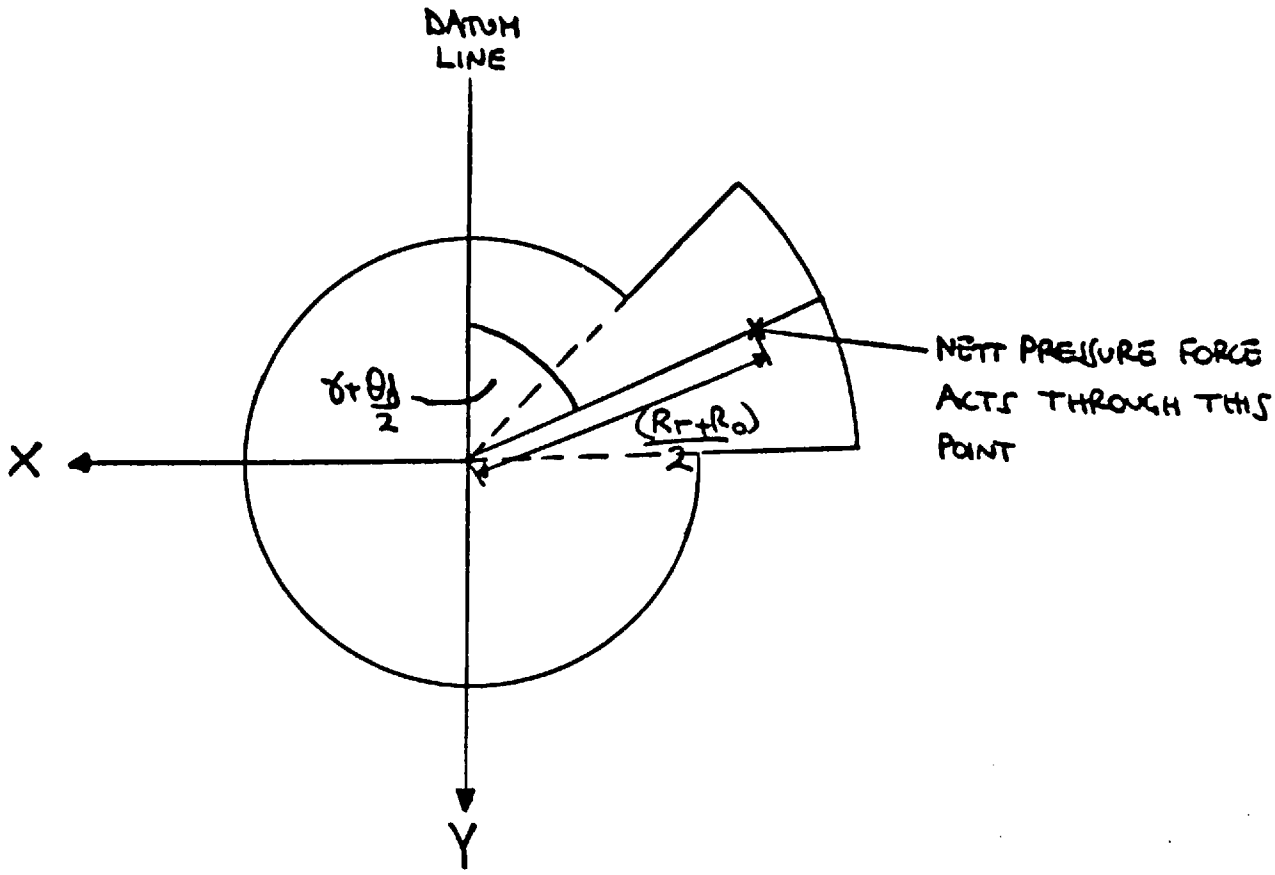

FIG. 3.12 CENTRIFUGAL FLIGHT FORCES

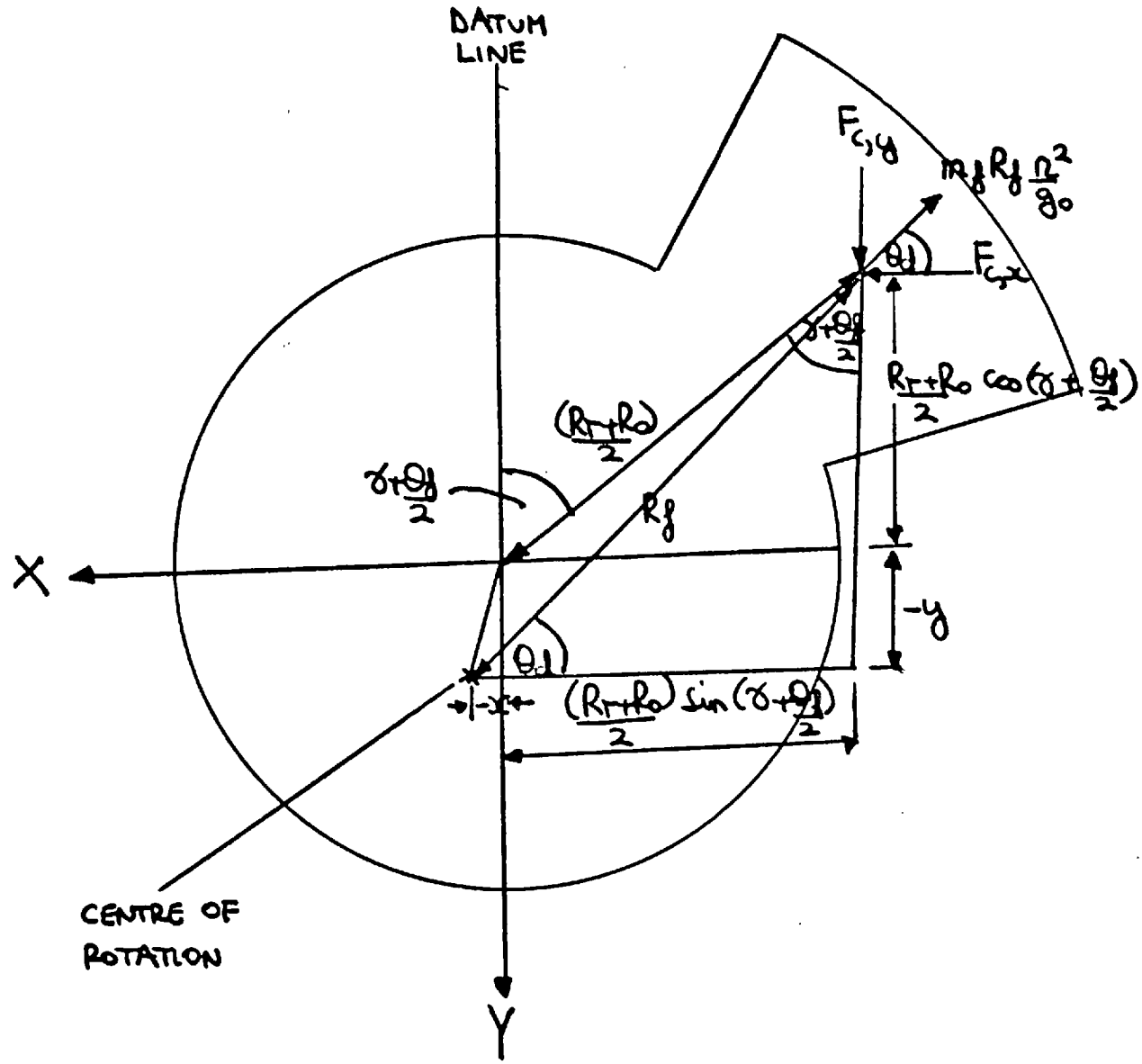

FIG. 3.13 CENTRIFUGAL FORCES CAUSED BY THE SCREW'S DISPLACED CENTRE OF GRAVITY

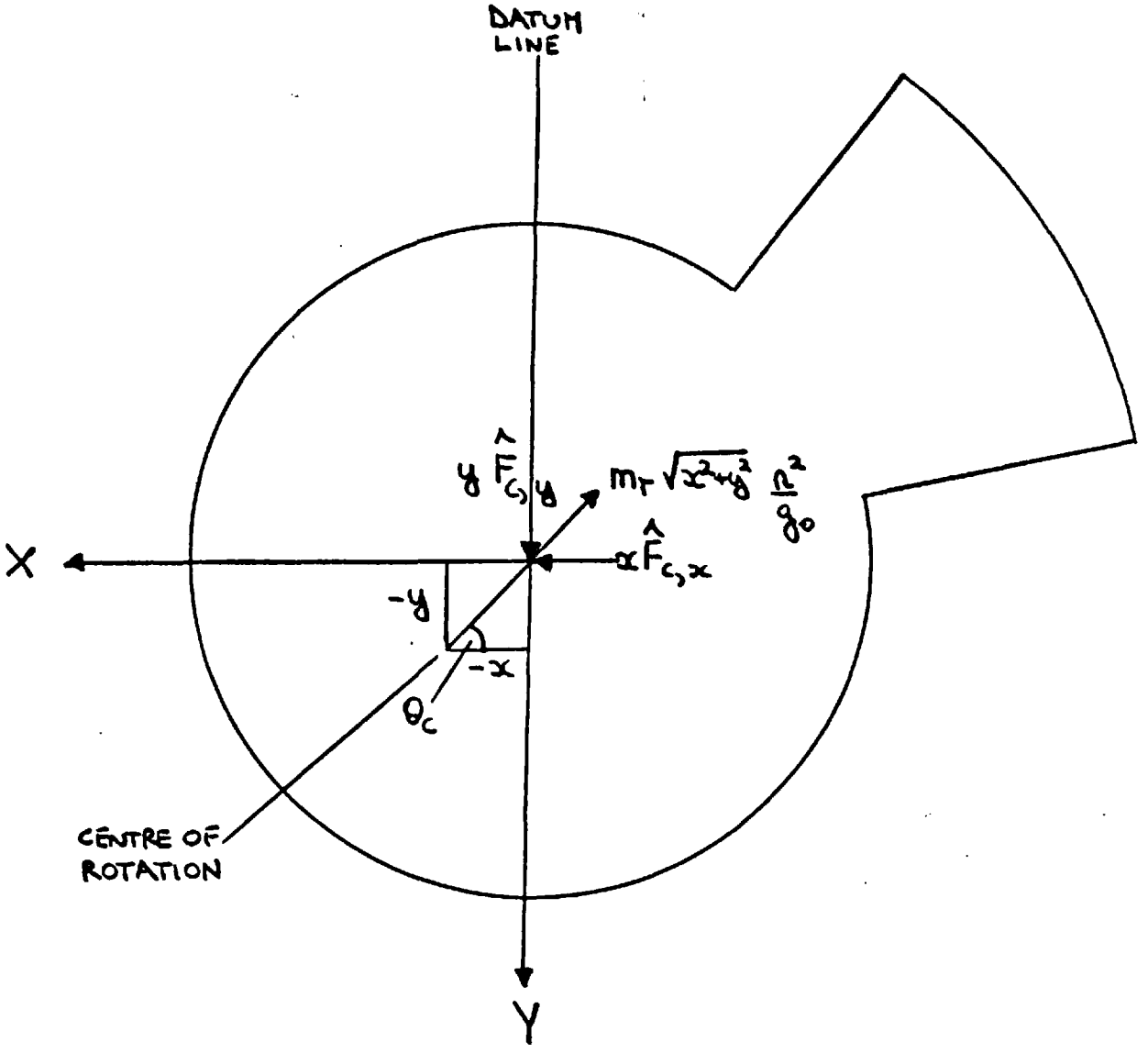

FIG. 3.14 WEIGHT OF THE SCREW

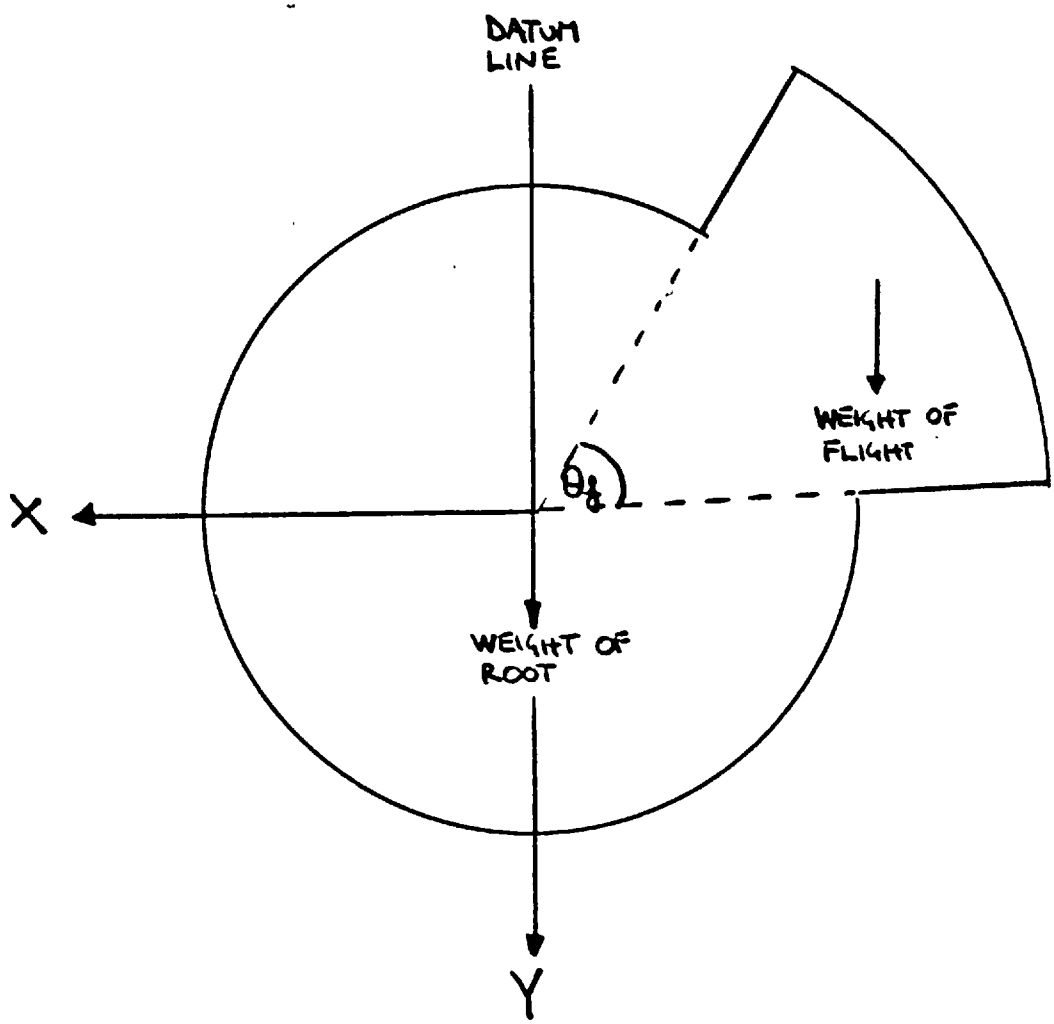

FIG. 3.15 INTERNAL AXIAL FORCE ACTING ON THE SCREW

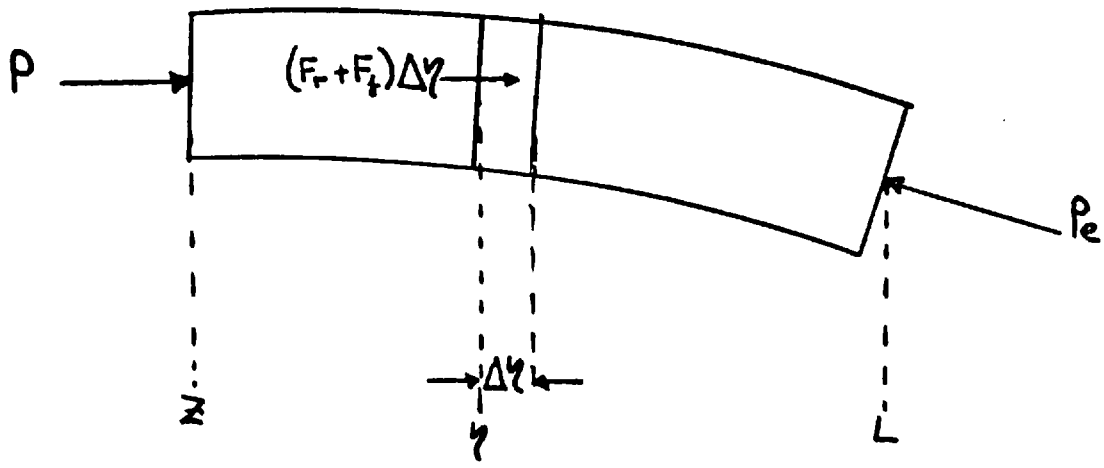

FIG. 3.16 AN ELEMENTAL AXIAL SLICE OF THE SCREW WITH SHEAR FORCES AND BENDING MOMENTS SHOWN

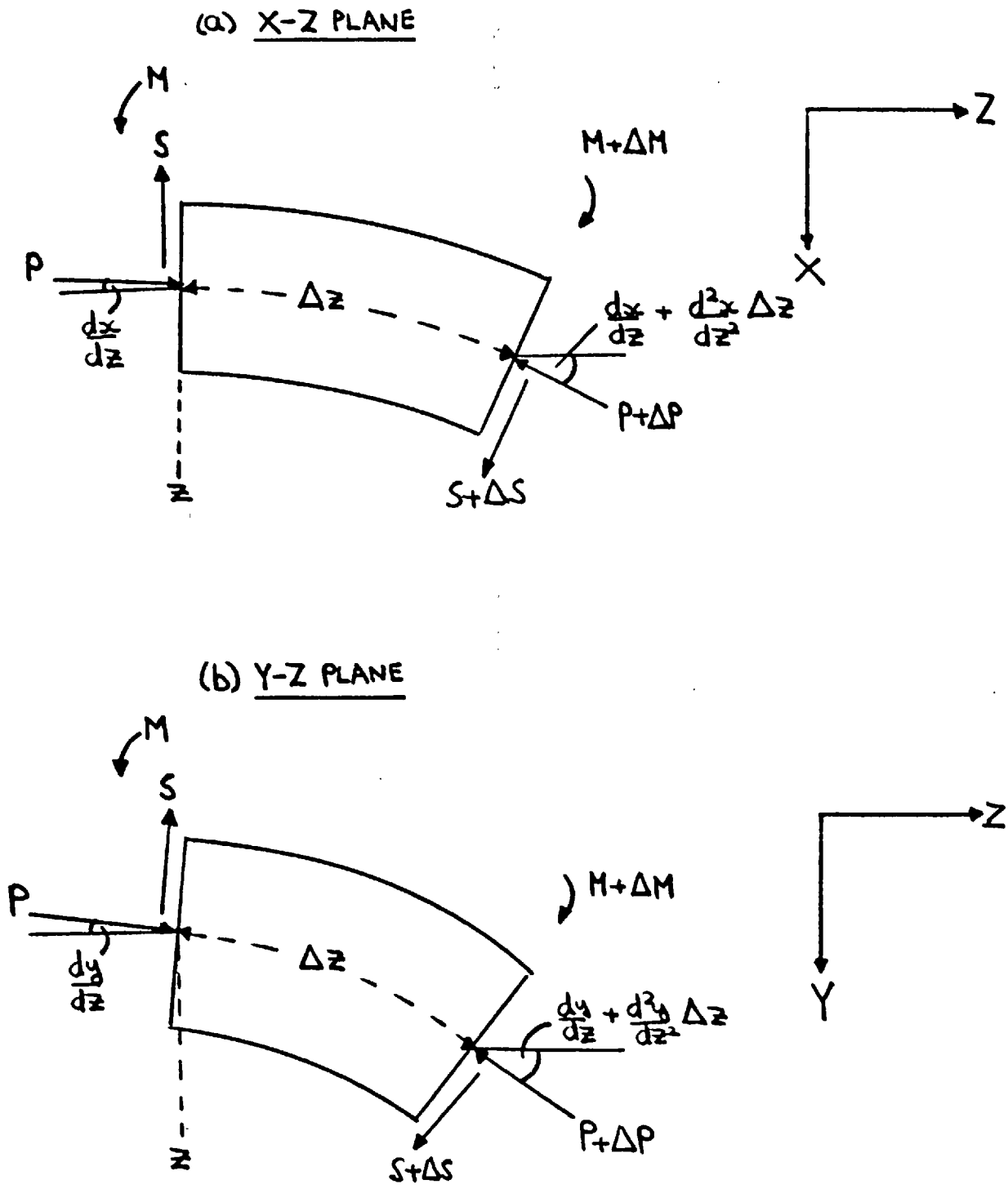

FIG. 3.17 SCREW SHANK HELD IN BEARINGS

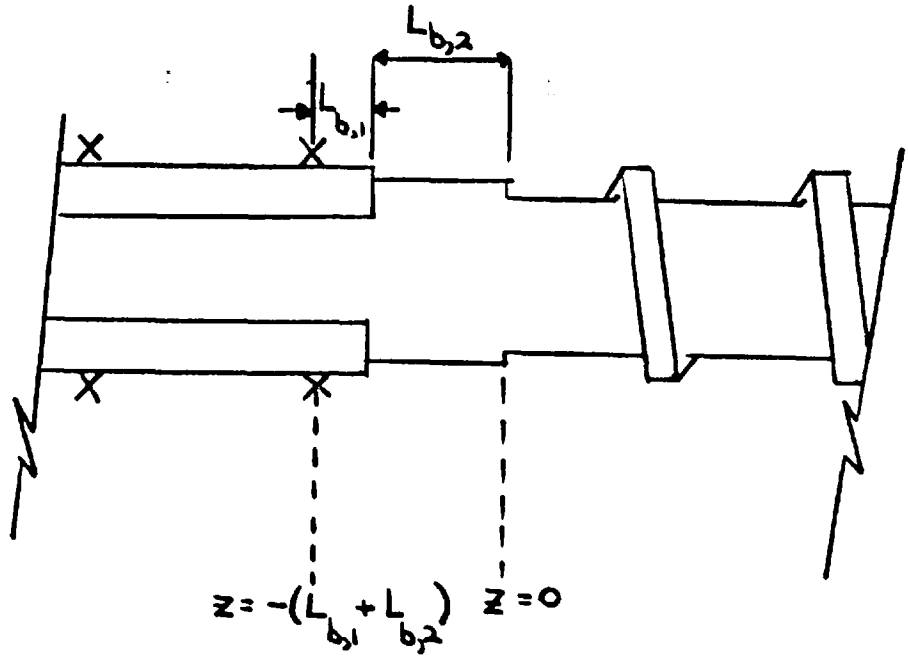

FIG. 3.18

Computer Program Flow Chart

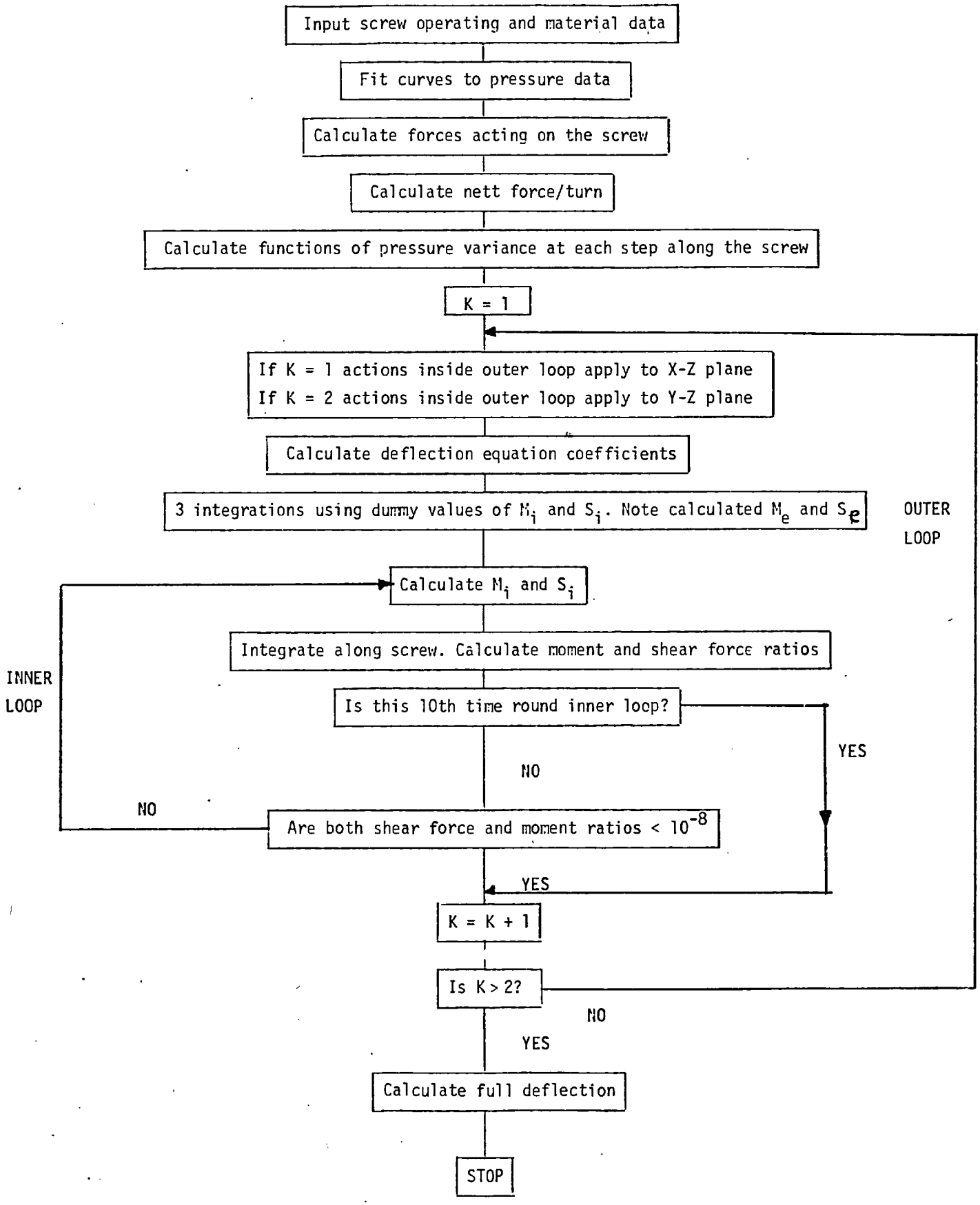

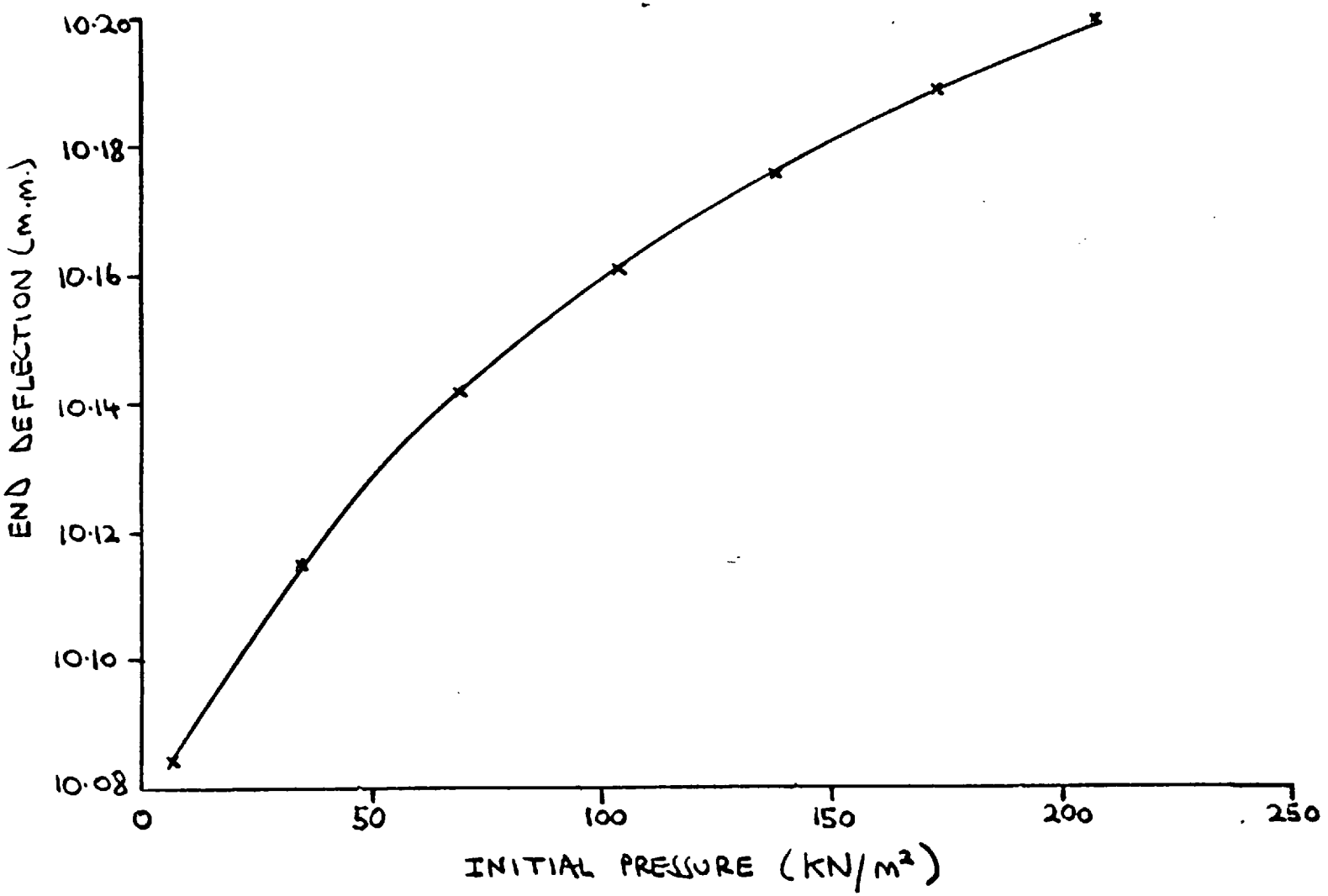

FIG. 3.19 THE EFFECT OF ASSUMED INITIAL PRESSURE ON THE END DEFLECTION IN EXPERIMENT 5

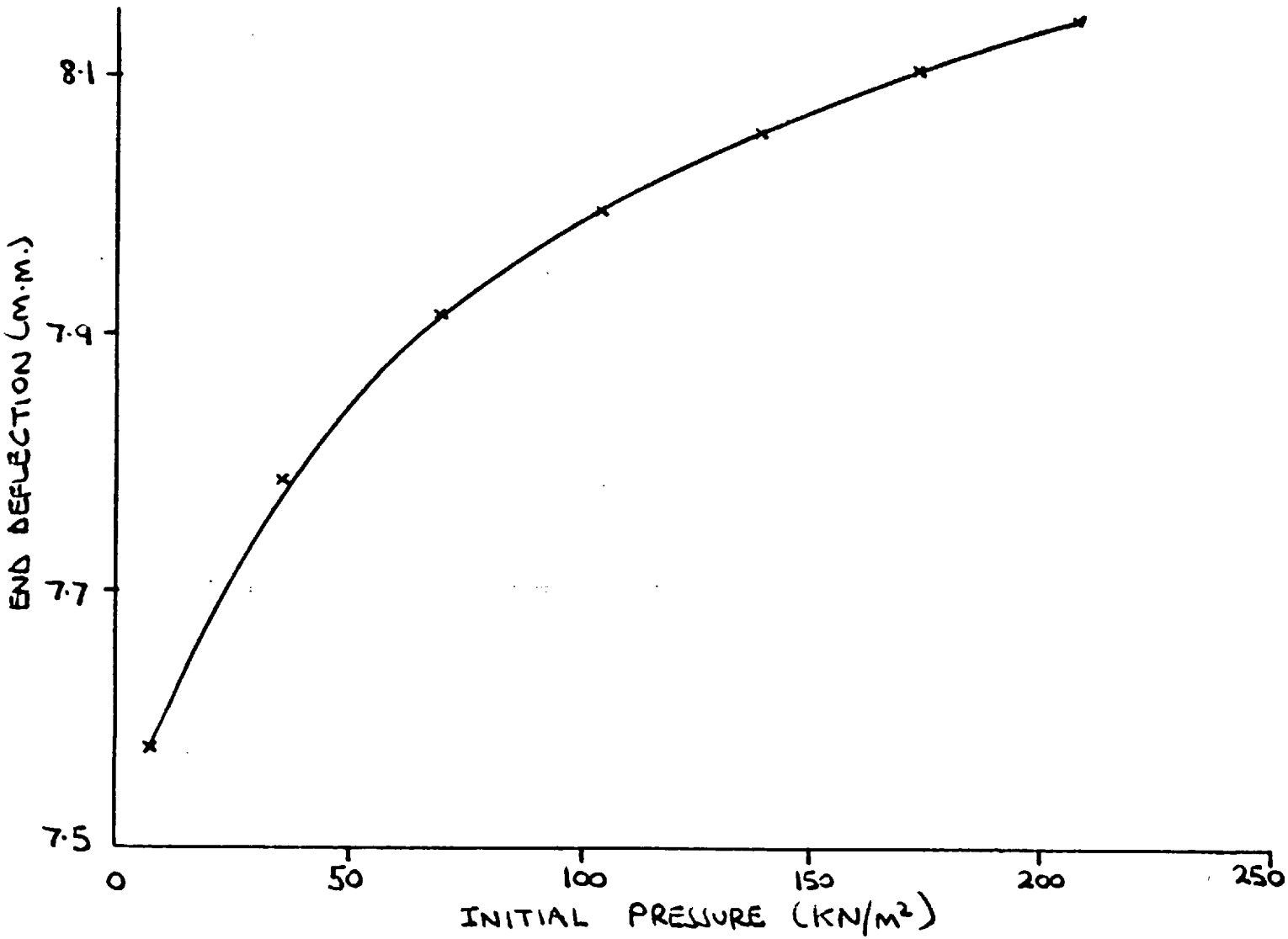

FIG. 3.20 THE EFFECT OF ASSUMED INITIAL PRESSURE ON THE END DEFLECTION IN EXPERIMENT 6

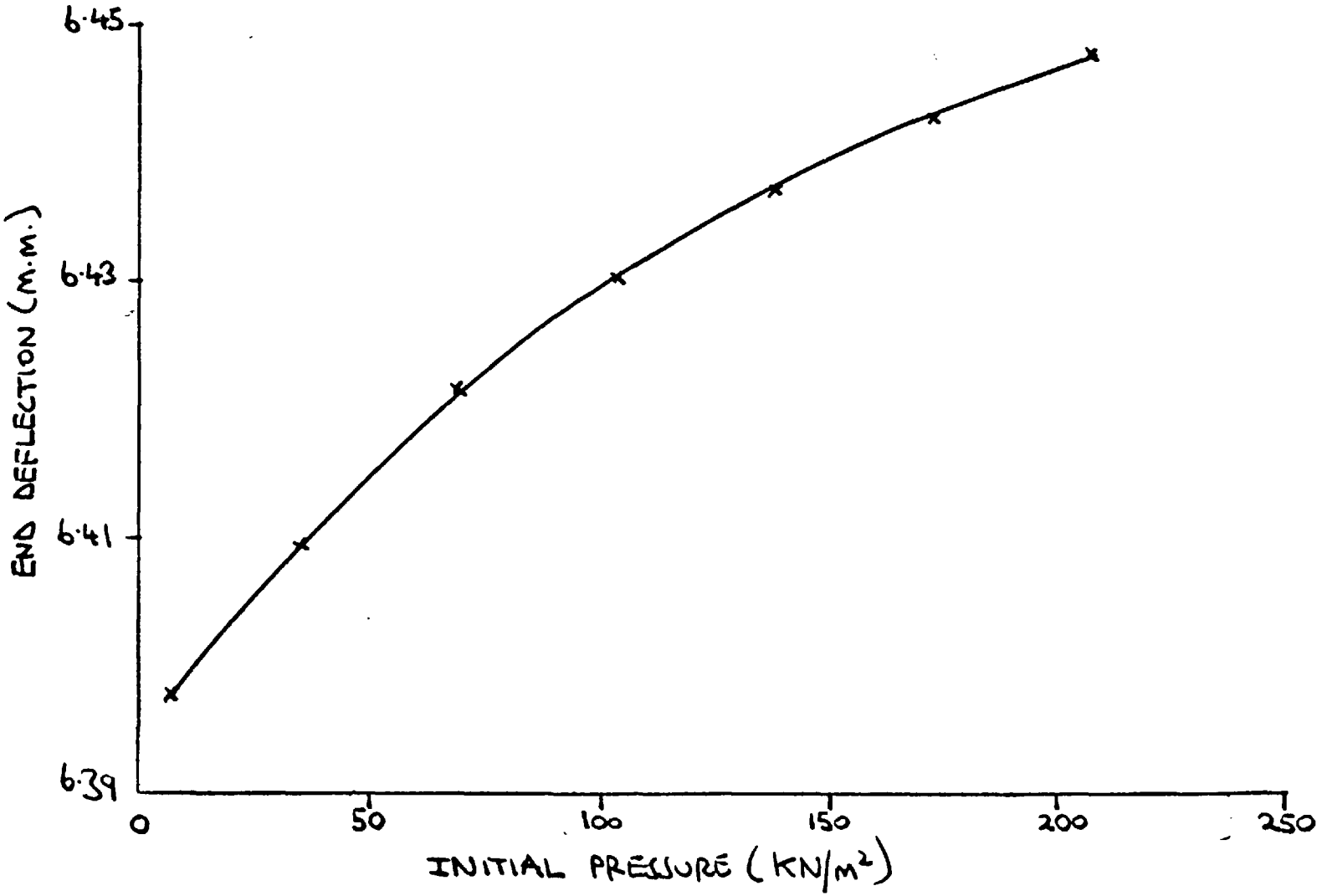

FIG. 3.21 THE EFFECT OF ASSUMED INITIAL PRESSURE ON THE END DEFLECTION IN EXPERIMENT 21

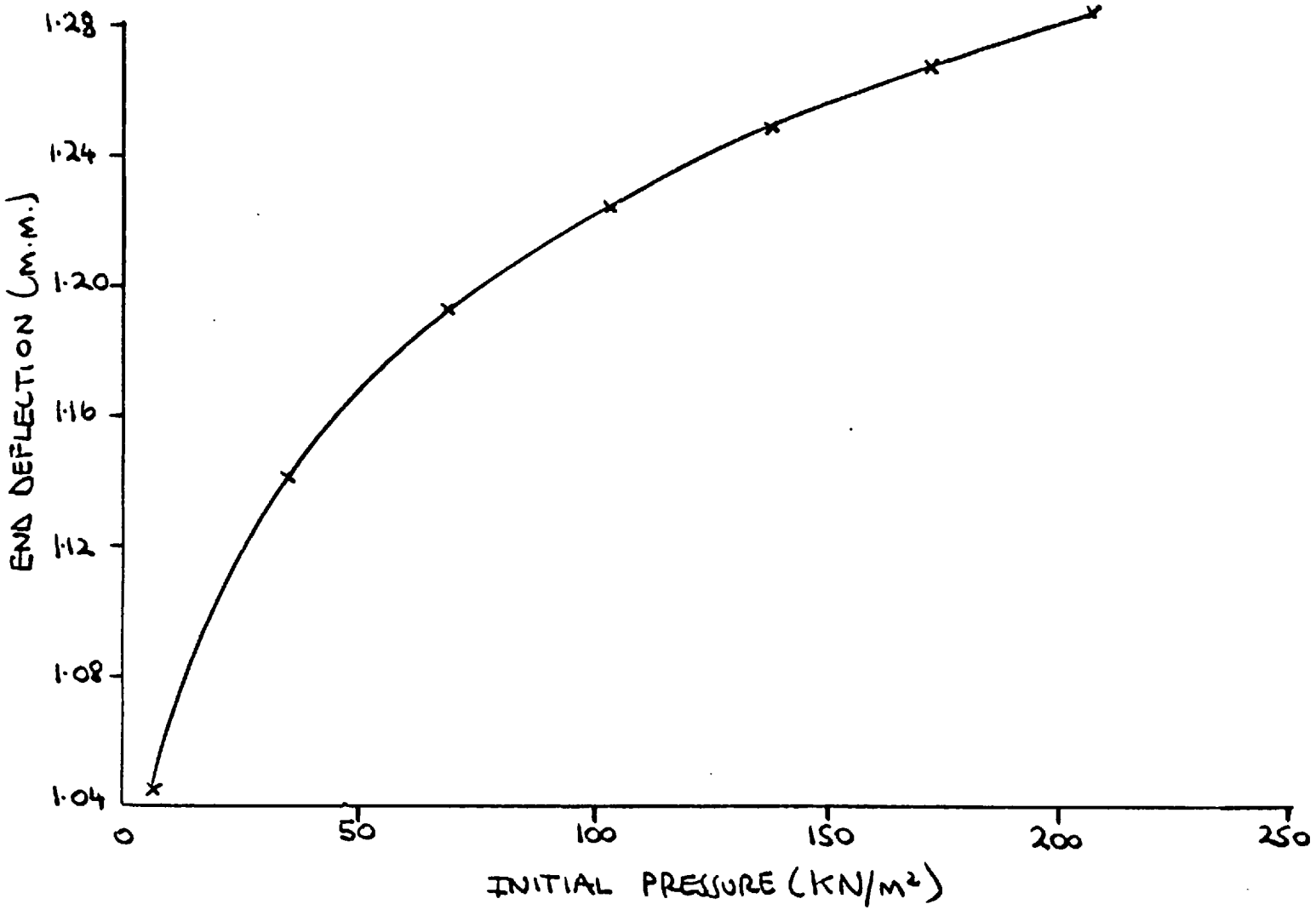

FIG. 3.22 THE EFFECT OF ASSUMED INITIAL PRESSURE ON THE END DEFLECTION IN EXPERIMENT 22

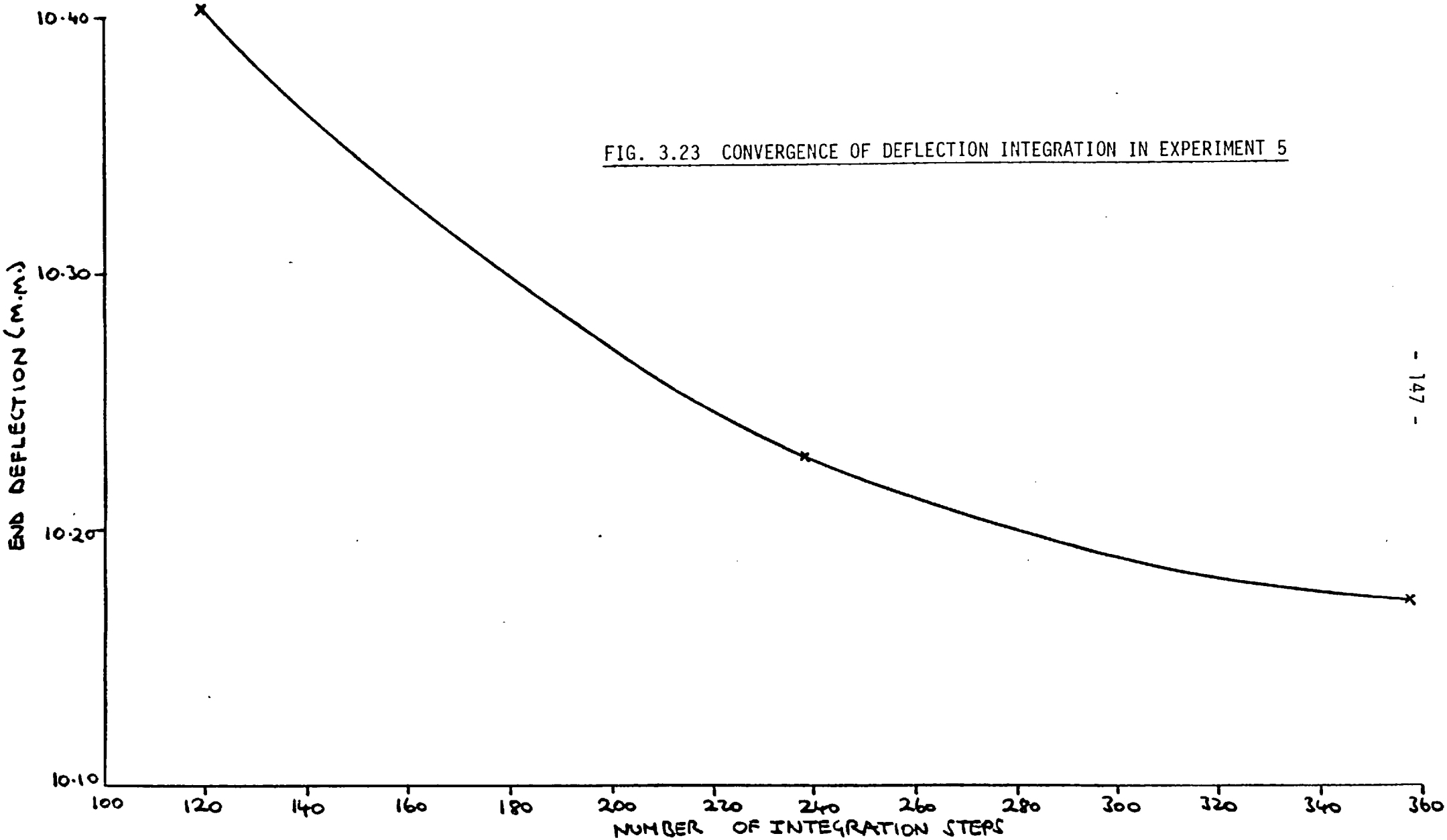

FIG. 3.23 CONVERGENCE OF DEFLECTION INTEGRATION IN EXPERIMENT 5

FIG. 3.24 CONVERGENCE OF DEFLECTION INTEGRATION IN EXPERIMENT 6

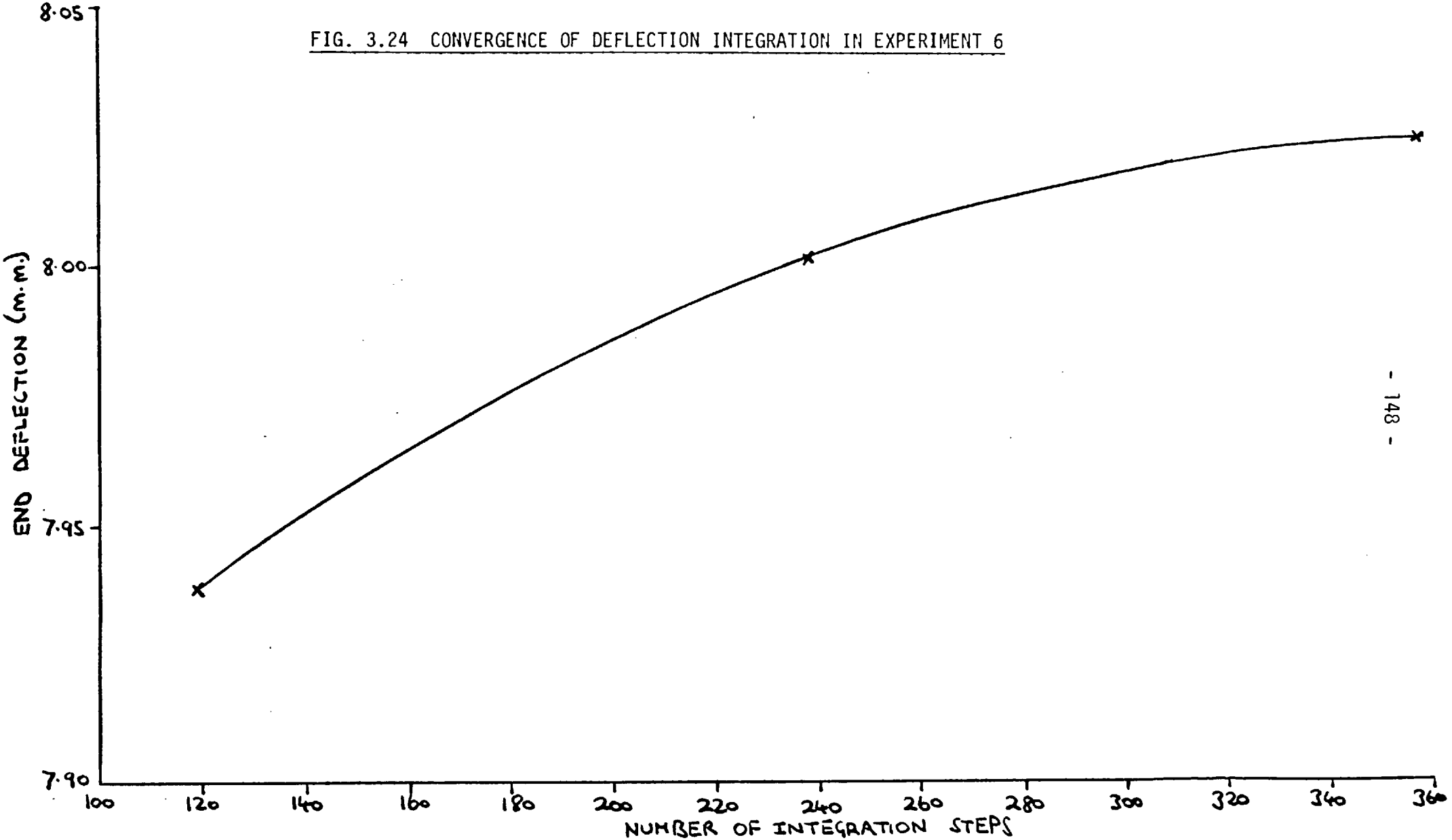

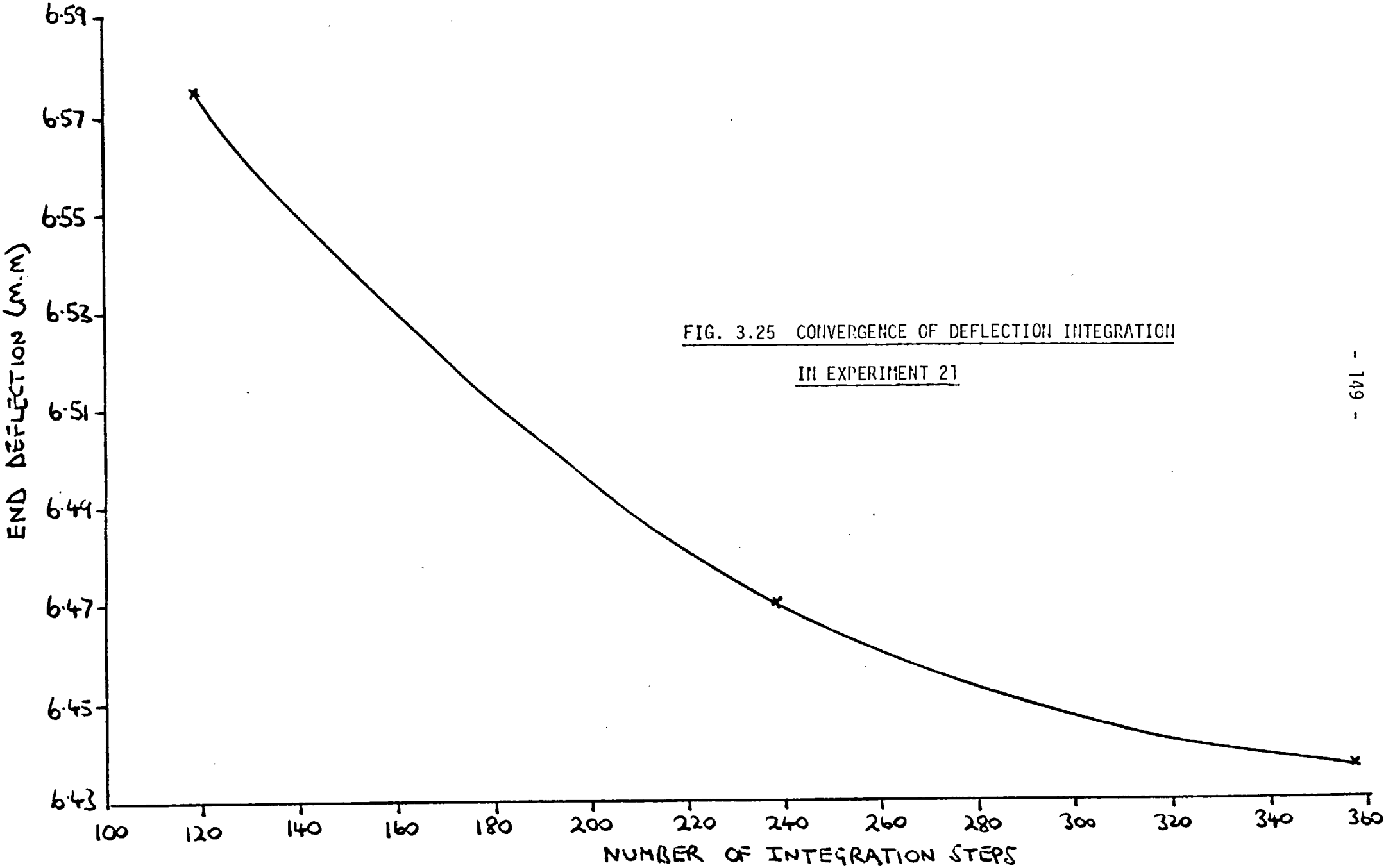

FIG. 3.25 CONVERGENCE OF DEFLECTION INTEGRATION IN EXPERIMENT 21

FIG. 3.26 CONVERGENCE OF DEFLECTION INTEGRATION IN EXPERIMENT 22

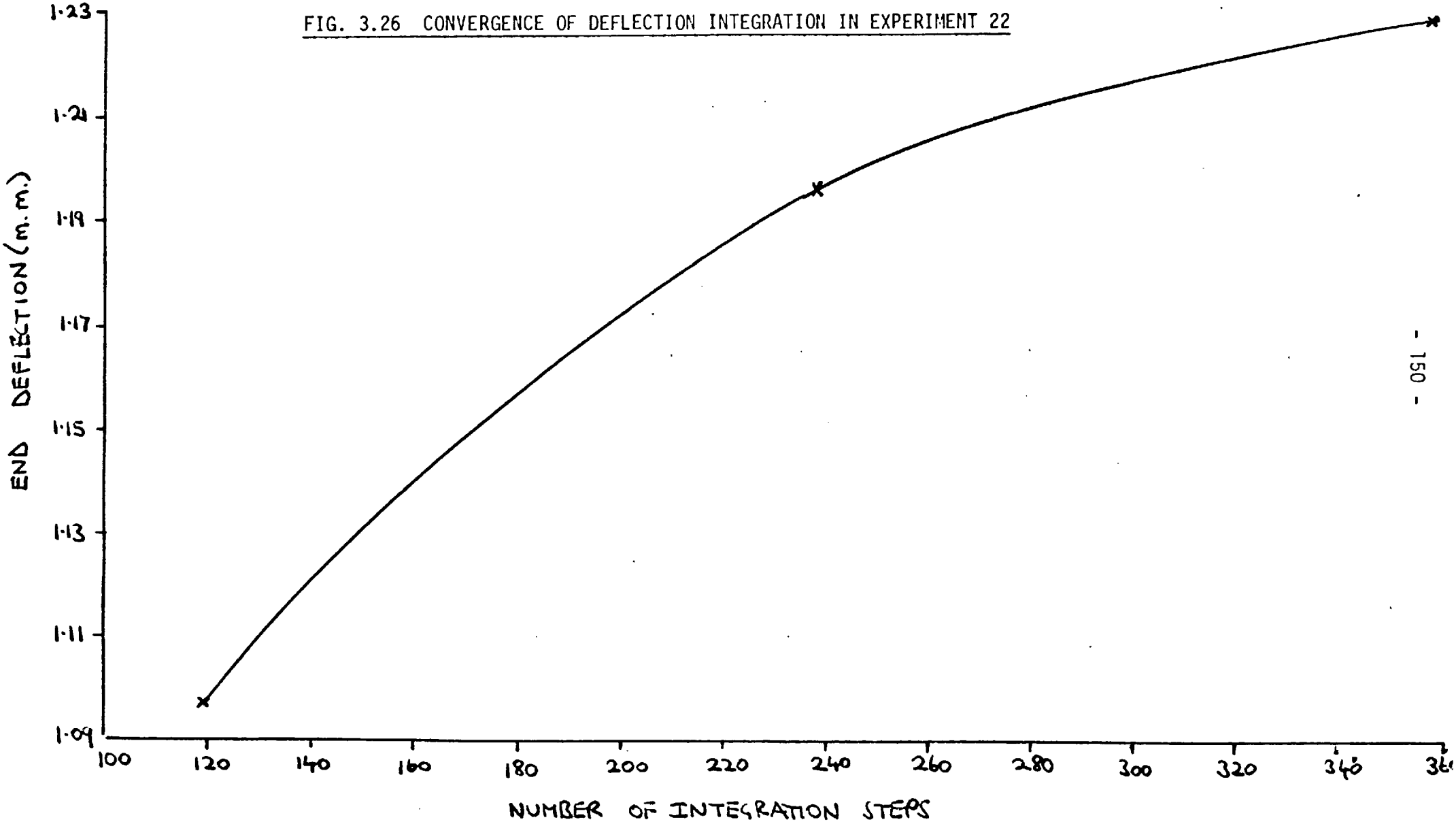

FIG. 3.27 END DEFLECTION VERSUS ROTATIONAL POSITION OF THE SCREW

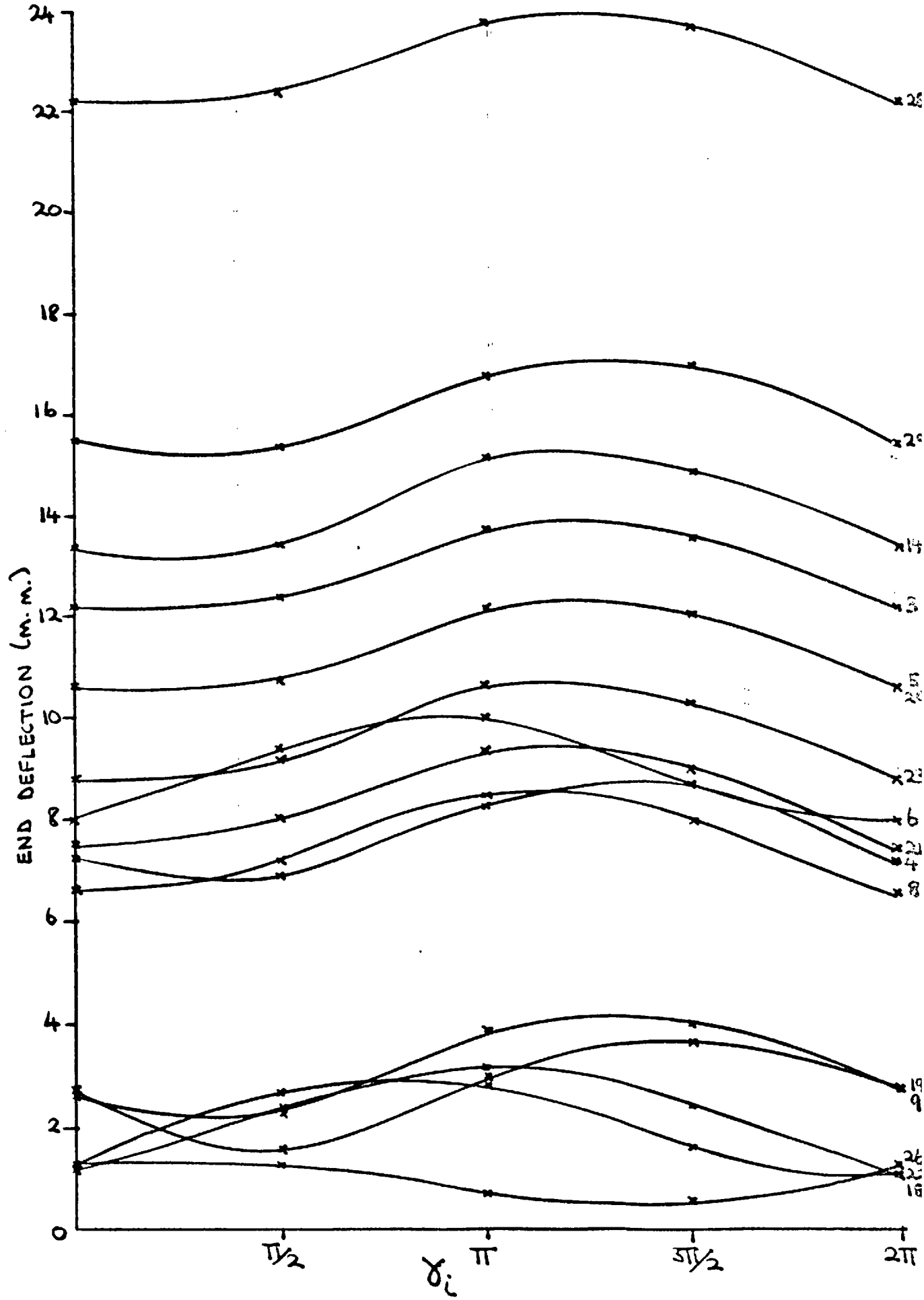

FIG. 3.28 END DEFLECTION VERSUS PRESSURE VARIANCE GRADIENT

SUMMATION ALONG THE SCREW: $\gamma_i = 0$

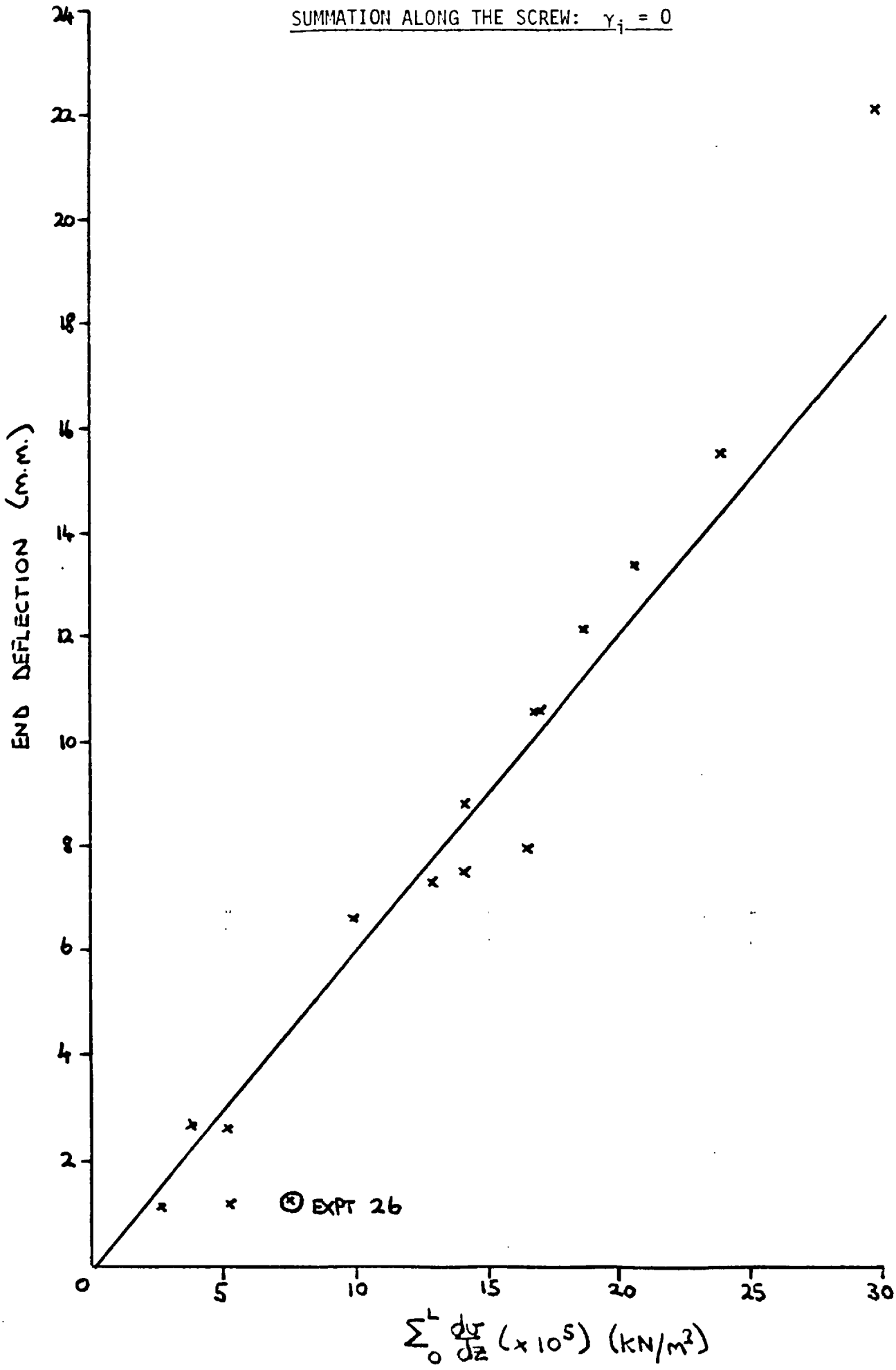

FIG. 3.29 END DEFLECTION VERSUS PRESSURE VARIANCE GRADIENT SUMMATION ALONG THE SCREW: $\gamma_i = \pi/2$

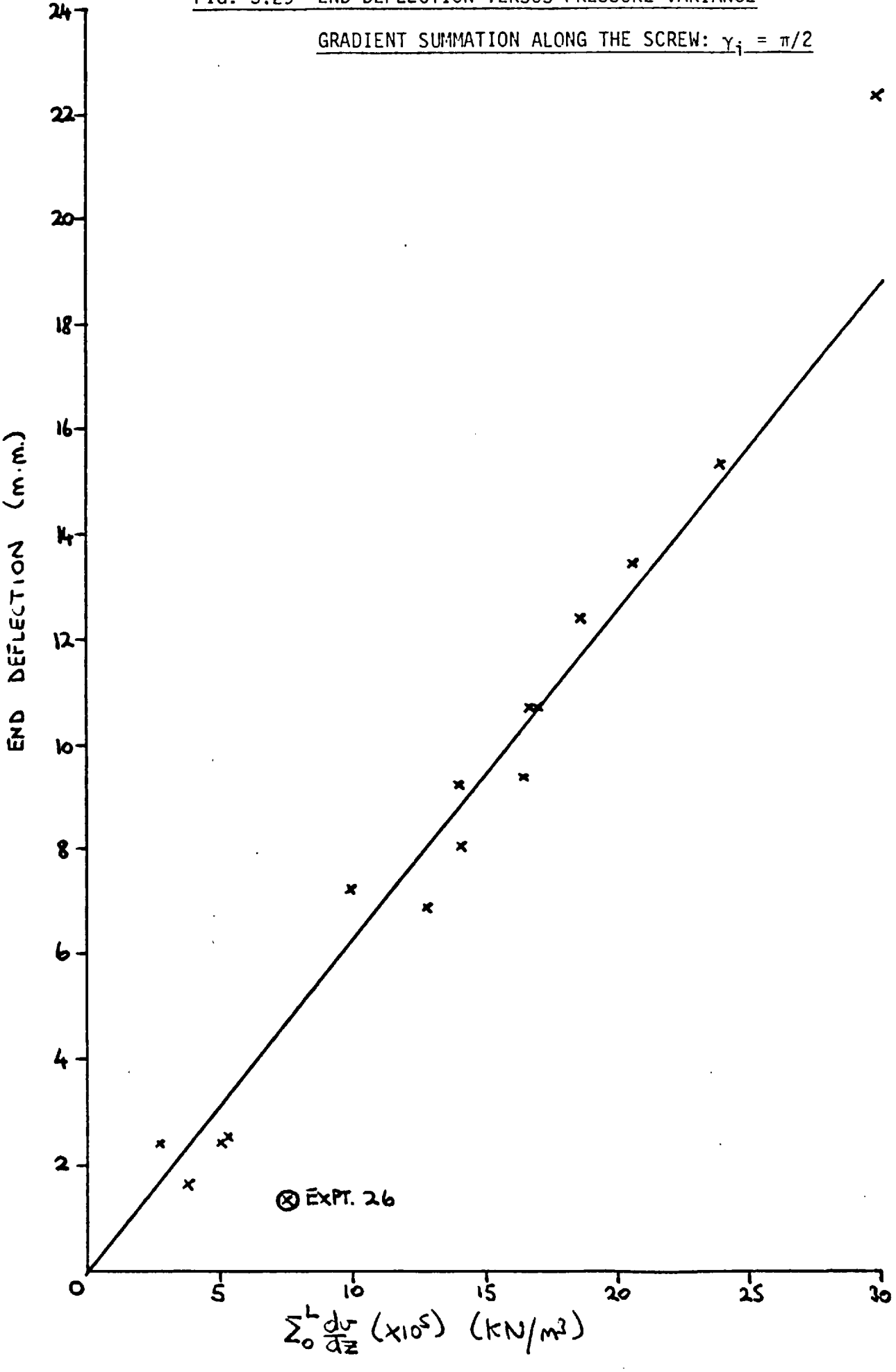

FIG. 3.30 END DEFLECTION VERSUS PRESSURE VARIANCE GRADIENT SUMMATION ALONG THE SCREW: $\gamma_i = \pi$

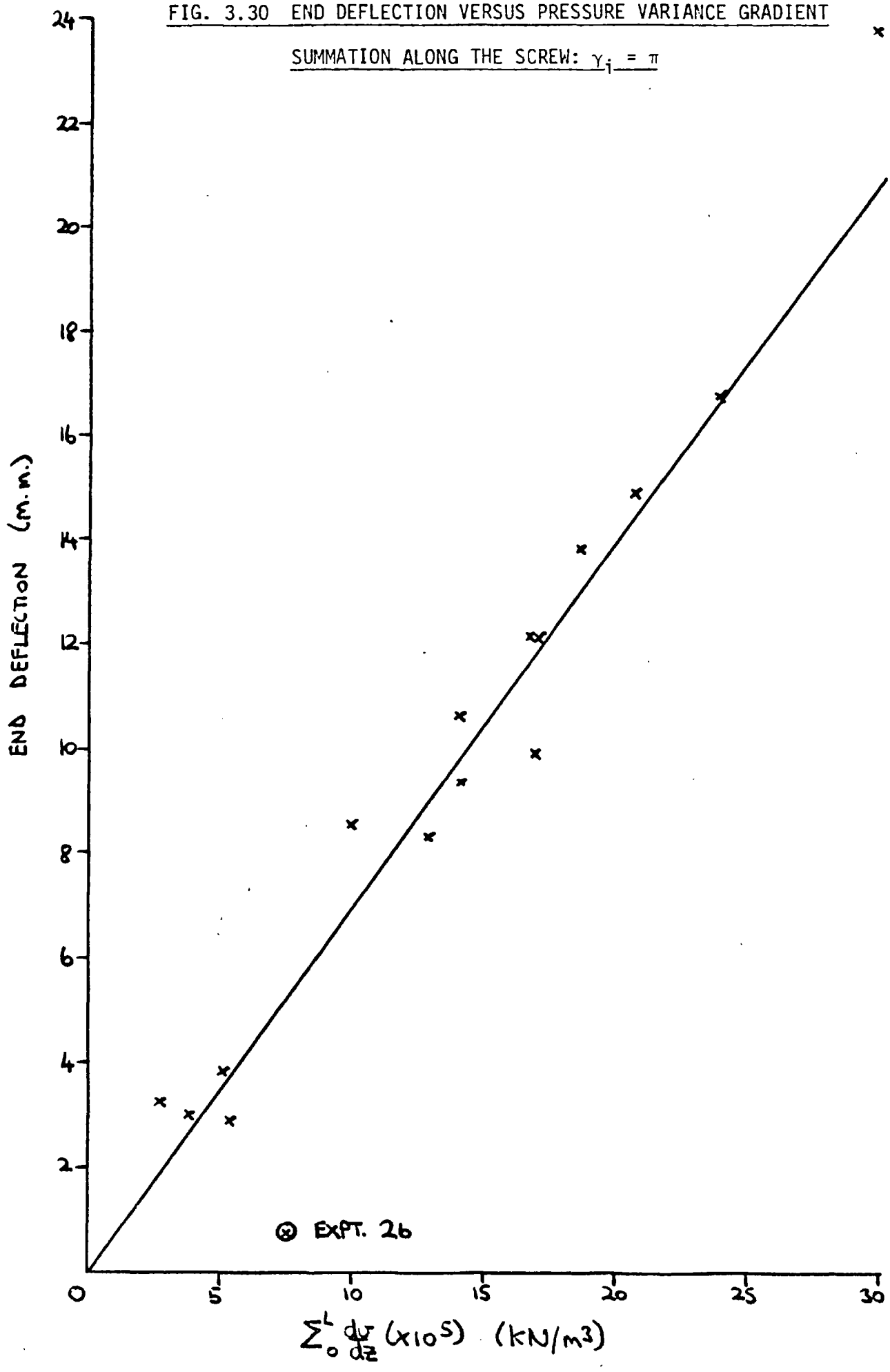

FIG. 3.31 END DEFLECTION VERSUS PRESSURE VARIANCE GRADIENT SUMMATION ALONG THE SCREW: $\gamma_i = 3\pi/2$

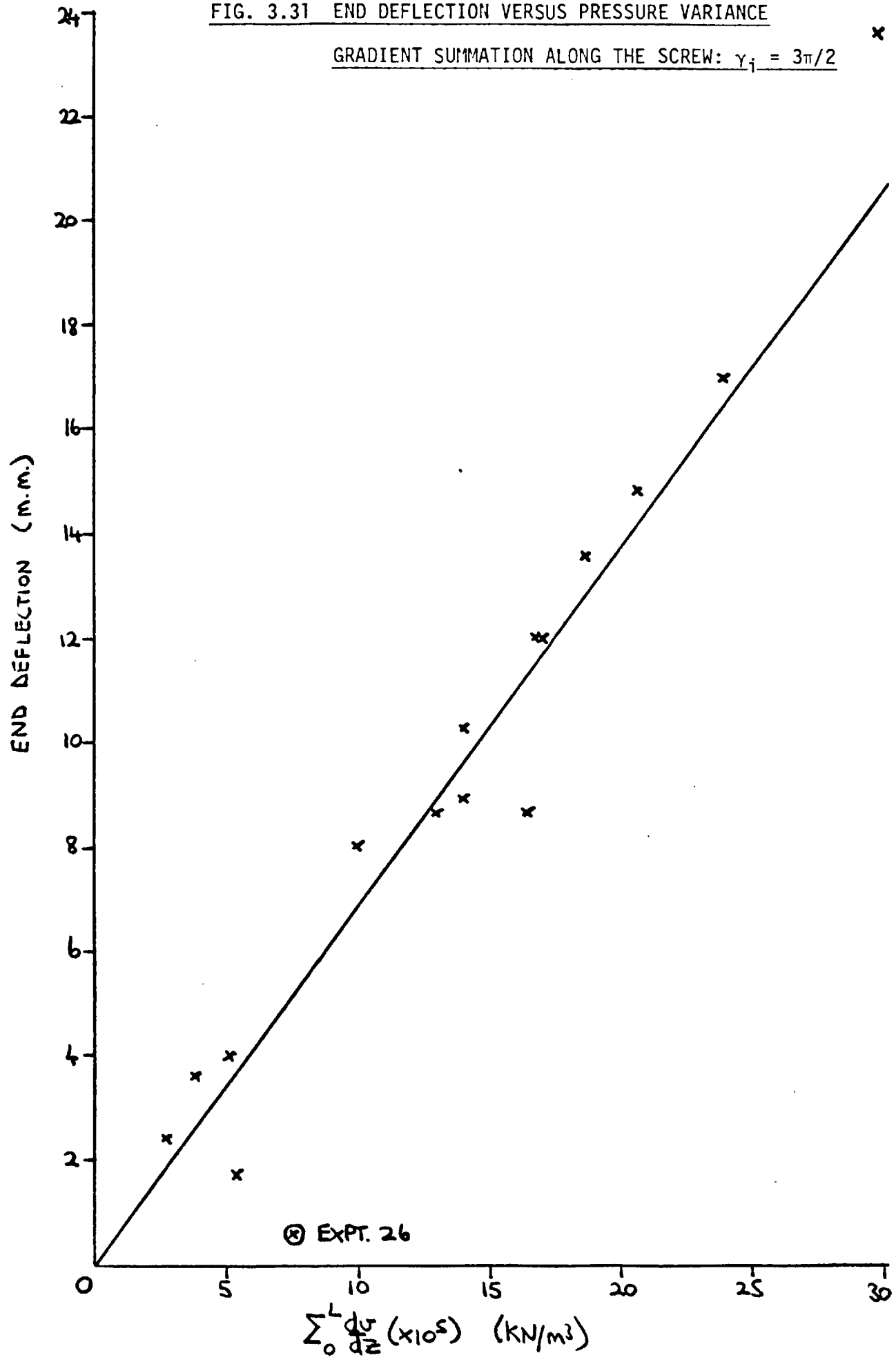

FIG. 3.32 END DEFLECTION VERSUS THE SUMMATION OF THE PRODUCT OF AXIAL POSITION AND THE ABSOLUTE VALUE OF PRESSURE VARIANCE GRADIENT ALONG THE SCREW: $\gamma_i = 0$

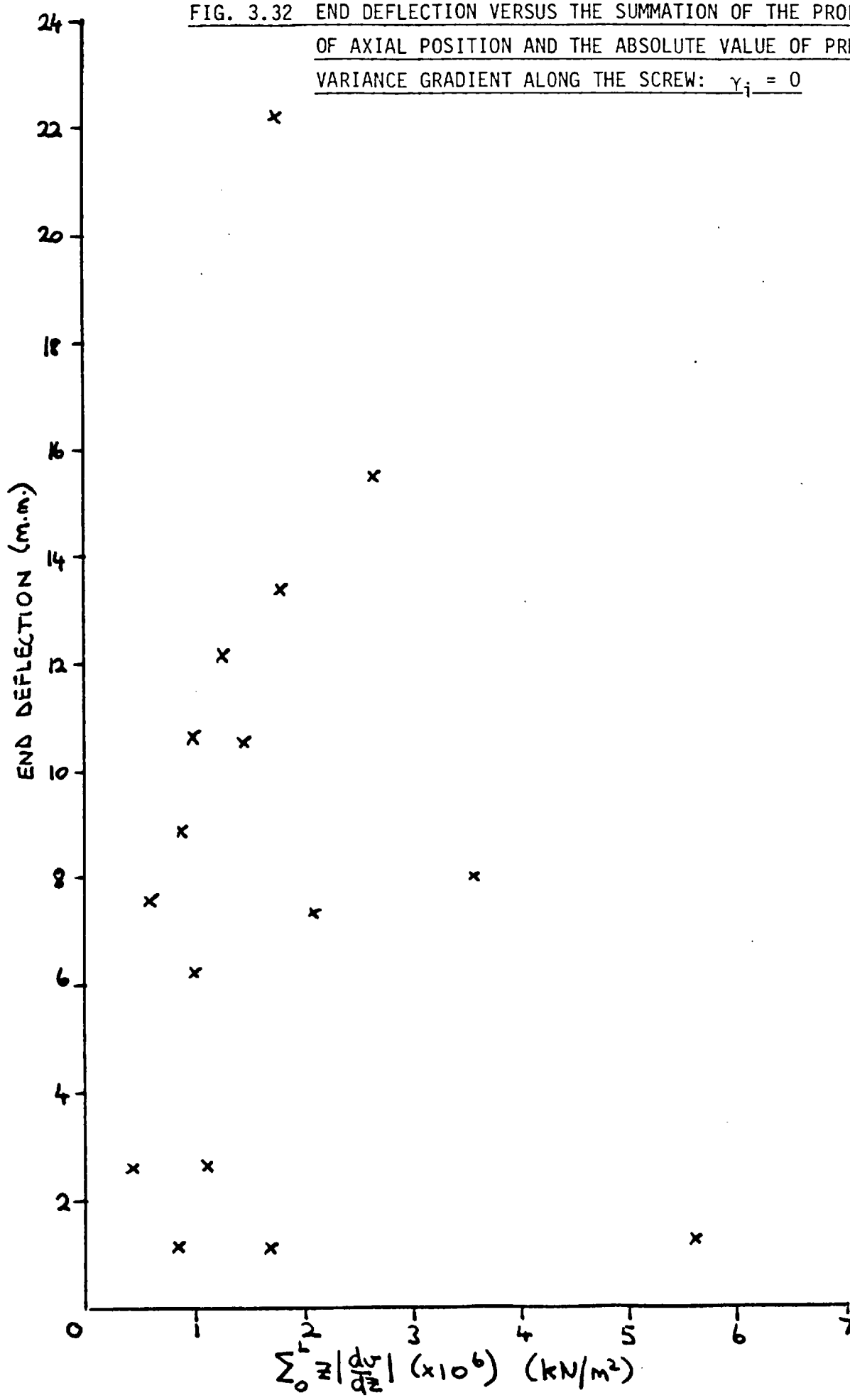

FIG. 3.33 END DEFLECTION VERSUS THE ABSOLUTE VALUE OF PRESSURE VARIANCE GRADIENT ALONG THE SCREW: $\gamma_i = 0$

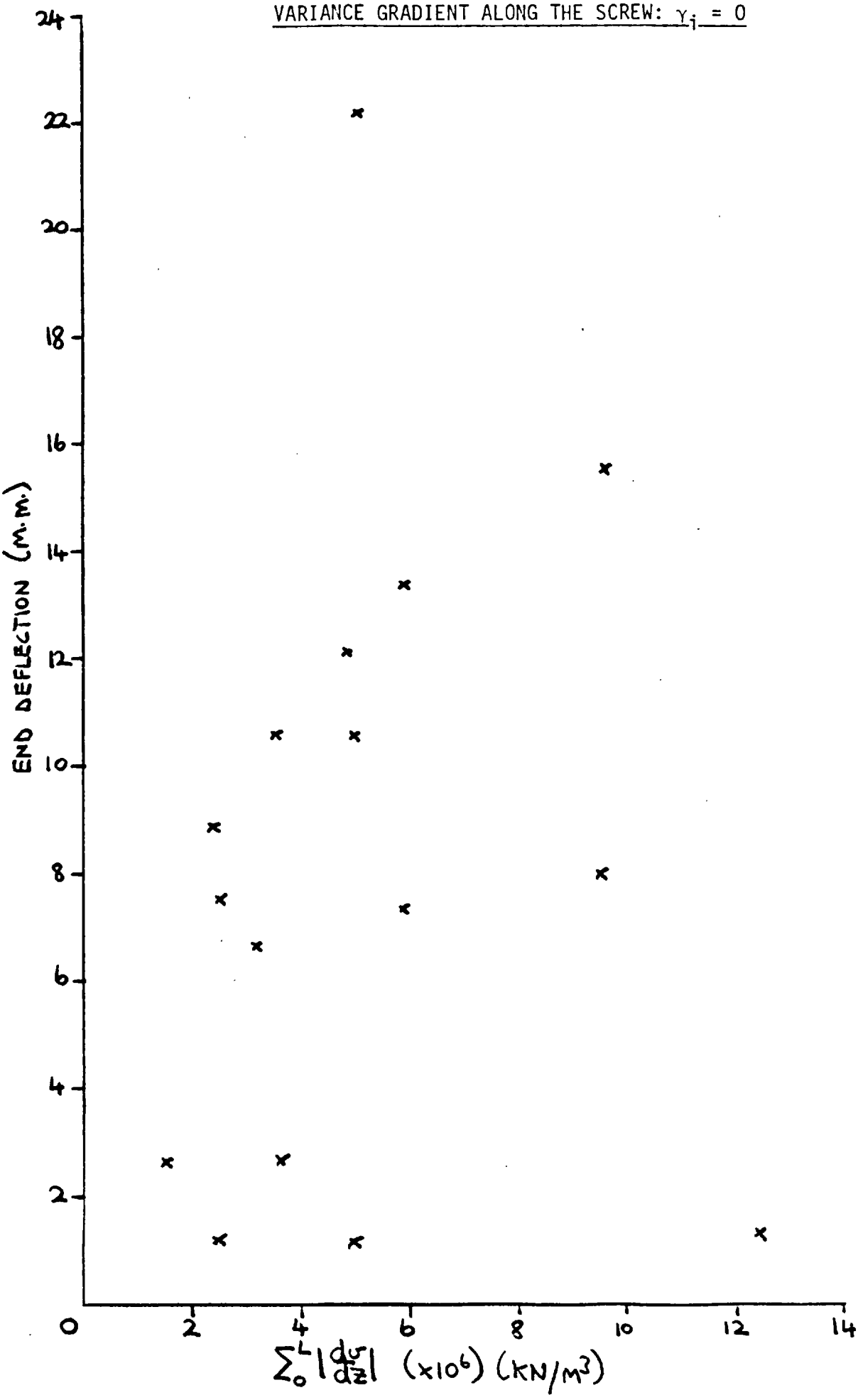

FIG. 3.34 X DEFLECTION FOR 3 COMPONENT FORCE SYSTEMS AS A PERCENTAGE OF THE X DEFLECTION FOR THE FULL FORCE SYSTEM VERSUS DEFLECTION

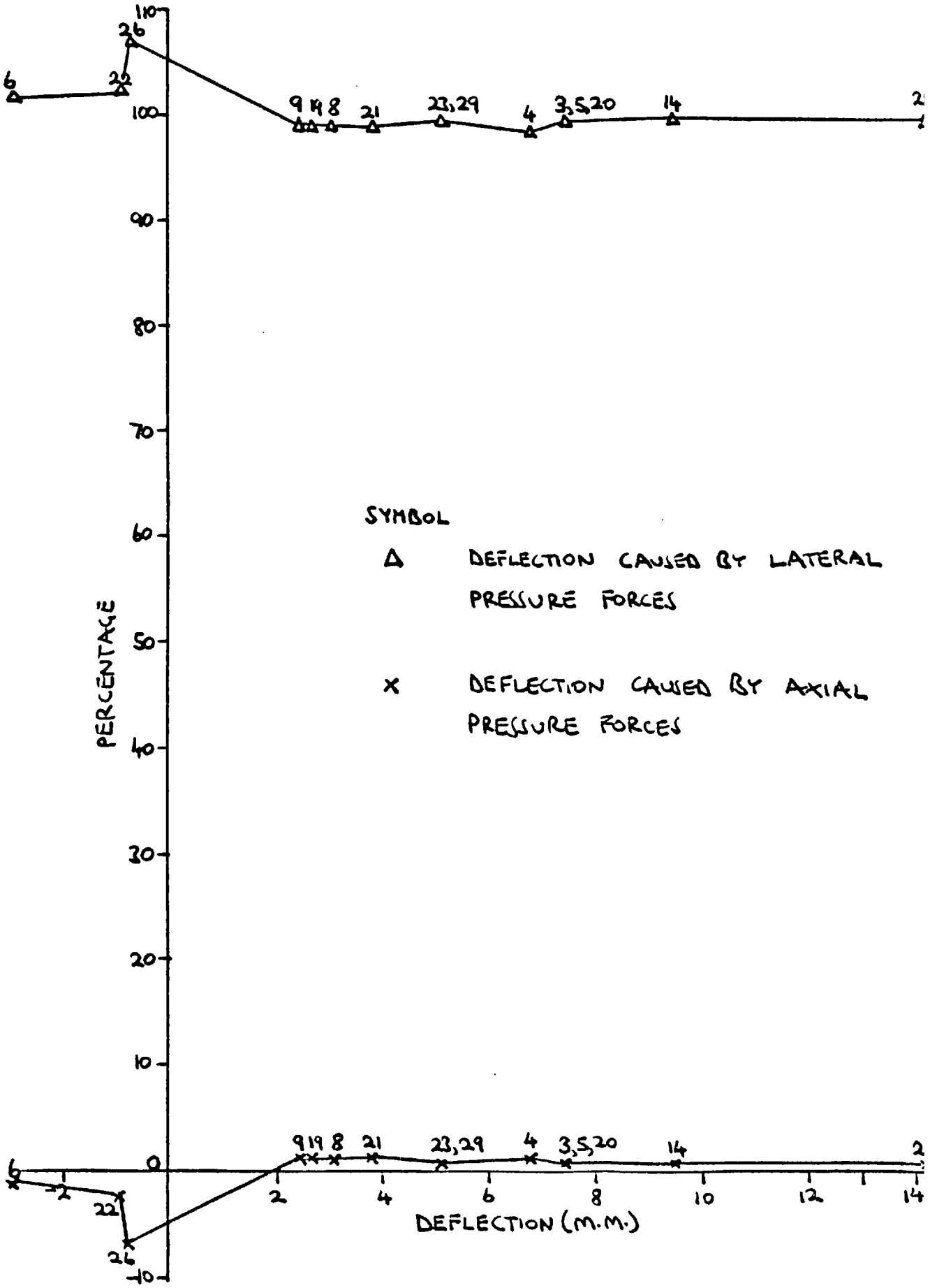

FIG. 3.35 Y DEFLECTION FOR 3 COMPONENT FORCE SYSTEMS AS A PERCENTAGE OF THE Y DEFLECTION FOR THE FULL FORCE SYSTEM VERSUS DEFLECTION

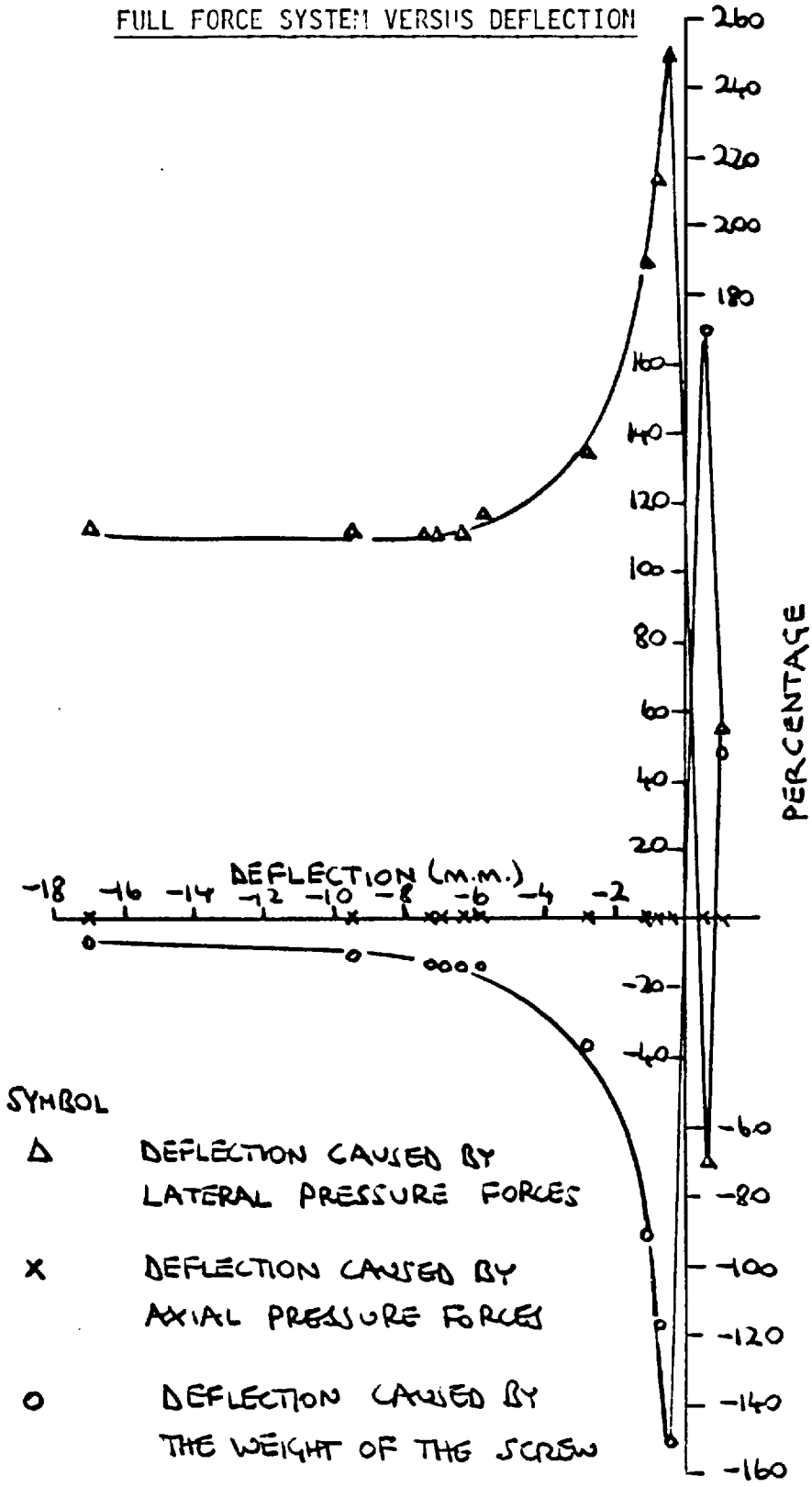

FIG. 3.36 END DEFLECTION/SCREW DIAMETER VERSUS SCREW DIAMETER FOR EXPERIMENT 3

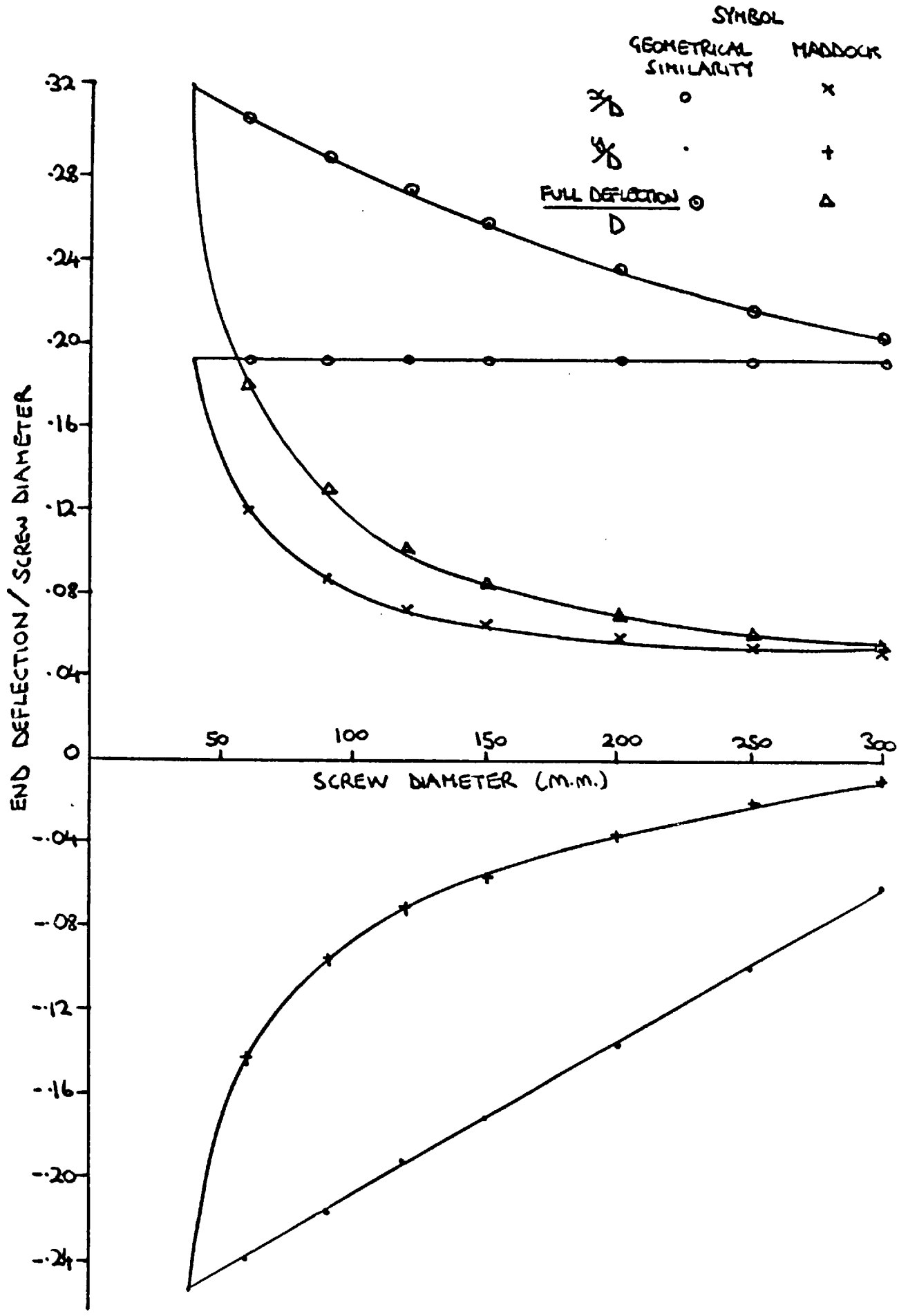

FIG. 3.37 END DEFLECTION/SCREW DIAMETER VERSUS SCREW DIAMETER FOR EXPERIMENT 28

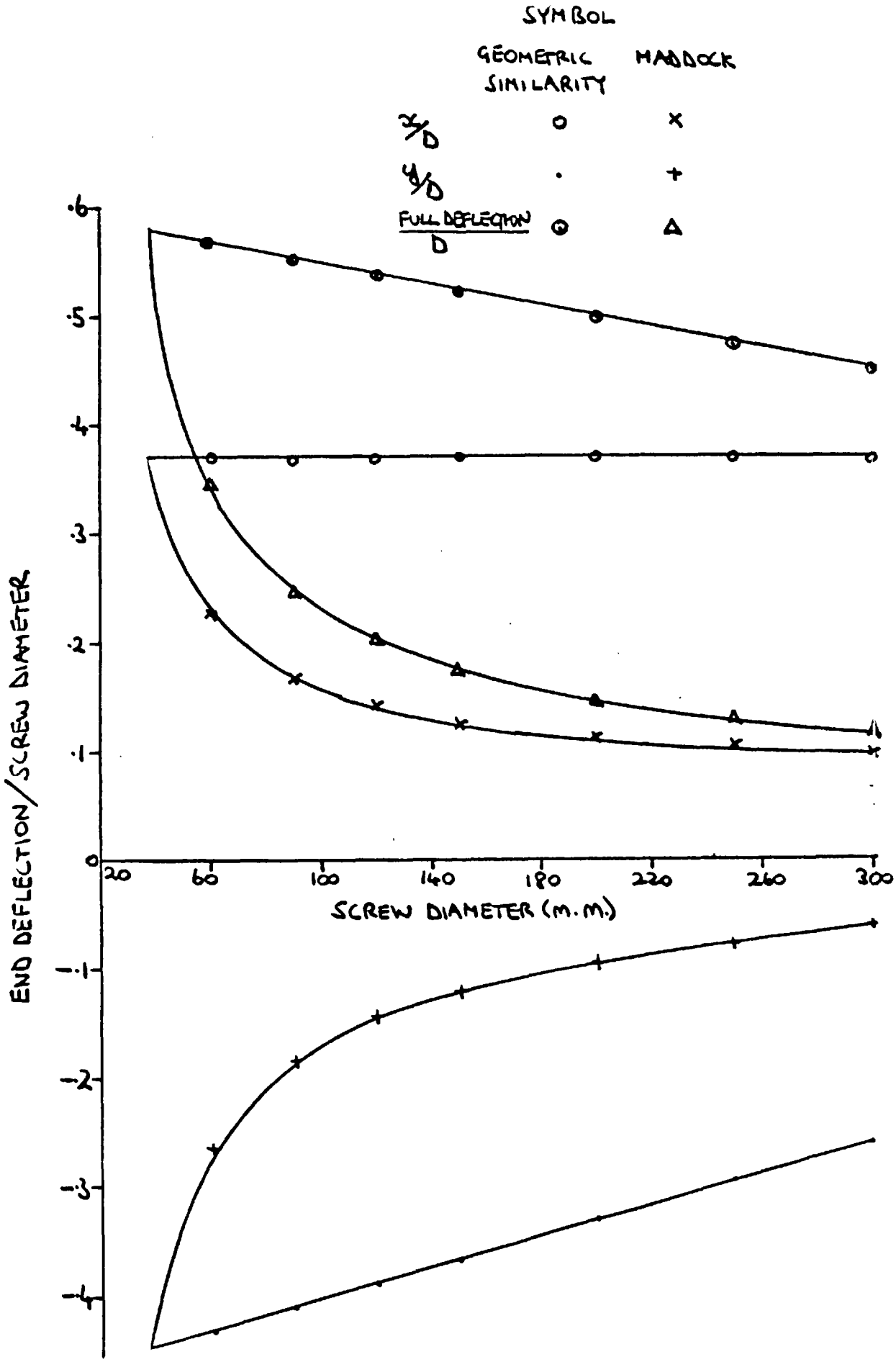

FIG. 3.38 END DEFLECTION/SCREW DIAMETER VERSUS SCREW DIAMETER

FOR EXPERIMENT 26

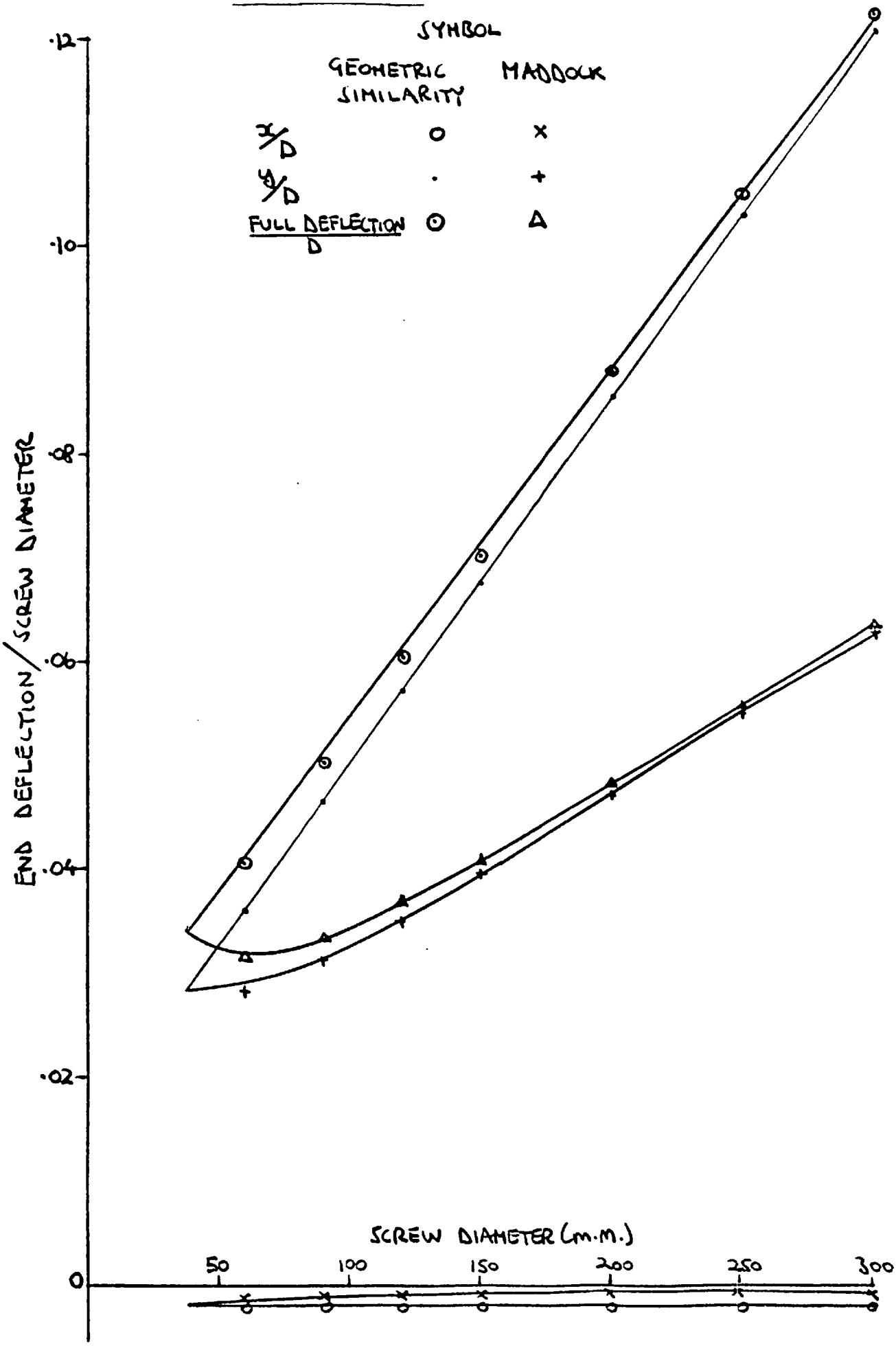

TABLE 3.1 EXTRUDER OPERATING CONDITIONS

Experiment	Polymer	Screw Speed (RPM)	Throughout Rate (GM/MIN)	Die Diameter (mm)
3	LDPE	40	97	2.4
4	LDPE	80	191	2.4
5	LDPE	40	83	1.6
6	LDPE	80	215	4.0
8	PP	40	80	1.6
9	PP	40	93	2.4
14	HDPE	40	81	1.6
18	P.E. POWDER	80	203	2.4
19	P.E. POWDER	40	115	2.4
20	P.E. POWDER	40	78	1.6
21	CRYSTAL POLYSTYRENE	40	128	1.6
22	"	80	266	4.0
23	"	40	110	2.4
26	RIGID PVC POWDER	40	185	2.4
28	LDPE	80	140	2.4
29	HDPE	80	137	2.4

TABLE 3.2 DIMENSIONS OF SCREWS

Screw	Length of screw (turns)	Length of feed (turns)	Length of compression (turns)	Length of metering (turns)	Feed root diameter (mm)	Metering root diameter (mm)
A	19.83	5.00	9.00	5.83	26.67	32.89
B	19.83	5.00	9.00	5.83	21.84	34.04

Both screws have an O.D. of 38.1 mm

TABLE 3.3 CIRCUMFERENTIAL INTEGRATION TESTS

Term in which integral occurs	Integral	Maximum percentage error along the screw
$F^*_{\ell,x}$	$R_o \int_{\gamma}^{\gamma+\theta_f} p_{\omega,z} \sin\omega d\omega + R_r \int_{\gamma+\theta_f}^{2\pi+\gamma} p_{\omega,z} \sin\omega \, d\omega$	.4
$F^*_{\ell,y}$	$R_o \int_{\gamma}^{\gamma+\theta_f} p_{\omega,z} \cos\omega d\omega + R_r \int_{\gamma+\theta_f}^{2\pi+\gamma} p_{\omega,z} \cos\omega d\omega$	.4
$M_{r,x}$	$\int_{\gamma+\theta_f}^{2\pi+\gamma} p_{\omega,z} \sin\omega d\omega$	.005
$M_{r,y}$	$\int_{\gamma+\theta_f}^{2\pi+\gamma} p_{\omega,z} \cos\omega \, d\omega$	.02

TABLE 3.3 CIRCUMFERENTIAL INTEGRATION TESTS (CONTINUED)

Term in which integral occurs	Integral	Maximum percentage error along the screw
F_r	$\int_{\gamma+\theta_f}^{2\pi+\gamma} p_{\omega,z}\, d\omega$	10^{-12}
$F^{***}_{\ell,x}$	$R_o^2 \int_{\gamma}^{\gamma+\theta_f} p_{\omega,z}\sin^2\omega d\omega + R_r^2 \int_{\gamma+\theta_f}^{2\pi+\gamma} p_{\omega,z}\sin^2\omega d\omega$	.009
$F^{***}_{\ell,y}$	$R_o^2 \int_{\gamma}^{\gamma+\theta_f} p_{\omega,z}\cos^2\omega d\omega + R_r^2 \int_{\gamma+\theta_f}^{2\pi+\gamma} p_{\omega,z}\cos^2\omega d\omega$	.008

TABLE 3.4 CONTRIBUTION OF TERMS IN DEFLECTION EQUATIONS TO THE END DEFLECTION

Non-zero Coefficients	Deflections (m.m.)			
	Expt. 5	Expt. 6	Expt. 21	Expt. 22
C_1	10.506	7.989	7.487	1.199
C_1, C_2	10.519	8.308	7.497	1.205
C_1, C_3	83.403	7.870	30.831	1.137
C_1, C_4	10.083	7.973	6.493	1.232
$C_1, M_{f,x}$ $M_{r,x}$	10.587	8.009	7.522	1.190

TABLE 3.5 THE MAXIMUM POLYMER FORCE/TURN TO PREVENT CONTACT BETWEEN THE SCREW AND BARREL

Experiment Number	Polymer	Screw Speed (rpm)	Throughput rate (gm/min)	Die Diameter (mm)	Maximum Force/Turn (Newtons)	AXIAL POSITION OF MAX. FORCE/TURN (L/D)
3	LDPE	40	97	2.4	46.3	9
4	LDPE	80	191	2.4	72.6	9
5	LDPE	40	83	1.6	58.6	9
6	LDPE	80	215	4.0	33.5	7
8	P.P.	40	80	1.6	35.0	8
9	P.P.	40	93	2.4	25.2	10
14	HDPE	40	81	1.6	68.0	7
18	P.E. POWDER	80	203	2.4	46.5	8
19	P.E. POWDER	40	115	2.4	47.0	9
20	P.E. POWDER	40	78	1.6	47.8	8
21	XTAL P.S.	40	128	1.6	34.5	8
22	XTAL P.S.	80	266	4.0	33.4	9
23	XTAL P.S.	40	110	2.4	32.7	8
26	RIGID PVC POWDER	40	185	2.4	139	15-19
28	LDPE	80	140	2.4	46.7	9
29	HDPE	80	137	2.4	32.3	9

CHAPTER FOUR

CONCLUDING DISCUSSION

It has been shown that a very favourable hydrodynamic/slip lubrication mechanism could prevail in extruders if the clearance between the screw and barrel were made large enough. In this regime considerable forces, up to 200 Newtons/turn for a 38.1 mm screw, are required to break down the lubricating polymer film between the flight tip and the barrel wall. Before this occurs the screw will not touch the barrel and no wear caused by metal-to-metal contact between the screw and barrel will occur.

The lateral forces acting on the screw, apart from a bent screw or misaligned screw, appear to be dominated by lateral pressure forces generated inside the extruder, not the weight of the screw as is commonly thought. The absolute pressure inside the extruder is not important, but there is virtually a linear relationship between screw end deflection and the absolute summation of the pressure variance gradient in the axial direction. If the screw length is of a non-integer number of turns then presumably the lateral forces have less chance of cancelling out, so it seems wise to choose a screw legnth of an integer number of turns. The 38.1 mm diameter screw considered in this investigation could support a lateral load of up to 200 Newtons/turn whilst extruding polyethylene and up to 120 Newtons/turn whilst extruding crystal polystyrene. These forces are well above the maximum calculated lateral forces/turn generated when the extruder processed polyethylene and crystal polystyrene (Table 3.5). If, however the generated forces are sufficiently large to break down this film, inferior boundary lubrication prevails and the screw and barrel will wear. The extent of this boundary lubrication

reduces with an increase in load of the order of 30% higher than the initial load required to breakdown the hydrodynamic/slip lubrication. At this point an extremely limited form of boundary lubrication prevails where presumably the wear rate is high but not quite as high as it would be if no lubrication occurred at all. Increases in lateral load do not ensure there is continuous full contact between the screw and barrel. Hydrodynamic/slip lubrication occurs when the nominal shear stress between the flight and the barrel is below a critical value, usually around $10^5 N/m^2$, but one which can be defined by simple rheometer work for any polymer. This slip phenomenon has previously been connected with melt fracture in an extruder die. If the shear stress exceeds $10^5 N/m^2$ then an extremely limited boundary lubrication prevails. Profiling the flight, which has previously been suggested, e.g. by Worth and Lai Fook (Ref. 26) will not improve the lubrication unless the new flight profile reduces the polymer shear stress below its critical value. Unfortunately the radial clearance to diameter ratio specified for most screws is .001:1. At the speeds most extruders are run at this ensures that the shear stress between the screw and barrel is greater than the critical shear stress. Consequently wear occurs as the unsupported screw grinds against the barrel wall. The wear rate will be reduced as the screw wears, the clearance increases and the shear stress drops below the critical value. Unfortunately if the initial clearance between the screw and the barrel is increased to ensure the shear stress is below the critical value the pumping and melting efficiency of the screw may suffer. There are three ways to limit metal-to-metal contact between the screw and barrel:

(i) Make the screw length an integer of turns.

(ii) Reduce the magnitude of the pressure variance gradient along the screw.

(iii) If the consequent reduction in pumping and melting rates is not large specify a clearance between the screw and barrel to ensure the shear stress is below the critical slip value, usually of the order of $10^5 N/m^2$.

Three areas of the investigation deserve further comment:

(i) Circumferential and axial components of shear stress acting on the screw were ignored in the deflection analysis because calculations showed them to be an order of magnitude smaller than the lateral pressure forces.

(ii) The force balance (Section 3.9.2) yields a term, $C_3\frac{dx}{dz}$, in the consequent differential equation. This is the lateral pressure force/unit length due to local deflection and pressure gradients. The effect of this term in producing large screw deflections is examined in Section 3.13. The term is then discarded in further analysis as not applicable to the real situation, where the barrel would act as a support for the screw before deflections of the size calculated were reached. The effect of this term deserves further study.

(iii) In Section 3.17.3 the end screw deflection is shown to be a linear function of $\Sigma_0^L \frac{dv}{dz}$, i.e. of the pressure variance gradient in the axial direction. The pressure variance, v, is the difference between maximum and minimum pressure seen at a slice taken perpendicular to the screw at axial position z, i.e. the pressure difference across the screw flight seen by a pressure transducer z along the screw. The relationship between the end deflection and $\Sigma_0^L \frac{dv}{dz}$ usefully simplifies the relatively complex loading situation, and enables a screw designer, without complex analysis, to concentrate on reducing screw deflections to a minimum.

NOTATION

Symbol	Description
A	area of shaft cross-section
A_r	area of screw root at axial position z in the compression section
a	arbitrary constant
C_1	constant coefficient in deflection differential equation derived from a force balance on an axial elemental screw slice
C_2	coefficient of deflection term in deflection differential equation derived from a force balance on an axial elemental screw slice
C_3	coefficient of deflection gradient term in the deflection differential equation derived from a force balance on an axial elemental screw slice
C_4	coefficient of the moment term in the deflection differential equation derived from a force balance in an axial elemental screw slice
D	barrel I.D.
E	Young's modulus
e	screw flight width perpendicular to the down channel direction
e_1	screw flight width perpendicular to the screw axis
$\hat{e}$	half the axial component of the flight width
$F_{c,x}$	X-component of the centrifugal force/unit length acting on the screw due to its flight
$F^*_{c,x}$	constant contribution to $F_{c,x}$

Symbol	Description
$F^{**}_{c,x}$	coefficient of the delfection term contribution to $F_{c,x}$
$\hat{F}_{c,x}$	X-component of the centrifugal force/unit length due to the screw's displaced centre of gravity
$F_{c,y}$	Y-component of the centrifugal force/unit length acting on the screw due to its flight
$F^{*}_{c,y}$	constant contribution to $F_{c,y}$
$F^{**}_{c,y}$	coefficient of the deflection term's contribution to $F_{c,y}$
$\hat{F}_{c,y}$	Y-component of the centrifugal force/unit length due to the screw's displaced centre of gravity
F_f	axial force/unit length caused by the pressure difference across the flight
$F_{\ell,x}$	lateral pressure force/unit length in the X-direction acting on an axial slice of the screw of original length Δz
$F^{*}_{\ell,x}$	constant contribution to $F_{\ell,x}$
$F^{**}_{\ell,x}$	coefficient of the deflection term's contribution to $F_{\ell,x}$
$F^{***}_{\ell,x}$	coefficient of the deflection gradient term's contribution to $F_{\ell,x}$
$F_{\ell,y}$	lateral pressure force/unit length in the Y-direction acting on an axial slice of the screw of original length Δz
$F^{*}_{\ell,y}$	constant contribution to $F_{\ell,y}$
$F^{**}_{\ell,y}$	coefficient of the deflection term's contribution to $F_{\ell,y}$

Symbol	Description
$F^{***}_{\ell,y}$	coefficient of the deflection gradient term's contribution to $F_{\ell,y}$
F_r	axial force/unit length acting on the screw' root in the compression section
F_W	screw weight/unit length
I	second moment of area of screw
j	number of axial curves fitted to circumferential pressure profiles
K	constant
L	screw or shaft length
$L_{b,1}$	length of screw's shank held in the bearing bush to the first bearing
$L_{b,2}$	length of the screw's shank between the end of the bearing bush and the start of the flighted section of the screw
L_f	representative flight length
L_p	screw pitch
M	bending moment at axial position z
M_e	bending moment at the end of the screw
$M_{f,x}$	X-component of the moment/unit length due to the pressure difference across the flight
$M_{f,y}$	Y-component of the moment/unit length due to the pressure difference across the flight
M_i	bending moment at the start of the screw
$M_{r,x}$	X-component of the moment/unit length due to the pressure acting on the screw's root in the compression section

Symbol	Description
$M_{r,y}$	Y-component of the moment/unit length due to the pressure acting on the screw's root in the compression section
m_f	mass/unit length of the flight
m_r	mass/unit length of the screw root
n	screw speed
p	axial force acting on the screw, z along the screw
Pe	axial back pressure force acting on the end of the screw
$p_{\omega,z}$	pressure acting on the screw at axial position z and angular position ω in the cross-section
p_z	average pressure at axial position z
R	screw radius with the value of R_o or R_r
R_a	radius of curvature of the axial slice length Δs
R_e	final screw root radius over length ΔL_r
R_f	distance between the centre of rotation of the screw and the centre of the flight
R_i	initial screw root radius over length ΔL_r
R_n	radius of curvature of the screw's neutral axis at position z and length Δz
$R_{n,x}$	the value of R_n in the X-Z plane
R_o	outside screw radius
R_r	screw root radius
r_t	resistance between screw section and barrel

Symbol	Description
r_1	voltage divider resistor
r_2	voltage divider resistor
r_3	current limiter resistor
S	shear force at axial position z
S_e	shear force at the end of the screw
S_f	force acting perpendicular to the flight due to the pressure difference across it
S_i	shear force at the start of the screw
s	screw section length
U	screw section's peripheral velocity
V	contact circuit voltage source
v	pressure variance
W	evenly distributed load
W_b	load bearing capacity of bearing or screw section
X	co-ordinate directions perpendicular to the screw's axis
x	X-component of screw deflection
x_e	X-component of screw end deflection
$x_{r,e}$	deflection at end of screw section
$x_{r,i}$	deflection at start of screw section
x_δ	X-component of full deflection of magnitude δ
Y	co-ordinate direction perpendicular to the screw axis, along which the screw's weight acts
y	Y-component of screw deflection
y_e	Y-component of screw end deflection
y_δ	Y-component of full deflection of magnitude δ

Symbol	Description
Z	co-ordinate direction along the screw's axis
z	axial position along the screw's axis

Greek Symbol

α_0	constant coefficient in the equation relating bending moment at the end of the screw to initial values of shear force and bending moment
α_1	coefficient of initial bending moment term in the equation relating the bending moment at the end of the screw to initial values of shear force and bending moment
α_2	coefficient of initial shear force term in the equation relating the bending moment at the end of the screw to initial values of shear force and bending moment
β_0	constant coefficient in the equation relating the shear force at the end of the screw to initial values of shear force and bending moment
β_1	coefficient of initial bending moment term in the equation relating the shear force at the end of the screw to initial values of shear force and bending moment
β_2	coefficient of initial shear force term in the equation relating the shear force at the end of the screw to initial values of shear force and bending moment
γ	angle between the datum line and the start of the screw flight at axial position z
γ_i	the value of γ at the start of the feed section

Greek symbol	Description
ΔF_r	elemental axial force/unit length due to the pressure acting on the screw root in the compression section
ΔL_r	screw root length over axial length Δz
ΔM	elemental change in bending moment from z to $z+\Delta z$
$\Delta p_{\omega,z}$	increase in pressure $\Delta p_{\omega,z}$ over axial elemental length Δs
ΔS	elemental increase in the shear force from z to $z+\Delta z$
Δs	the new length of an axial elemental screw slice, of original length z, due to screw bending
Δz	length of elemental axial slice, z along the screw's axis
$\Delta\omega$	angle subtended by a section of the screw's cross section, ω from the datum line
δ	nominal radial clearance between screw and barrel
ε	eccentricity ratio
η	axial co-ordinate between z and L
θ_a	angle subtended by the screw's neutral axis over a length Δz
θ_c	angle between the horizontal and the line connecting the screw's centre of rotation to its centre of gravity
θ_d	angle between the horizontal and the line connecting the centre of the flight to the screw's centre of rotation
θ_f	angle subtended by the flight at the centre of the screw root
θ_g	the local rotation of an elemental axial slice of the screw of length Δz

Greek symbol	Description
θ_h	helix angle
θr	taper of the screw's root
$\theta_{r,f}$	angle between the horizontal and the line connecting the centre of the screw's root and the centre of the flight
μ	polymer viscosity
ρ	screw density
ω	angle between the datum line and an elemental section of the screw's cross-section

REFERENCES

1. Maddock, B.H. "Effect of wear on the delivery capacity of extruder screws'. SPE Jl., 1959, 15 (No. 5), 433.
2. Barr, R.A. and Chung, C.I. 'Effects of radial screw clearance on extruder performance'. SPE Jl., 1966, 22 (No. 6), 71.
3. Klein, I. 'Predicting the effect of screw wear on performance of plasticating extruders'. Poly. Eng. Sci., 1975, 15 (No. 6), 444.
4. Cameron, A. Principles of lubrication. Longmans.
5. Summers-Smith, D. An introduction to tribology in industry. Machinery Publishing Co. London (1969).
6. Pugh. Practical Lubrication. Newnes-Butterworths.
7. Furey, M.J. 'Contact and friction between sliding surfaces'. ASLE. Trans., 1961, 4, 1.
8. Tallian, T.E. et al. 'Lubricant films in rolling contact of rough surfaces'. ASLE Trans., 1964, 7, 109.
9. Renfrew and Morgan. Polyethylene second edition. Iliffe.
10. Modern Plastics Encyclopedia. McGraw-Hill (1976-77).
11. Pearson, J.R.A. and Petrie, C.J.S. Proc. 4th Inst. Conf. Rheol., part 3, Lee, E.H., Ed., Interscience, New York, 1965, 265.
12. Kennaway, A. 'Some recent developments in extrusion'. Plast. Prog. Lond., 1957.
13. Benbow, J.J. and Lamb, P. 'New aspects of melt fracture'. SPE Trans., 1963, 3 (No. 1), 1.
14. Berger, R. 'Wandhaftung beim viskasen flieben van polymerschmelzen, insbesondere durch kapillaren-eine literaturstudie'. Plaste und Kautschuk, 1972, 19 (No. 2), 113.

15. Worth, R.A., Helmy, H.A.A. and Parnaby, J. 'Wall slip and its implication in the design of plastics melt fed extruders'. Poly. Eng. Sci., 1977, 17 (No. 4), 257.

16. Cogswell, F.N., private communication.

17. Fenner, R.T. and Williams, J.G. 'Some melt flow and mechanical design aspects of large extruders'. Poly. Eng. Sci., 1971, 11 (No. 6), 474.

18. Newland, D.E. 'Whirling of a cantiliver elastic shaft subjected to external pressure'. J. Mech. Engng Sci., 1972, 14 (No. 1) 11.

19. Edmondson, I.R. 'The melting of polymers in single screw extruders'. Ph.D. Thesis, Imperial College, London University, 1973.

20. Lovegrove, J. 'Solids flow in a polymer extruder'. Ph.D. Thesis, Imperial College, London University, 1972.

21. Zienkiewicz, O.C. The finite element method in engineering science. McGraw-Hill, London (1971).

22. Newland, D.E. 'Deflection equation for the buckling of an elastic column subjected to surface pressure'. Research note, University of Sheffield.

23. Timoshenko, S.P. and Gere, J.M. Theory of elastic stability. McGraw-Hill, New York (1961).

24. Maddock, B.H. 'Extruder scale-up theory'. SPE Jl. 1959, 983.

25. Pearson, J.R.A. 'On the scale-up of single-screw extruders for polymer processing'. Plastics and Rubber Processing, 1976, 113.

26. Worth, R.A. and Lai Fook, R.A. 'Factors affecting the wear of extruder screws'. PRI Conf. Interplas., 1977.